Pontifícia Universidade Católica
do Rio de Janeiro

Giulia Simão Barreto de Sousa

Stability and thermal degradation of photo-crosslinked polyethylene pipes for geothermal energy storage applications

Tese de Doutorado

Thesis presented to the Programa de Pós–graduação em Engenharia Química, de Materiais e Processos Ambientais, do Departamento de Engenharia Química e de Materiais da PUC-Rio in partial fulfillment of the requirements for the degree of Doutor em Engenharia Química, de Materiais e Processos Ambientais.

Advisor : Prof. José Roberto Moraes d'Almeida
Co-advisor: Prof. Mikael Skrifvars

Rio de Janeiro
February 2025

Pontifícia Universidade Católica
do Rio de Janeiro

Giulia Simão Barreto de Sousa

Stability and thermal degradation of photo-crosslinked polyethylene pipes for geothermal energy storage applications

Thesis presented to the Programa de Pós–graduação em Engenharia Química, de Materiais e Processos Ambientais da PUC-Rio in partial fulfillment of the requirements for the degree of Doutor em Engenharia Química, de Materiais e Processos Ambientais. Approved by the Examination Committee:

Prof. José Roberto Moraes d'Almeida
Advisor
Department of Engenharia Química e de Materiais – PUC-Rio

Prof. Mikael Skrifvars
Co-advisor
University de Borås - UB

DSc. Marcos Henrique de Pinho Maurício
Pontifícia Universidade Católica do Rio de Janeiro – PUC-Rio

Prof. Marysilvia Ferreira da Costa
Universidade Federal do Rio de Janeiro - UFRJ

Prof. Laura Hecker de Carvalho
Universidade Federal de Campina Grande - UFCG

PhD. Sunil Kumar Lindström Ramamoorthy
University de Borås - UB

Rio de Janeiro, February the 27th, 2025

Giulia Simão Barreto de Sousa

Earned a Bachelor's degree in Mechanical Engineering from Rio de Janeiro State University, Brazil, in 2019. Completed a Master of Science in Materials Science and Engineering at the Pontifical Catholic University of Rio de Janeiro in 2021. Pursued a PhD in Materials Science and Engineering, with emphasis on advanced polymer research.

Bibliographic data

Simão Barreto de Sousa, Giulia

Stability and thermal degradation of photo-crosslinked polyethylene pipes for geothermal energy storage applications / Giulia Simão Barreto de Sousa; advisor: José Roberto Moraes d'Almeida; co-advisor: Mikael Skrifvars. – 2025.

147 f: il. color. ; 30 cm

Tese (doutorado) - Pontifícia Universidade Católica do Rio de Janeiro, Departamento de Engenharia Química e de Materiais, 2025.

Inclui bibliografia

1. Engenharia Química – Teses. 2. Engenharia de Materiais – Teses. 3. Polietileno curado por UV. 4. Degradação do polietileno. 5. RMN no estado sólido. 6. RMN de ângulo mágico giratório. 7. RMN estática de prótons. 8. Massa molar entre reticulações.
I. d'Almeida, José Roberto Moraes. II. Skrifvars, Mikael. III. Pontifícia Universidade Católica do Rio de Janeiro. Departamento de Engenharia Química e de Materiais. IV. Título.

CDD: 620.11

To my found family in life.

To my partner Chris for your incredible support and love. Thank you for always making me laugh, even on the toughest days.

To my oldest friends in life, Juliana, Sara and Carol. I love you all deeply and treasure the way we're always there for one another, no matter how far apart we may live or how different our lives may be. Thank you for your unwavering understanding and support. It means the world to me.

To my friends/family from Rio who I absolutely adore, specially Marcello T., Paula, Renan, Anna Carol, Deja, Lucas X., Karina and Marcelinho. You've become such an important part of my life and I'm so grateful for the all the moments we had together.

To my friends/family in Sweden, specially Sabrina, Samira, Tuĝba, Linus, Lea, Matilda, Sharmeen and Negar. You made a cold and distant land feel like a home.

Acknowledgments

I would like to first thank my advisor, José Roberto, for his unwavering support, encouragement, and guidance throughout this journey. Your lectures back in my UERJ days were a big inspiration and played a huge role in my decision to pursue a master's degree and a research career in materials science and engineering. Your mentorship has helped me stay on track and keep pushing forward despite of the challenges inherent in this academic path.

I would also like to thank my co-advisor, Mikael, for all the support and for welcoming me into the Polymer Technology Group at UB. Being part of such a collaborative group taught me so much and gave me a new appreciation for polymer research.

I would also like to thank all the colleagues that were essential for the elaboration if this work: Andrew, Ivo, Sabrina, Matilda, Shahab, Ville, Magnus, Andreas, Kristina, Jonas and Adib.

This study was financed in part by the Coordenação de Aperfeiçoamento de Pessoal de Nível Superior - Brasil (CAPES) - Finance Code 001.

This study was financed in part by the National Council for Scientific and Technological Development (CNPq) [grant number 141161/2021-3].

Abstract

Simão Barreto de Sousa, Giulia; d'Almeida, José Roberto Moraes (Advisor); Skrifvars, Mikael (Co-Advisor). **Stability and thermal degradation of photo-crosslinked polyethylene pipes for geothermal energy storage applications**. Rio de Janeiro, 2025. 147p. Tese de Doutorado – Departamento de Engenharia Química e de Materiais, Pontifícia Universidade Católica do Rio de Janeiro.

This study provides a comprehensive evaluation of the degradation and stability of crosslinked polyethylene (PEX) pipes designed for high-temperature borehole thermal energy storage (BTES) systems. Special attention is given to a novel type of PEX pipe manufactured using a photo-initiated crosslinking (PEX-e) process. Two formulations, PEX-e1 and PEX-e2, were assessed and compared with commercial peroxide-crosslinked polyethylene (PEX-a) and non-crosslinked bimodal polyethylene (PE100) pipes. The first phase of the study focused on the characterization of the pipes in their "as-received" condition to evaluate their morphology and properties post-processing. The degree of crosslinking was quantified through gel content and the crosslink density was determined through dynamic mechanical analysis (DMA). Phase composition and molecular mobility were examined using static ^{1}H nuclear magnetic resonance (NMR) and differential scanning calorimetry (DSC), while oxidative stability was evaluated using oxidation induction time (OIT) measurements. Both PEX-e formulations exhibited elevated crosslinking degrees and high OIT values. The second phase of the study involved a detailed analysis of thermo-oxidative degradation and stability through ageing tests. This was achieved by immersing pipes in water at BTES service temperatures for 210 days. Changes were monitored using advanced analytical techniques, including fourier transform infrared spectroscopy (FTIR), ^{1}H and ^{13}C NMR, colorimetry, and DMA. Results revealed that physical ageing dominated the first 30 days, while over time, chain scission was identified as the primary degradation mechanism, with PEX-a being the most severely affected. Interestingly, despite the high OIT levels, both PEX-e exhibit accelerated AO depletion during prolonged exposure to hot water. These findings highlight the importance of long-term ageing tests at service conditions and underscore the need for further optimization of PEX-e formulations specifically tailored for BTES service conditions.

Keywords

UV-cured polyethylene; Polyethylene degradation; Solid state NMR; Magic spinning angle NMR; 1H static NMR; Molecular weight between crosslinks.

Resumo

Simão Barreto de Sousa, Giulia; d'Almeida, José Roberto Moraes; Skrifvars, Mikael. **Estabilidade e degradação térmica de tubos de polietileno foto-reticulado para aplicação em armazenamento de energia geotérmica**. Rio de Janeiro, 2025. 147p. Tese de Doutorado – Departamento de Engenharia Química e de Materiais, Pontifícia Universidade Católica do Rio de Janeiro.

Este estudo avalia a degradação e a estabilidade de tubos de polietileno reticulado (PEX) projetados para sistemas de armazenamento de energia geotérmica em poços (*borehole thermal energy storage* - BTES). O foco principal é dado a um novo tipo de tubo PEX, fabricado por meio de um processo de reticulação fotoinduzida (PEX-e). Foram analisadas duas formulações desse material, PEX-e1 e PEX-e2, comparando-as com tubos comerciais de polietileno reticulado por peróxido (PEX-a) e de polietileno bimodal não reticulado (PE100). Na primeira etapa, os tubos foram caracterizados em sua condição "como recebidos", a fim de investigar a morfologia e as propriedades após o processamento. O grau de reticulação foi avaliado por meio do teor de gel, enquanto a densidade de reticulação foi determinada utilizando análise mecânica dinâmica (DMA). A composição das fases e a mobilidade molecular foram examinadas por ressonância magnética nuclear (RMN) de prótons e calorimetria exploratória diferencial (DSC), enquanto a estabilidade oxidativa foi medida pelo tempo de indução de oxidação (OIT). Ambas as formulações PEX-e apresentaram elevado grau de reticulação e altos valores de OIT. Na segunda etapa, foi feita uma análise detalhada do envelhecimento de longo prazo. Para isso, os tubos foram submetidos a imersão em água na temperatura de serviço dos sistemas por 210 dias. Alterações nas propriedades foram monitoradas por técnicas como espectroscopia no infravermelho por transformada de Fourier (FTIR), RMN de prótons e carbono-13, colorimetria e DMA. Os resultados indicaram que o envelhecimento físico predominou nos primeiros 30 dias, enquanto, ao longo do tempo, a cisão de cadeias tornou-se o principal mecanismo de degradação. Apesar dos altos níveis iniciais de OIT, ambos os tubos PEX-e apresentaram declínio acelerado de antioxidantes após exposição prolongada. Esses achados ressaltam a necessidade de otimização das formulações PEX-e para melhorar sua estabilidade e durabilidade em aplicações BTES de alta temperatura.

Palavras-chave

Polietileno curado por UV; Degradação do polietileno; RMN no estado sólido; RMN de ângulo mágico giratório; RMN estática de prótons; Massa molar entre reticulações;.

Table of contents

List of figures

List of tables

1
Introduction

1.1
Motivation

Thermal energy storage (TES) systems offer a sustainable and efficient solution for balancing the time disparity between energy production and consumption. Among the various TES technologies, borehole thermal energy storage (BTES) is particularly attractive due to its comparatively low operational costs and minimal environmental impact [1].

BTES systems consist of a network of heat exchange pipes, typically made from high-density polyethylene (HDPE) or crosslinked polyethylene (PEX) [2, 3]. These systems operate within a temperature range of approximately 5 °C to 90 °C [2, 4]. While higher temperatures enhance system efficiency, they also pose challenges regarding polymer stability. Elevated temperatures combined with oxygen exposure can lead to thermo-oxidative degradation, resulting in a loss of mechanical properties and, in severe cases, premature failure of system components [5–8].

For high-temperature applications (above 80°C), PEX is often preferred over HDPE due to its superior thermal stability [9–12]. Among the commercially available PEX types, peroxide crosslinked polyethylene (PEX-a) is the most commonly used in heating and hot-water transportation systems [13, 14]. However, the PEX-a production process presents several drawbacks, including a low crosslinking rate, heat sensitivity, and the generation of unwanted volatile by-products [15, 16]. These limitations have driven efforts within the pipe industry to identify more efficient and sustainable alternatives [17, 18].

One promising innovation is photo-crosslinked polyethylene (PEX-e), a material initially developed in the 1990s for applications such as films and cable insulation. Recently, this technology has garnered interest from the pipe industry due to its advantages, including higher production efficiency, reduced energy consumption, and the absence of volatile chemical emissions [15, 17, 18]. Despite these benefits, the use of photo-crosslinking in pipes and tubing remains unexplored in scientific literature.

This study addresses this knowledge gap by investigating the morphology

and physical properties of PEX-e pipes specifically designed for BTES systems. Emphasis is placed on assessing their long-term stability, a critical factor for ensuring performance and reliability in thermal energy storage applications. By exploring the suitability of PEX-e for BTES systems, this work contributes to advancing materials for sustainable energy storage solutions.

1.2 Objectives

The objective of this study is to assess the suitability of photo-crosslinked polyethylene (PEX-e) pipes for borehole thermal energy storage (BTES) applications. First, an extensive literature review was conducted to provide a comprehensive understanding of the application, the manufacturing processes of PEX pipes, the current state of the art in PEX degradation and stability. For the experimental work, two PEX-e formulations, designated as PEX-e1 and PEX-e2, were evaluated and systematically compared to commercial peroxide-crosslinked polyethylene (PEX-a) and non-crosslinked polyethylene (PE100) pipes to benchmark their relative performance.

The experimental work was conducted in two phases:

1. Initial characterization: Pipes were analyzed in their "as-received" condition to examine their morphology and physical properties following the manufacturing process.

2. Long-term ageing analysis: Thermo-oxidative degradation and stability were assessed through prolonged exposure to hot water, with the goal of monitoring morphological changes and identifying the primary degradation mechanisms.

Overall, this study aims to provide a comprehensive understanding of the stability and degradation of PEX-e pipes in demanding BTES conditions.

1.3 Thesis scope

This thesis is organized as follows:

Chapter 1: Introduction

This chapter introduces the motivation behind the research and outlines the objectives of the thesis.

Chapter 2: Literature Review

A comprehensive literature review is presented, covering the application of Borehole Thermal Energy Storage (BTES) systems, the manufacturing and

crosslinking processes of polyethylene pipes, the morphological aspects and their relationship with practical properties and the current state of knowledge on polyethylene degradation and stability.

Chapter 3: Characterization of Photo-Crosslinked Polyethylene Pipes for Geothermal Energy Storage

This chapter presents the first research paper, focusing on the characterization of photo-crosslinked polyethylene (PEX-e) pipes after processing, including an analysis of their morphology and physical properties.

Chapter 4: Thermo-Oxidative Ageing of Photo-Crosslinked Polyethylene Pipes for Thermal Energy Storage

This chapter presents the second research paper, corresponding to the second stage of the experimental work. It examines the thermo-oxidative degradation and stability of the PEX-e pipes through long-term ageing tests, focusing on the effects of prolonged exposure to hot water.

Chapter 5: Conclusions and Future Work Suggestions

This chapter provides the final conclusions drawn from the research, summarizing key findings. Additionally, suggestions for future research directions are proposed.

2
Literature review

2.1
Borehole thermal energy storage systems

In response to the growing environmental crisis, many countries have committed to reducing greenhouse gas (GHG) emissions. The energy sector accounts for approximately 35% of total GHG emissions, with a substantial portion stemming from heating and cooling activities [1]. Addressing this challenge requires significant investment in sustainable resources for heating and cooling systems on a district or city scale. District heating and cooling (DHC) systems provide an efficient, large-scale energy solution with the potential to significantly reduce GHG emissions. A critical component of DHC systems is thermal energy storage, which plays a crucial role in improving their overall efficiency and performance [1].

Several approaches can be employed for thermal energy storage purposes, including tank thermal energy storage, pit thermal energy storage, aquifer thermal energy storage, and borehole thermal energy storage (BTES). Among these, BTES is often preferred due to its high capacity for seasonal storage, lower maintenance costs and fewer environmental considerations [1].

BTES can be integrated with other renewable energy sources, such as solar power to provide heating, cooling, and dehumidification for residential and commercial buildings, as well as for industrial and horticultural processes. Figure 2.1 shows an example of a typical vertical BTES system integrated with a solar thermal collector, a combined heat and power (CHP) plant, and a gas boiler linked to a DHC network [19]. This type of integration is particularly advantageous in high-latitude countries like Sweden, where solar energy availability is abundant during summer but scarce in winter, when peak heating demand occurs. This seasonal mismatch between energy supply and demand can be addressed effectively by storing excess heat produced during high-production periods for later use [20]. Furthermore, industrial waste heat can be stored via BTES arrays and recycled for DHC applications, further enhancing energy efficiency and sustainability [2, 21].

The principle behind BTES involves injecting or extracting heat from

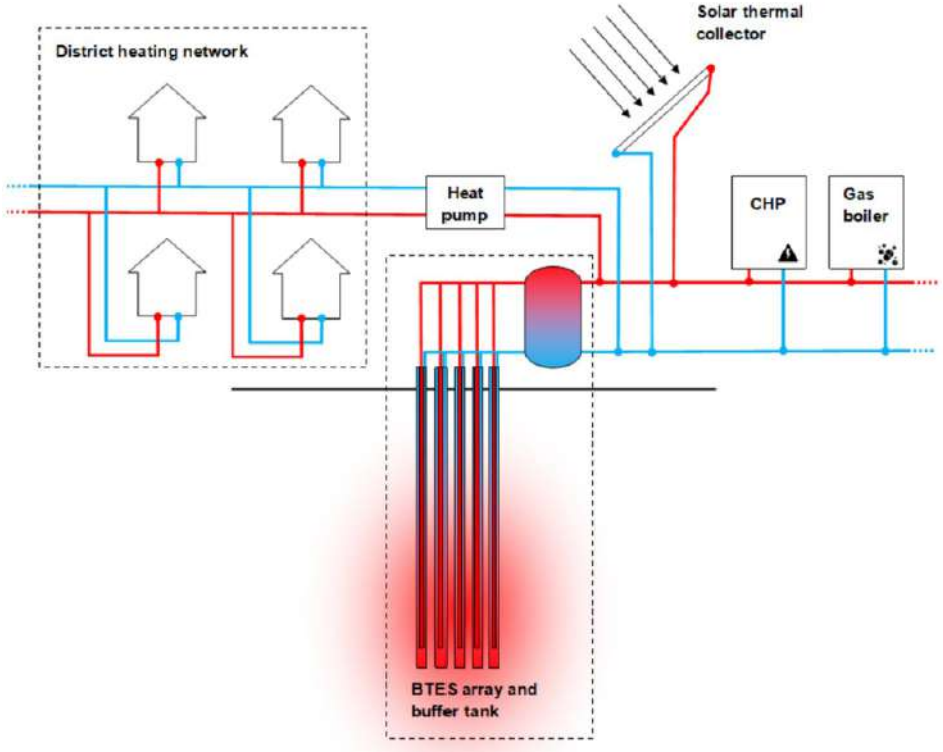

Figure 2.1: Schematics of borehole thermal energy storage array with sources and end-users [19].

underground layers of rock and soil through a network of borehole heat exchangers (BHEs) [1, 22]. A BHE typically consists of a borehole with a diameter between 100 and 150 mm, drilled to depths ranging from 35 m to 350 m [2]. While different configurations are possible, the most common setup is the single U-tube, which features up-flow and down-flow shanks installed within vertical boreholes, as illustrated in Figure 2.2 [2, 20]. Alternatively, coaxial pipes or double-U pipes can also be used. A heat transfer fluid, typically a glycol/water mixture, is circulated through these pipes via a heat pump.

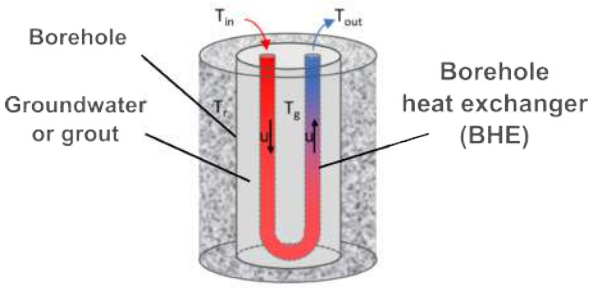

Figure 2.2: Single U-tube borehole heat exchanger. Modified from reference [20].

.

The composition of the BHE borehole filling depends on the geological environment [22]. In areas where the rocks are not fully lithified or self-supporting, or where the water table is low, the borehole must be filled with a low-permeability, thermally-enhanced grout. This grout material ensures the structural stability of the system and acts as a thermally conductive connection between the heat exchange pipe and the surrounding geological environment. In contrast, in hard crystalline rock environments, such as those composed of gneisses, granites, or schists, BHE boreholes are typically filled with groundwater. Groundwater systems generally exhibit lower thermal resistance to heat flow compared to grouted systems, resulting in higher efficiency [2]. This is particularly common in Scandinavian countries and was the type of borehole configuration considered for this study.

BHE systems typically operate within a temperature range of approximately 5 °C to 90 °C [1, 22]. The U-tubes used in BHEs are commonly made of high-density polyethylene (HDPE) with an outside diameter of 32-40 mm [2]. Material selection is critical to ensure not only system efficiency, but also durability. Kupfernagel et al. [23] evaluated the impact of operational temperature changes on the hydraulic conductivity of BHEs made of HDPE. Results revealed that hydrophobic character of HDPE pipes as well as its high coefficient of thermal expansion were the key weaknesses compromising system integrity over numerous heating/cooling cycles [23].

Many efforts have been made to enhance the thermal properties of HDPE pipes [22, 24, 25]. Incorporating talc particles into the HDPE matrix has shown promising results, including a reduction in the thermal expansion coefficient and an increase in thermal conductivity [22, 26]. Mehrjerdi [22] demonstrated that the enhanced thermal conductivity of talc-filled HDPE pipes can reduce the borehole thermal resistance by up to 21%, thereby increasing system efficiency. However, the addition of talc also led to a significant decline in thermal-oxidative stability, with a notable reduction in oxidation induction time. Similar findings were reported for HDPE resins filled with soapstone, a talc-rich mineral [27]. It is hypothesized that talc particles may adsorb stabilizers on their surfaces, reducing their effectiveness and consequently shortening the service life of the pipes [22, 27].

Ensuring the thermal stability of BTES pipes is critical, as these systems operate under conditions of elevated temperatures and oxygen exposure, which can cause thermo-oxidative degradation, loss of mechanical properties, and premature failure. To address these challenges, crosslinking has emerged as a promising approach to enhance the durability and thermal stability of PE pipes [9–12]. Studies have highlighted the potential of crosslinked

polyethylene (PEX) as a material for thermal energy storage applications [25, 28, 29]. For instance, Han et al. [28] demonstrated that PEX sheets exhibited significantly improved thermal stability and resistance to thermo-oxidative degradation compared to un-crosslinked HDPE after 400 heating/cooling cycles. Furthermore, crosslinking has been shown to enhance resistance to slow crack growth (SCG) [30], which is widely recognized as the leading cause of failure in PE pipes [7].

Given these advantages, PEX pipes emerge as a promising material choice for BTES systems. However, as Boneh et al. [31] emphasized, the suitability of different PEX materials for energy storage applications depends on achieving sufficient high-temperature stability, which is the main focus of the present study.

2.2 Crosslinked polyethylene pipes

The crosslinking process transforms the linear polymer structure of polyethylene into a three-dimensional, mesh-like network by forming covalent bonds between polymer chains [32]. This process is initiated through a free-radical reaction driven by chemical agents or by physical means. Accordingly, the commercially available methodologies are broadly categorized into chemical and physical methods, as illustrated in Figure 2.3.

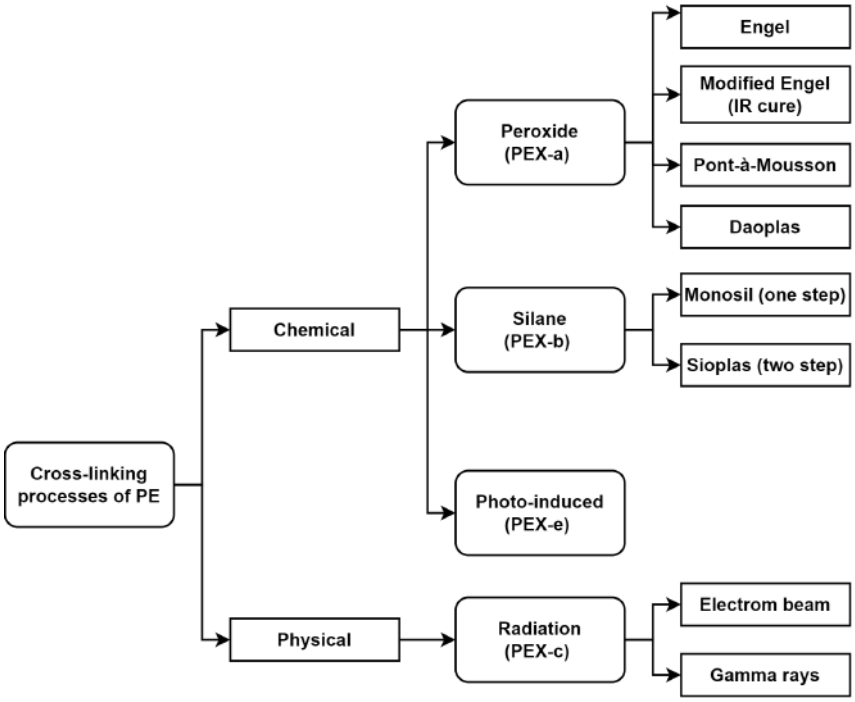

Figure 2.3: Schematics illustrating the crosslinking processes commonly utilized for production of PEX pipes.

The three most commonly used methods for producing PEX pipes are peroxide-induced (PEX-a), silane-induced (PEX-b), and radiation-induced (PEX-c) crosslinking. Among these, PEX-a pipes are the most widely used for potable water transport and heating applications due to its high degree of crosslinking and superior mechanical properties [13, 14].

Recently, photo-crosslinked polyethylene (PEX-e) has emerged as a promising alternative to PEX-a. The PEX-e process offers several advantages, including higher production efficiency, reduced energy consumption, and the absence of volatile chemical emissions during manufacturing [15, 17, 18, 33]. These benefits make PEX-e an attractive option for the pipe industry, and it is of particular interest in this study. A detailed description of each crosslinking method is provided in the following sections.

2.2.1 Peroxide-induced crosslinking

In the PEX-a process, peroxide molecules decompose at elevated temperatures (170°C to 250 °C), producing free radicals. These radicals abstract hydrogen from the polymer chain, forming alkyl radicals that initiate crosslinking reactions by bonding with nearby polymer chains to create a three-dimensional network [34–36]. Organic peroxides are commercially attractive free-radical initiators due to their room temperature-stability and temperature-dependent decomposition rates [16]. Common commercial organic peroxides for chemical crosslinking include di-tert-butyl cumyl peroxide (BCUP) and dicumyl peroxide (DCP) [35]. Figure 2.4 illustrates the mechanism of PE crosslinking using DCP [36].

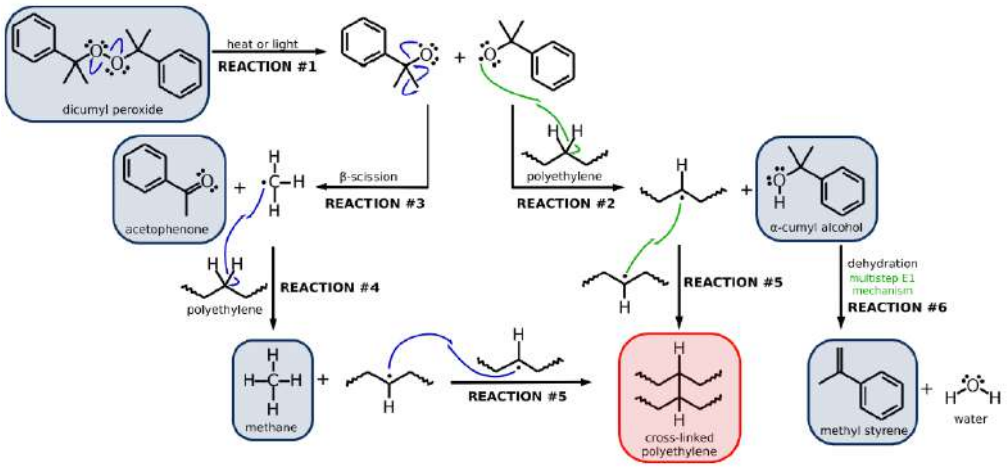

Figure 2.4: Schematics of PEX-a crosslinking process with DCP agent [36].

Peroxide-induced crosslinking occurs in three primary steps. First, radical formation is initiated through the thermolytic decomposition of the peroxide.

The O−O bond of peroxides (∼150 kJ/mol) preferentially breaks due to its lower bond energy compared to the carbon-hydrogen bond (∼350 kJ/mol) [37]. Peroxide radicals ($RO^{\bullet}$) abstract hydrogen from the PE substrate, forming stable ROH species and polymer radicals [37, 38]. This exothermic reaction, with an activation energy of approximately 25 kJ/mol, occurs at temperatures above the PE melt point. Finally, termination reactions occur via two mechanisms: combination and disproportionation. In the combination process, adjacent radicals covalently bond, creating crosslinks and consequently, increasing molecular weight. In disproportionation reactions no changes occur in molecular weight, as no covalent bonds are made. Radicals containing β-hydrogen undergo a hydrogen exchange, forming non-reactive species [37].

Competing side reactions involving peroxide radicals can reduce the crosslinking efficiency. A notable side reaction is β-scission of alkoxy radicals, which produces lower-energy hydrocarbon radicals and carbonyl-containing species. The prevalence of side reactions depends on the radical structure, peroxide concentration, and reaction temperature [36, 37]. Akbarian et al. [36] used molecular dynamics simulations and experimental methods, such as Fourier transform infrared (FTIR) mapping and wide-angle X-ray scattering (WAXS), to investigate peroxide-induced PE crosslinking. They found that moderate DCP-to-PE ratios (∼0.4) enhanced crosslinking, while excessive DCP-to-PE ratios (>0.5) led to unfavorable side reactions, reducing crosslinking concentrations and increasing by-products. Similarly, increasing the reaction temperature up to 500 K improved crosslinking, whereas increasing the temperature above that threshold had an adverse effect on crosslinking degree [36].

The peroxide crosslinking process has been refined over time to maximize desired products, minimize side reactions, and ensure consistent end-product quality [37]. Several commercial variations of this process exist. The Engel process, developed by Thomas Engel in the late 1960s, was the first commercially available method. It involves sintering a granulated blend of PE, peroxide, and stabilizers under controlled temperatures [38]. Crosslinking occurs during extrusion through a heated die under high pressure, typically applied to HDPE [39].

The Engel process has notable drawbacks, including slow production rates and non-homogeneous crosslinking distribution. To address these limitations, alternative methodologies have been developed. One widely adopted approach involves the use of double-screw extruders followed by an infrared oven. In this process, the non-crosslinked pipe is first extruded at temperatures below the decomposition point of the peroxide. Immediately thereafter, it is

subjected to infrared heating to initiate crosslinking [40, 41]. Infrared heating ensures rapid and uniform heating of the pipe wall, thereby promoting efficient and more homogeneous crosslinking.

Figure 2.5 shows a modern production line for PEX-a pipes using a modified Engel process with infrared-induced crosslinking. Pre-mixed PE, peroxide agent, and additives are extruded through a double-screw extruder. The pipe then goes through the infrared oven, where crosslinking occurs. The pipes are then cooled and calibrated for dimensional accuracy. For heating applications, the extrusion of external oxygen barrier layers are also required [42]. These layers prevent oxygen permeability, which can lead to corrosion in systems such as underfloor heating. The oxygen barrier is applied via an adhesive layer on the outer surface of the heated PEX pipe, ensuring functionality in closed systems [38]. At the end of the production line, pipes are coiled for storage and distribution [18]. The PEX-a pipes analyzed in the present study were manufactured using this methodology.

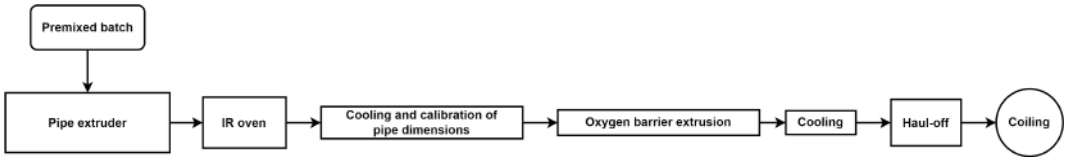

Figure 2.5: Schematic representation of a production line for PEX-a pipes designed for heating system applications. (This figure is based on the firsthand observations and experiences of the author within the industry).

Other alternative peroxide-crosslinking methodologies, though less commonly applied to pipes, include the Pont-à-Mousson and Daoplas methods. The Pont-à-Mousson method is used for crosslinking low- and medium-density polyethylene or high-density polyethylene with low molecular weight [39]. This two-step process involves mixing and extruding PE with peroxide below the peroxide decomposition temperature, followed by immersion in a high-temperature salt bath to initiate crosslinking [35]. Precise temperature control is crucial in this method to prevent premature crosslinking.

The Daoplas method addresses the concern about temperature control by introducing the peroxide initiator after extrusion. In this process, the extruded pipe is surrounded by a peroxide-containing medium, and crosslinking is carried out downstream under high temperature and pressure [35, 39]. However, the Daoplas method requires additional equipment and faces limitations regarding peroxide diffusion rates, which affects crosslink distribution.

Overall, peroxide-induced crosslinking offers several advantages, such as the ability to integrate crosslinking into the production line, low material costs, and high crosslinking degrees (70–90%) [16, 18]. Nonetheless, limitations in-

clude the formation of unwanted low-molecular-weight by-products like water, methane, acetophenone, cumyl alcohol, and α-methyl styrene [43]. Elimination of these by-products require prolonged degassing at high temperatures and effective ventilation systems to mitigate health risks for workers [43]. Additionally, PEX-a systems are energy-intensive, require substantial capital investments, and have relatively low production rates [16].

2.2.2 Silane-induced crosslinking

Chemical crosslinking can also be accomplished by the use of silane coupling agents [16, 35, 39]. Silane coupling agents are silicon-based organic chemicals with standard formula of X_3Si-Y, where X represents a hydrolyzable group such as ethoxy or methoxy, Y is a functional group, e.g., amino, methoxy, acetoxy, epoxy, that reacts with water to form silanol (Si−OH) [39]. Vinyl alkoxy silanes are suitable compounds for crosslinking purposes due to their double bonds and ability to rapid crosslink, with vinyltrimethoxysilane being the most common silane used in manufacturing of PEX-b [39].

The general methodology for silane crosslinking comprises at least two stages, that can be done consecutively (one step) or separately (two steps). In the first step, a silane agent is grafted into PE via its vinyl groups through a free radical reaction [16, 39]. Initiation of the free radical reaction is facilitated by a relatively small amount of peroxide. In the second step, the crosslinkable PE undergoes crosslinking via exposure to hot water or steam with the aid of a catalyst. Moisture induces hydrolysis of silane alkoxy groups, leading to the subsequent condensation of hydroxyl groups to form stable siloxane linkages (crosslinks) [39]. A fundamental difference of this process is that the resultant crosslinks between PE chains are not carbon-carbon bonds as in the case of PEX-a and PEX-c. The crosslinks in PEX-b are constituted of oxygen-silicon covalent bonds, i.e., siloxane "bridges".

The grafting process can be conducted while the polymer is still in the molten state, but typically, the crosslinking reaction takes place in the solid state (70-95 °C), after molding the grafted polymer into the final product shape [35, 38]. There are two primary processes for crosslinking PE with moisture-cured vinyl silanes: Monosil and Sioplas process.

The Monosil process, proposed by BICC Limited and Establishments Maillefer SA in 1974 is a one-step process that involves a continuous feeding of liquids during extrusion [38, 39]. The specially designed extruder is equipped with a long barrier screw (high L:D ratio) and an injection system. Silane is grafted into PE and the injected end-product is crosslinked in the presence of

moisture [39]. This speeds up production but poses safety problems owing to the volatile and flammable nature of silanes [38]. Additionally, there is a risk of premature and excessive crosslinking [39].

The Sioplas process was developed in 1968 by Midland Silicones Co [39]. In this method, a blend of silane and peroxide is added to molten PE, initiating the silane grafting reaction. Typically, this reaction is achieved by reactive extrusion. High-shear compounding extruders, such as co-rotating twin-screw extruders with L:D ratio range of 30 to 36, are commonly used [39]. Following the grafting process, the polymer undergoes pelletization and can be stored in dry conditions up to 6 months [38, 39]. In the second step, a masterbatch, composed of PE pellets, catalyst and stabilizing additives, is mixed with the grafted pellets in a typical ratio of 5:95 [39]. The resulting mixture is melted and extruded. Crosslinking occurs in a water bath or in a steam sauna at temperatures of 70-90°C [38, 39]. The state-of-the-art of the Sioplas process, including schematics of the typical industrial line for the manufacturing of PEX products can be found in reference [39]. Advantages of the Sioplas method include high output rates, low scrap generation, and the ability to utilize conventional extrusion equipment.

In general, the silane crosslinking processes offer flexibility in formulation and a broad processing window. The design of the crosslinking bridges may vary a lot according to the structure of the alkoxy-silane used, allowing for tailored properties in the final PEX product [16]. The rate of crosslinking is influenced by factors such as catalyst type, crosslinking temperature and diffusion rate of water throughout the fabricated product. The formulation can be highly specialized and tailored to the specif application of the end-product [37]. Drawbacks include high materials costs and low degree of crosslinking relative to PEX-a, typically (65-70%) [16, 18].

2.2.3 Radiation-induced crosslinking

In the radiation method, the solid polymer is exposed to high-energy sources such as X-rays, gamma rays, or electron beams. These high-energy particles penetrate the polymer, elevating its molecular energy to an excited state and leading to the formation of free radical species [37]. Covalent bonds are then formed between free radicals in adjacent chains, resulting in crosslinking.

A significant concern with this method is that radiation can also cause chain scission, potentially leading to degradation and a reduction in molecular weight [16, 38]. In fact, both chain scission and crosslinking typically occur

simultaneously and competitively. The predominant phenomenon depends on several factors, including the polymer's sensitivity to radiation effects (chemical yield), the irradiation dose and rate, the presence of stabilizers, and the process environment [38].

Radiation crosslinking is conducted in the solid state, after the pipe is molded into its final shape, typically within an inert atmosphere to prevent oxidative degradation [16, 39]. There are two predominant methods for radiation-induced crosslinking in polyethylene: gamma (γ) radiation and electron beam radiation (EBR). In the gamma radiation method, the pipe is exposed to a radioactive isotope such as Cobalt 60 (Co^{60})) or Cesium 137 (Cs^{137}). Conversely, in EBR, high-energy electrons are employed to irradiate the polymer molecules [38].

Electron beams are more commonly used as a industrial radiation source due to their capacity to deliver high doses rapidly with higher control over the radiation dose [35, 39, 43]. However, EBR is limited by its short penetration depth, restricting the thickness of the crosslinkable products to less than 10 cm [16]. On the other hand, gamma radiation readily penetrates thicker PE samples, but its use is challenging to control since it involves a nuclear process [39, 43].

Several kinds of electron beam accelerators are commercially available such as direct current, electrodynamic direct current, radio-frequency linear accelerators, magnetic induction, and continuous wave machines [38]. In practical terms, the PE pipe is extruded normally, and afterwards crosslinking is achieved offline, i.e. outside the pipe production line, by exposure of the pipe to radiation in an appropriately shielded cell. The crosslinking density of PEX-c typically falls within the 70-75% range. Careful control of irradiation time is crucial, as excessive exposure can lead to product discoloration and increased brittleness [18].

The radiation method offers several advantages, including a rapid crosslinking rate in comparison to conventional chemical processes, which are limited by heat or water diffusion. It is considered a relatively clean process, requiring no chemicals or initiators, leading to non-harmful by-products such as H_2 and low-molecular-weight hydrocarbons that are easily removed [43]. Additionally, it is a temperature-independent process, enabling the incorporation of temperature-sensitive additives such as metal hydrates [37].

Nevertheless, this method has notable drawbacks, including the high capital costs involved in establishing a commercial manufacturing facility, which serves as a barrier for numerous industries across all scales. Moreover, the hazardous potential of radiation is another relevant disadvantage of this

method. Standard legislation mandates the construction of thick, high-density concrete walls to shield the environment, and stringent precautions are imposed to protect operators from radiation [37, 38, 43].

2.2.4 Photo-initiated crosslinking

In the PEX-e process, the PE formulation contains a photo-initiator additive, which absorbs UV light, undergoes photo-excitation, and abstracts hydrogen atoms from the polymer backbone [15, 44].

Although the concept of using photo-initiators was initially explored in the 1950s, no commercial process for photo-induced crosslinking emerged in the subsequent decades due to challenges such as low penetration depth (less than 1 mm) and slow crosslinking rates [44]. However, pioneering research in the 1990s by Chen and Rånby [44–51] demonstrated that photo-initiated crosslinking of polyethylene could be optimized for high efficiency if conducted at temperatures above the polymer's melting point.

Extensive studies explored various photo-initiators, crosslinking agents, and experimental conditions for the photo-crosslinking of polyethylene films and extruded filaments [44–51]. Results showed that employing benzophenone (BP) or a chlorinated BP derivative as the photo-initiator, auxiliary crosslinking agents such as triallyl cyanurate (TAC), and elevated temperatures (above the melting point) enabled a high degree of crosslinking (gel content $\geq 90\%$) within 15 seconds of irradiation [44]. Among the 18 photo-initiators tested by Chen and Rånby [44], 4-chlorobenzophenone proved to be the most effective. Additionally, the presence of a nitrogen atmosphere during crosslinking was found to be critical for achieving the desired gel content [44].

One key issue identified in this method was the pre-oxidation of the polymer during photo-crosslinking, which can adversely affect the polymer's durability [48]. However, optimized stabilizer formulations significantly mitigated this issue. Specifically, a formulation incorporating the antioxidant Irganox B215 and small amounts of the hindered amine photo-stabilizer Tinuvin 770 effectively prevented oxidation during processing [48].

Recent studies have focused on industrial applications of photo-crosslinking, particularly for cable insulation [15, 52–54]. These investigations have provided detailed insights into the reaction mechanisms of photo-initiated crosslinking. Figure 2.6 shows schematic representation of the photo-initiated crosslinking reactions of PE molecules by using photo-initiator BP and auxiliary crosslinking agent triallyl isocyanurate (TAIC) [15]. In this system, the photo-initiator (PI) absorbs UV light, transitions to an excited triplet state,

and subsequently abstracts hydrogen atoms from polyethylene molecules, forming free radicals on both the polymer chains and the hydrogenated PI molecules [15, 44]. A small fraction of PI molecules form non-volatile by-products during this process. The radical PI molecules then react with the auxiliary crosslinking agent (CA), generating allyl radicals that subsequently polymerize. This process results in transient free radicals on both PE and CA molecules, which chemically bond to form crosslinks. Three main crosslink configurations are possible: PE-PE, PE-CA-PE, and PE[CA]-PE, where [CA] denotes a copolymer segment of CA. The statistical probability of each configuration is governed by reaction kinetics [15].

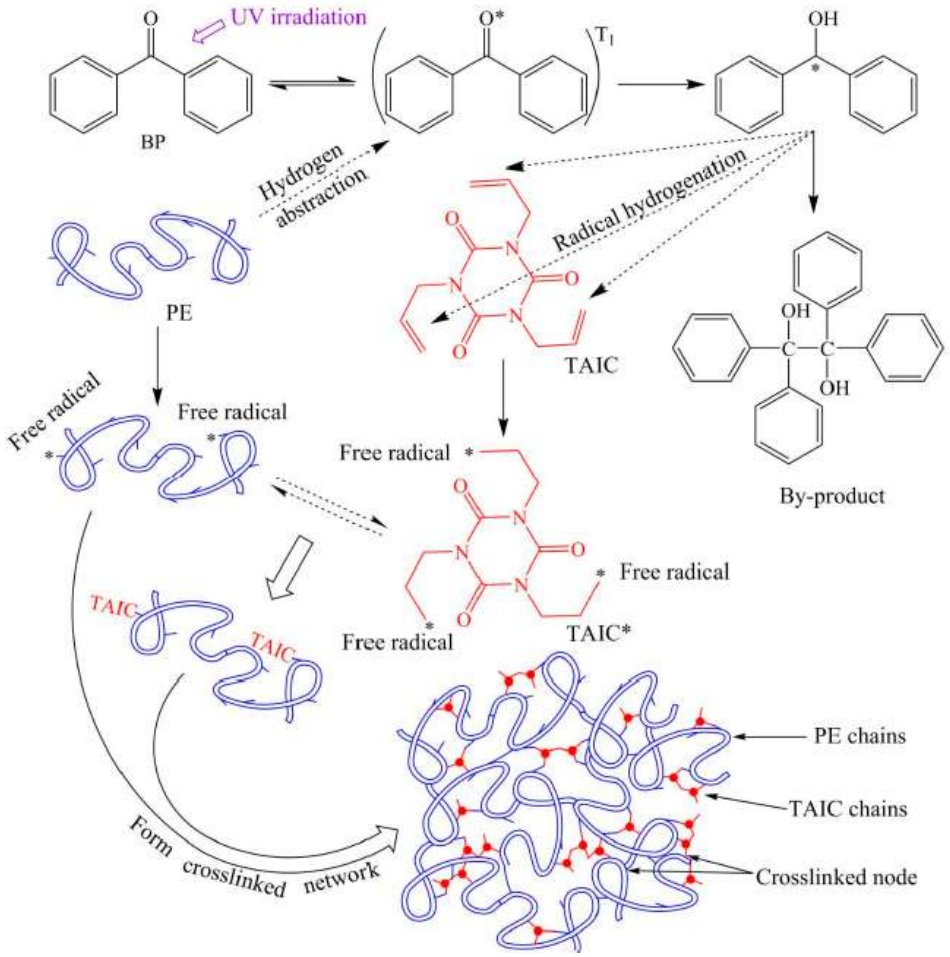

Figure 2.6: Schematic crosslinking reaction of polyethylene initiated by UV irradiation. Sourced from reference [15].

Recently, the PEX-e process has attracted significant interest from the pipe industry [17, 18, 33]. Figure 2.7 illustrates a modern commercial production line for PEX-e pipes. In this process, a batch mixture containing the structural polymer (HDPE), along with photo-initiators and other additives, including auxiliary crosslinking agents, stabilizers, and processing aids, is premixed in a rotation mixer. The batch is then fed into a double-screw

extruder, and immediately after extrusion, the molten pipes pass through an irradiation unit equipped with UV lamps to initiate crosslinking.

For pipes intended for heating systems, the production line also includes the extrusion of oxygen barrier layers. Because photo-initiated crosslinking is temperature-independent, immediate cooling after crosslinking is not required, which allows the oxygen barrier extrusion step to be positioned upstream in the production line, reducing the process to a single cooling stage. This flexibility represents a significant improvement over the PEX-a process.

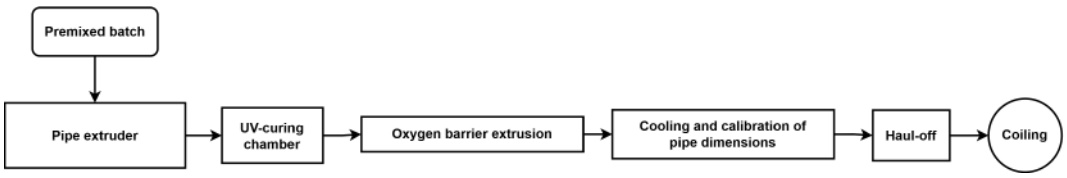

Figure 2.7: Schematic representation of a production line for PEX-e pipes. (This figure is based on the firsthand observations and experiences of the author within the industry).

Both PEX-a and PEX-e processes have as key advantage the ability to perform crosslinking inline with pipe production, which results in higher production efficiency and lower operating costs. In contrast, the PEX-b process requires offline crosslinking due to time-consuming nature of the process, which relies on the diffusion of moisture into the polymer. Similarly, the PEX-c process is limited by the size, complexity, and safety risks associated with electron beam equipment, which prevent its use as an inline crosslinking solution. By comparison, the UV source used in PEX-e is significantly smaller, easier to configure, more cost-effective, and safer to operate [55].

Photo-crosslinking also offers distinct advantages over the peroxide-induced (PEX-a) process. Comparatively, the UV process is considered more environmental friendly due to the absence of volatile chemical emissions and lower energy consumption [15]. Additional benefits include a higher crosslinking rate, which results in a greater production efficiency.

Despite these advantages, no commercial PEX-e products are currently available on the market. Further optimization of formulations and processing conditions is needed to achieve pipes with the desired properties. This highlights the need for continued research in this area. Furthermore, the lack of information on the scientific literature about PEX-e in pipe applications underscores the importance and novelty of the present study.

2.3 Polyethylene degradation and stability

Polyolefins, as aliphatic hydrocarbons, are susceptible to degradation when subjected to high temperatures and/or radiation in the presence of oxygen. This process, commonly referred to as ageing, can lead to either chain scission or uncontrolled crosslinking between chains [5, 56]. Thermal-oxidation is induced by free radicals and can be intensified by elevated temperatures combined with mechanical stress, metal catalyst residues, and/or radiation [56]. Photo-oxidation, on the other hand, relies on the existence of UV-absorbing chromophores such as catalyst residues, pigments, processing aids, flame retardants, or any organic molecules containing double bonds [57]. Thermo- and photo-oxidative degradation reactions can occur throughout the life cycle of PE and PEX pipes, spanning from the manufacturing process to installation and service. The degradation process is often manifested by changes in molecular weight distribution, embrittlement, surface cracking, discoloration and loss of mechanical properties, ultimately leading to failure [11, 56, 58].

The degradation process can be divided into initiation, propagation and branching reactions [56]. Initiation of degradation occurs through the formation of alkyl radicals via either hydrogen abstraction (Equation 2-1) or chain cleavage (Equation 2-2). The C-C cleavage (bond dissociation energy ∼349 kJ/mol) is primarily caused by high temperatures or high shear processing, such as extrusion. On the other hand, C-H cleavage (bond dissociation energy ∼410 kJ/mol) typically results from chemical or radiation attack, occurring more readily at elevated temperatures [5].

$$\mathrm{R{-}H} \longrightarrow \mathrm{R^{\bullet}} + \mathrm{H^{\bullet}} \tag{2-1}$$

$$\mathrm{R{-}R} \longrightarrow \mathrm{R^{\bullet}} + \mathrm{R^{\bullet}} \tag{2-2}$$

The polymer radicals formed may either recombine, i.e., crosslink, or react with other molecules, further propagating the degradation process [5]. During propagation, the alkyl free radicals react with oxygen, forming highly unstable peroxy radicals (Equation 2-3) [5, 11]. These peroxy radicals, in turn, can extract hydrogen atoms from the PE backbone, leading to the formation of hydroperoxides (Equation 2-4), which are the key intermediate species in PE oxidation.

$$\mathrm{R^{\bullet}} + \mathrm{O_2} \longrightarrow \mathrm{ROO^{\bullet}} \tag{2-3}$$

$$\mathrm{ROO^{\bullet}} + \mathrm{RH} \longrightarrow \mathrm{ROOH} + \mathrm{R^{\bullet}} \tag{2-4}$$

Hydroperoxides are inherently unstable and prone to degradation, yielding alkoxy and hydroxyl radicals (Equation 2-5) These radical are both capable of abstracting hydrogen atoms from adjacent polymer chains, which can lead to branching, formation of water, alcohol and more alkyl radicals capable of further reactions [5, 56].

$$\mathrm{ROOH} \longrightarrow \mathrm{RO}^{\bullet} + \mathrm{OH}^{\bullet} \tag{2-5}$$

Stabilizing additives are incorporated in all commercial grades of PE to provide protection against degradation during manufacturing process and service life [58]. These additives can be classified according to their mechanism of action as (1) antioxidants and (2) UV light stabilizers [5, 6]. Commercially, different combinations of these stabilizing additives are employed to optimize protection based on specific applications requirements.

Antioxidant (AO) compounds play a crucial role in impeding the propagation of free-radical oxidation reactions and can be categorized into primary and secondary AOs. Primary AOs act either as hydrogen donors, reacting preferentially with backbone peroxyl radicals, or as free-radical scavengers that mitigate material degradation by forming stable radical species [59].

Sterically hindered phenols, such as Irganox 1010, Irganox 1076, and Irganox 1330 are among the most commonly used primary AOs. Their structure is shown in Figure 2.8 [5]. The term "sterically hindered" pertains to their structure, where each molecule's reactive hydroxyl (OH) group is attached to its phenolic ring at a point shielded by hydrocarbon units connected to each neighboring carbon atom in the ring. This structure enables the molecule to donate a hydrogen atom from its OH group, deactivating free radicals, while transforming itself into a stable, inactive phenoxy radical [56]. When appropriately incorporated into the polymer matrix, phenolic AOs can provide both melt processing stability and long-term oxidative stability [56].

Secondary AOs prevent propagation by decomposing hydroperoxides into more stable alcohol forms. Phosphite-based and thioester-based compounds are commonly employed for this purpose [5, 56]. Typically, a synergistic effect can be obtained by combination of primary and secondary AOs, not only improving the polymer's resistance to degradation, but also reducing costs by decreasing the required amount of expensive primary AOs [6, 56]. Moreover, phosphites and hindered phenol AOs can be combined as dry blends to simplify handling and feeding [56].

UV light stabilizers act as UV absorbers or as radical scavengers (hindered amine light stabilizers - HALS), preventing and/or interrupting photo-oxidation [57]. UV absorbers protect the polymer against photo-oxidation by

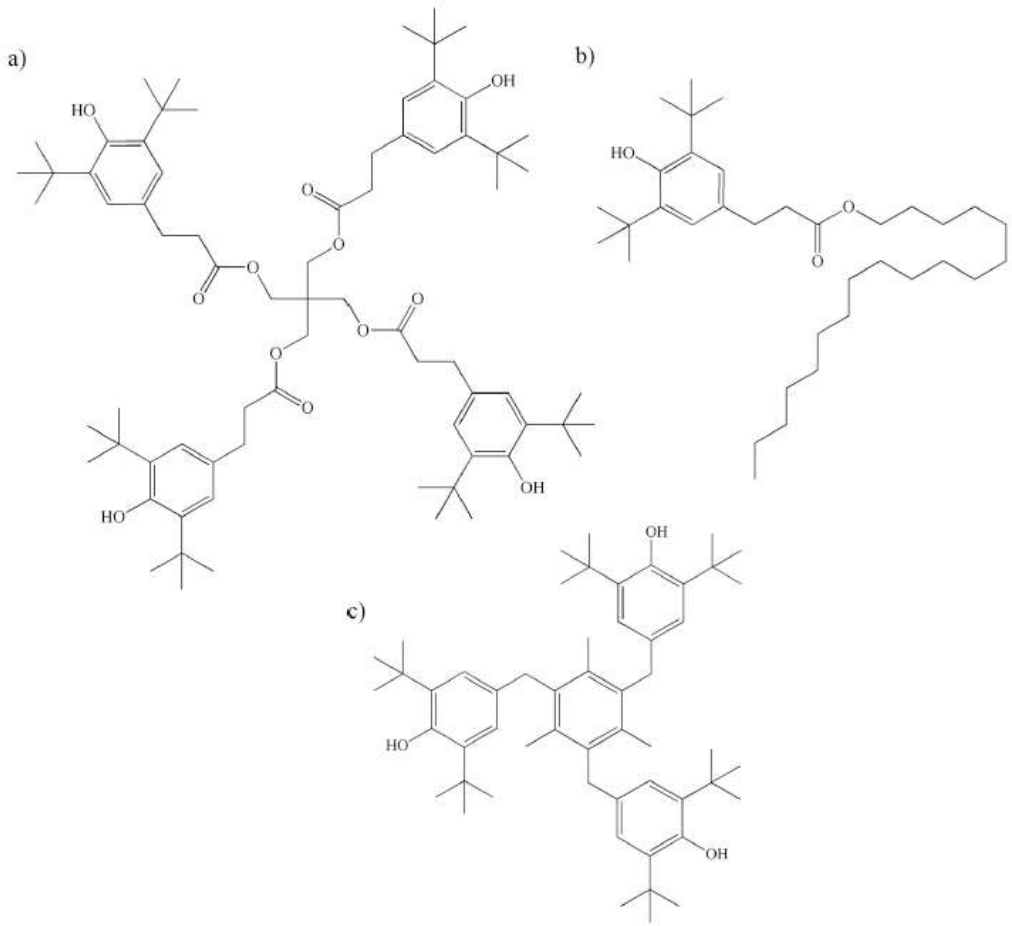

Figure 2.8: Structure of a) Irganox 1010, b) Irganox 1076 and c) Irganox 1330. [5].

preferentially absorbing harmful UV radiation and dissipating it as thermal energy. HALS, such as Tinuvin 770 and Tinuvin 622, act as radical scavengers, offering long-term UV protection by neutralizing free radicals formed during UV degradation [5].

The stabilization of PEX involves mechanisms similar to those established for non-crosslinked PE [58]. However, the combination of different stabilizing additives can significantly affect the morphology of the crosslinked regions. For example, Hirabayashi et al. [12] evaluated PEX-a pipes manufactured using various combinations of phenol antioxidants, HALS, and metal deactivators. The specimens underwent hydrostatic and hydrodynamic tests, and the structure of the crosslinked regions was analyzed using nuclear magnetic resonance (NMR). Their results demonstrated that variations in antioxidant combinations resulted in distinct crosslinking degree and crosslink dispersion. This difference in crosslinking morphology significantly affected the failure times of the pipes.

Similarly, Qing and Rånby [48] observed slight differences in the crosslink-

ing degree (gel content) of PEX-e filaments after incorporating small amounts of the HALS additive Tinuvin 770. Their study further revealed that combining the antioxidant Irganox B215 with HALS Tinuvin 770 effectively mitigated thermo-oxidation during photo-crosslinking. However, this combination also led to a slight decrease in gel content as a trade-off [48].

During pipe manufacturing and service life, stabilizing additives are chemically consumed and can also undergo degradation reactions that reduce their efficacy. Many additives have ester linkages that are vulnerable to hydrolysis and photo-degradation. As a result of these reactions, the molecular volume is reduced, potentially leading to the leaching of additives into the water that flows through the pipe [11]. While active AO is available in the pipe, extensive polymer degradation is not expected. However, localized degradation, specially on the surface and outer layers of the pipe, has been reported prior to complete AO depletion [8, 60].

2.3.1 Antioxidant performance and formation degradation products

Infrared (IR) spectroscopy is widely used technique for analysis of stabilizer consumption and formation of degradation products in PE/PEX pipes [5, 6, 59, 61]. Maria [5] employed IR microscopy to evaluate the performance of various stabilizing additive formulations in PE pipes subjected to photo-oxidative ageing tests. This approach proved effective in monitoring both the depletion of stabilizers and the associated morphological changes resulting from photo-oxidative degradation.

To quantify the stabilizer Irganox 1010, a calibration curve based on IR absorbance was developed. The analysis revealed a linear correlation between the loss of the AO and the UV radiation dose. Pipes exposed to UV radiation exhibited pronounced AO depletion on the exposed surface, an effect that was further intensified by elevated temperatures. IR spectroscopy was also effective in revealing the formation of oxidation products, marked by the disappearance of vinyl unsaturations originally present in PE and the formation of trans-vinylene groups. Interestingly, no significant changes in crystallinity were detected as a result of UV radiation exposure.

Al-Malaika et al. [14] investigated the long-term stability of PEX-a pipes stabilized with reactive (graftable) antioxidants (r-AOs). These pipes were compared to commercial PEX-a pipes stabilized with the conventional hindered phenol antioxidant, Irganox 1076. Both types of pipes were subjected to a hydrostatic pressure test, with water inside and air outside, at a temperature of 115 °C and a pressure of 2.5 MPa. The results showed that the pipe

containing the conventional antioxidant combination failed after just over one year, whereas the pipe containing the graftable AOs exhibited significantly greater longevity before failure. FTIR analysis of the fractured pipe surfaces revealed formation of degradation products containing carbonyl groups and double bonds (Figure 2.9). This analysis confirmed that the failure of these pipes was primarily due to chemical degradation processes.

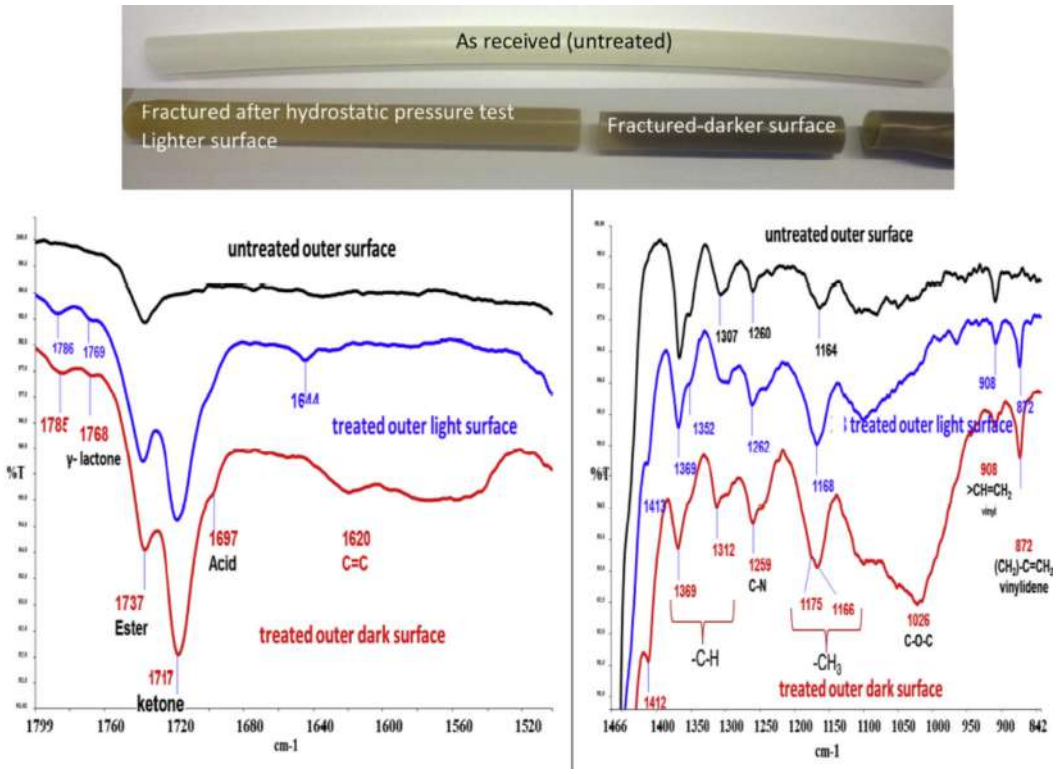

Figure 2.9: Formation of oxidation products on the surface of commercial PEX-a pipe [14].

Hiles et al. [11] developed a methodology to characterize and compare different PEX-a pipe formulations using transmission IR spectroscopy, coupled with principal component analysis and machine learning. Twenty-two absorbance bands characteristic of molecular vibrations in PE and additives, were used to classify and compare three pipe formulations that differed either in the additive package used or in the peroxide employed for crosslinking. These reference bands are shown in Figure 2.10 and detailed in Table 2.1. The analysis revealed that the primary source of variance in the FTIR data was attributed to the choice of the peroxide agent [11].

In a subsequent study, Grossutti et al. [59] utilized principal component analysis (PCA) of IR microscopy data to identify and track changes to stabilizing additives in segments of PEX-a pipes subjected to ageing tests at elevated temperatures. IR image spectra were obtained from axial slices of virgin pipes and pipes subjected to two distinct ageing protocols: immersion in

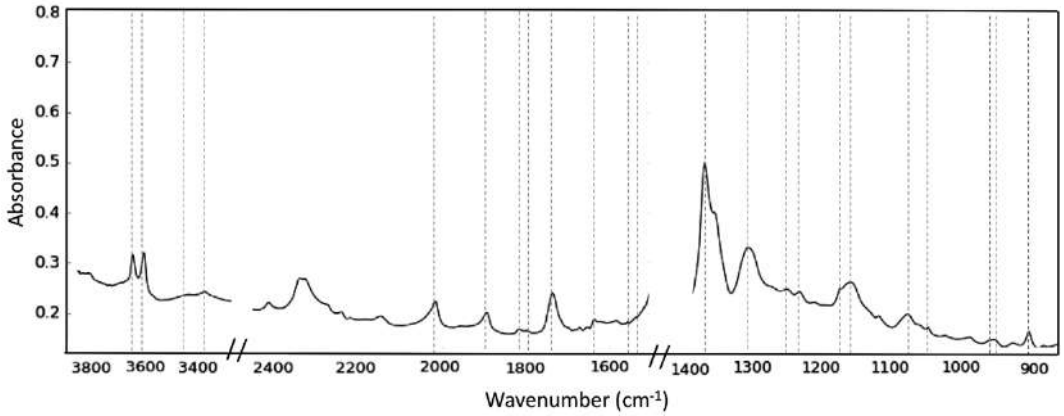

Figure 2.10: Representative baseline-corrected infrared absorption spectrum of a PEX-a pipe showing absorbance bands of interest [11].

Table 2.1: Vibrational bands detected in PEX-a pipe IR spectrum [11].

Wavelength	Band assignment
908 cm^{-1}	PE vinyl unsaturation CH=CH_2 H out of plane bending
956 cm^{-1}	PE trans unsaturation CH=CH H out of plane bending
964 cm^{-1}	PE trans unsaturation CH=CH H out of plane bending
1051 cm^{-1}	Crystalline PE
1079 cm^{-1}	Amorphous PE C−C stretching
1160 cm^{-1}	Ester C−O−C from additive
1176 cm^{-1}	Crystalline PE
1234 cm^{-1}	Phenolic C−OH from additive
1249 cm^{-1}	Unassigned
1305 cm^{-1}	Amorphous PE CH_2 wagging
1367 cm^{-1}	Amorphous PE CH_2 wagging
1531 cm^{-1}	Triazine ring from additive
1569 cm^{-1}	Triazine ring from additive
1639 cm^{-1}	PE chain unsaturation C=C stretching
1739 cm^{-1}	Carbonyl stretching from additive
1799 cm^{-1}	Unassigned
1818 cm^{-1}	Unassigned
1895 cm^{-1}	Crystalline PE
3371 cm^{-1}	Unassigned
3436 cm^{-1}	Unassigned
3606 cm^{-1}	Phenol O−H stretching from additive
3648 cm^{-1}	Phenol O−H stretching from additive

hot air (85 °C) or hot water (85 °C) for 21 days. Figure 2.11 shows the ageing time averaged spectra for all the samples.

Comparison between the spectra of the laboratory-aged specimens and samples from service pipes used for hot water transportation revealed that hot water, opposed to hot air, chlorine, or pressure, was the primary component driving AO depletion in the service pipe [59].

In a more recent work, Grossutti et al. [13] employed hyperspectral IR imageing combined with machine learning to identify physico-chemical factors of ageing and degradation in PEX-a pipes. IR measurements were performed on virgin, aged, and service (cracked and not cracked) PEX-a pipe cross-sections. The aged pipe samples were immersed in distilled water at 80 psi and temperatures between 70 °C and 90 °C. Spectral differences observed between virgin, service, and cracked pipes are shown in the IR spectra generated by the

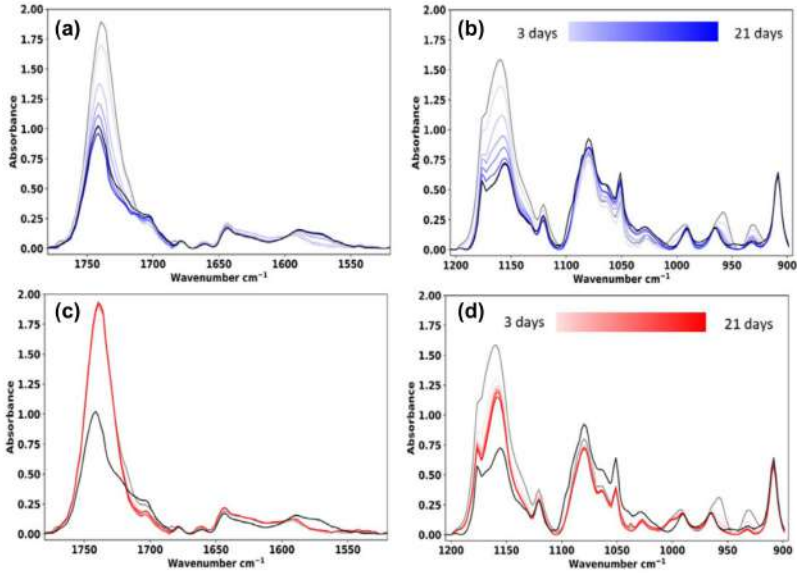

Figure 2.11: Average spectra for the hot water aged samples (carbonyl (a) and fingerprint (b) regions), and hot air aged samples (carbonyl (c) and fingerprint (d) regions). The virgin (gray) and in-service (black) pipe spectra are also shown in (a)–(d) [59].

deep generative model (Figure 2.12). Three distinct physico-chemical factors were analyzed, namely:

- L1: stabilizing additive ester hydrolysis;
- L2: amorphous PE oxidation and chain scission
- L3: degradation characterized by the increased carbonyl and conjugated alkene content.

In Figure 2.12.a, its possible to see the changes attributed to hot water-driven hydrolysis of stabilizing additive ester linkages. The absorbance peaks 1740 cm^{-1} and 1170 cm^{-1}, that correspond to ester C=O and C−O groups, presented large decreases, while peaks at 1700 cm^{-1} and 1570 cm^{-1}, corresponding to carboxylic acid C=O and carboxylate COO^{-} groups, increased in intensity. These changes were present, at different intensities, throughout the bulk of all in-service samples, regardless of the presence of cracks [13].

Figure 2.12.b shows the changes in the IR spectra attributed to oxidative degradation and chain scission of amorphous PE components of the PEX-a pipe matrix. It was noted that the absorbance peaks at 1720 cm^{-1} and 908 cm^{-1} increased in the service pipe, relative to the virgin pipe. These peaks correspond to major products of PE degradation: ketone carbonyl and terminal vinyl groups, respectively. Additionally, major decrease occurred in the 1400-1275 cm^{-1} region that is associated with the PE backbone C−C stretching modes. It is important to note that, even though oxidative degradation and

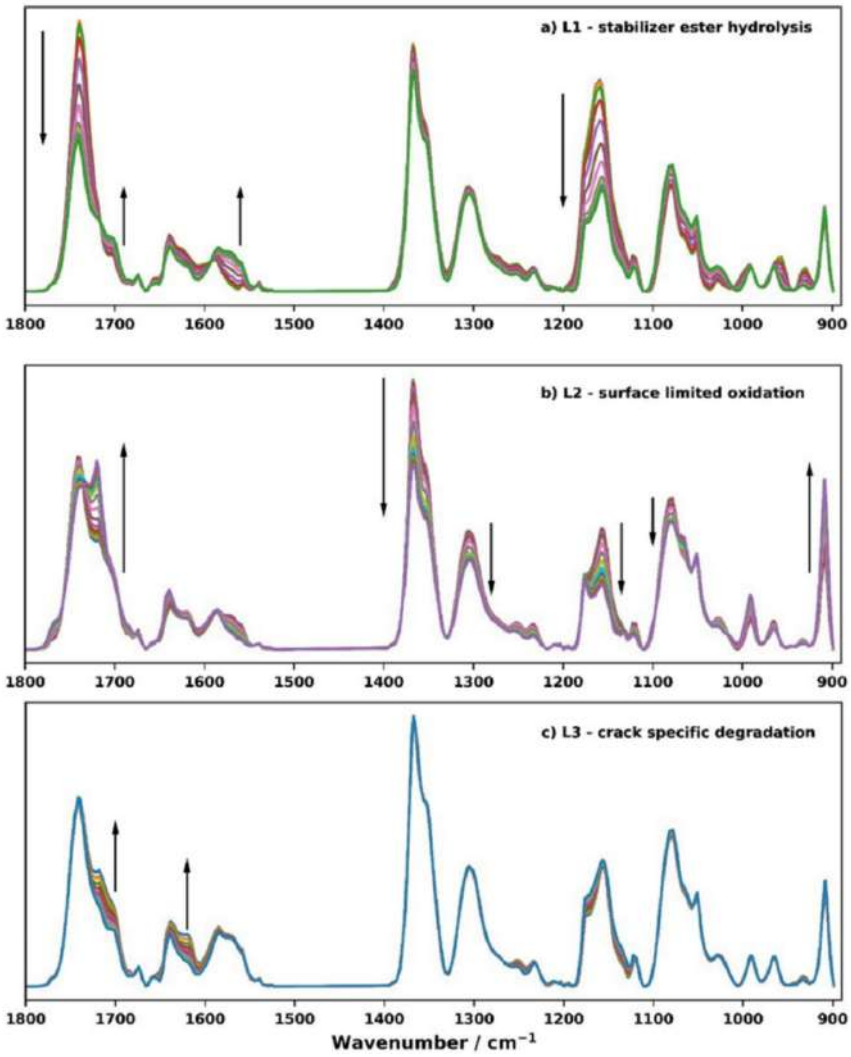

Figure 2.12: Decoder generated IR spectra of PEX-a pipe for latent dimension traversals of the (a) most informative latent dimension L1, the (b) second most informative latent dimension L2, and the (c) third most informative latent dimension L3. The arrows indicate the direction of change for the major peaks as the given latent dimension is traversed from negative to positive values. The absorbance bands in the 1400-1200 cm^{-1} frequency window are shown at 30% of their original intensity to clearly visualize changes across the entire spectrum. The saturated CH_2 bending modes, in the 1520-1400 cm^{-1} region, are omitted from the spectrum [13].

chain scission are considered important factors that lead to cracking, the above mentioned spectral changes were also observed in samples without cracks [13].

In Figure 2.12.c, the elevated ketone carbonyl and conjugated alkene content, detected by the increased in the absorbance peaks at 1720 cm^{-1} and 1620 cm^{-1}, respectively, were only observed at the immediate vicinity of cracks. Notably, elevated levels of amorphous PE oxidation and chain scission were also observed near the cracks. These findings suggested that these physico-chemical changes, described by L2 and L3, are related to crack progression in PEX-a

pipes [13].

Xu et al. [62] used FTIR spectroscopy to investigate the stabilization of PEX-b films with varying concentrations of Irganox 1076. A phase separation was observed at concentrations exceeding 0.9 wt% ($\sim$ 1.6 $\times$ 10^{-2} mol/L), attributed to the limited solubility of Irganox in PE. As emphasized by the authors, the solubility of hindered phenols in polyolefins is generally low due to their significant differences in polarity. During high-temperature processing operations, AOs are highly soluble in polymers. However, during cooling, as the polymer crystallizes and the solubility of the AO in the amorphous phase decreases, the polymer can rapidly become supersaturated with AO. This supersaturation leads to phase separation, causing exudation and blooming of AO on the sample surface.

Notably, differences were observed in the infrared absorption bands of the AO depending on its physical state. The ester carbonyl ($C = O$) group of Irganox 1076 dissolved in PE appeared at 1741–1740 cm^{-1}, whereas AO crystals at the surface exhibited peaks around 1736–1733 cm^{-1}. The blooming of Irganox 1076 onto the polymer film surface was further confirmed by optical microscopy, as shown in Figure 2.13.

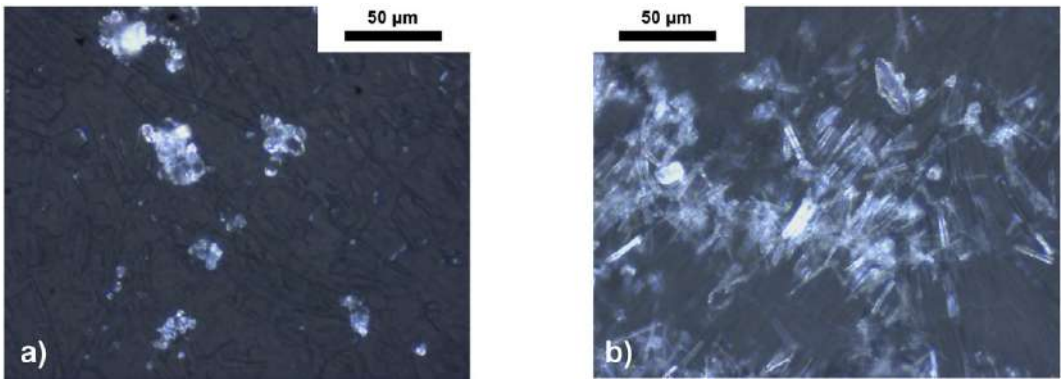

Figure 2.13: Micrographs of the surface of a Si-XLPE film stabilized with Irganox 1076: a) before, and b) after one week of thermal treatment at 70 °C under vacuum (with G = 500x) [62].

In a subsequent study, Xu et al. [63] investigated whether AO crystals contribute to polymer stabilization. This was accomplished by conducting ageing tests in air at different temperature and monitoring the consumption of AO and the formation of oxidation products (from both AO and the polymer matrix) using FTIR spectroscopy. To distinguish the ageing products of phenolic antioxidants from those of PE, the authors conducted thermal ageing of pure Irganox 1076 in air at 130 °C (Figure 2.14). The observed spectral changes indicated alterations in the chemical structure of the AO due to thermal degradation.

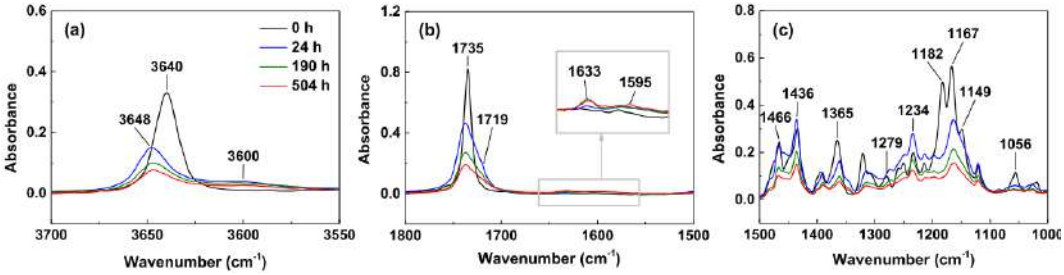

Figure 2.14: Changes in the FTIR spectrum in transmission mode of the pure Irganox 1076 powder during its thermal ageing at 130 °C in air: (a) between 3700 and 3550 cm^{-1}, (b) between 180 0-150 0 $cm^{-1}1$, and (c) between 1500-1000 cm^{-1} [63].

Figure 2.15 illustrates the potential reaction pathways for the thermal degradation of pure phenolic AO or polyolefins stabilized with phenolic AO. During oxidative ageing, the first radical species formed are phenoxyl radicals, which are generated through the reaction of the phenol group with various dehydrogenating agents, such as peroxyl radicals ($ROO^{\bullet}$) or molecular oxygen. These phenoxyl radicals can then undergo a series of transformations, producing a variety of degradation products, with quinone methides being the primary product [63]. In the FTIR spectra, these species are observed at approximately 1630–1640 cm^{-1} (C=O stretching) and 1590–1610 cm^{-1} (C=C stretching).

Cinnamate species can also be detected, as they are generated by the intramolecular rearrangement of quinone methides, as depicted in Figure 2.15. Due to the conjugation effect in unsaturated esters like cinnamates, these species typically appear at slightly lower wavenumbers than those of saturated esters, specifically in the range of 1710–1730 cm^{-1}. The IR band observed around 1719 cm^{-1} in Figure 2.14 was attributed to cinnamate species [63].

PEX-b films stabilized with a standard antioxidant concentration (0.6 wt%) and an excess concentration (2.1 wt%) were aged in air at different temperatures, exhibiting similar behavior in terms of antioxidant depletion. A key finding was that, although some chemical degradation of the antioxidant was observed, the initial depletion was primarily caused by its physical loss through evaporation. The comparison of oxidation induction periods at 130 °C revealed that an excess of antioxidant contributed to enhanced polymer stabilization during thermal ageing. This effect was attributed to the increased solubilization of antioxidants during prolonged thermal exposure [63].

Bredács et al. [8] employed FTIR microscopy combined with PCA to distinguish the ageing products of phenolic antioxidants from those of PE. The analysis revealed a small-scale migration of antioxidants from the bulk

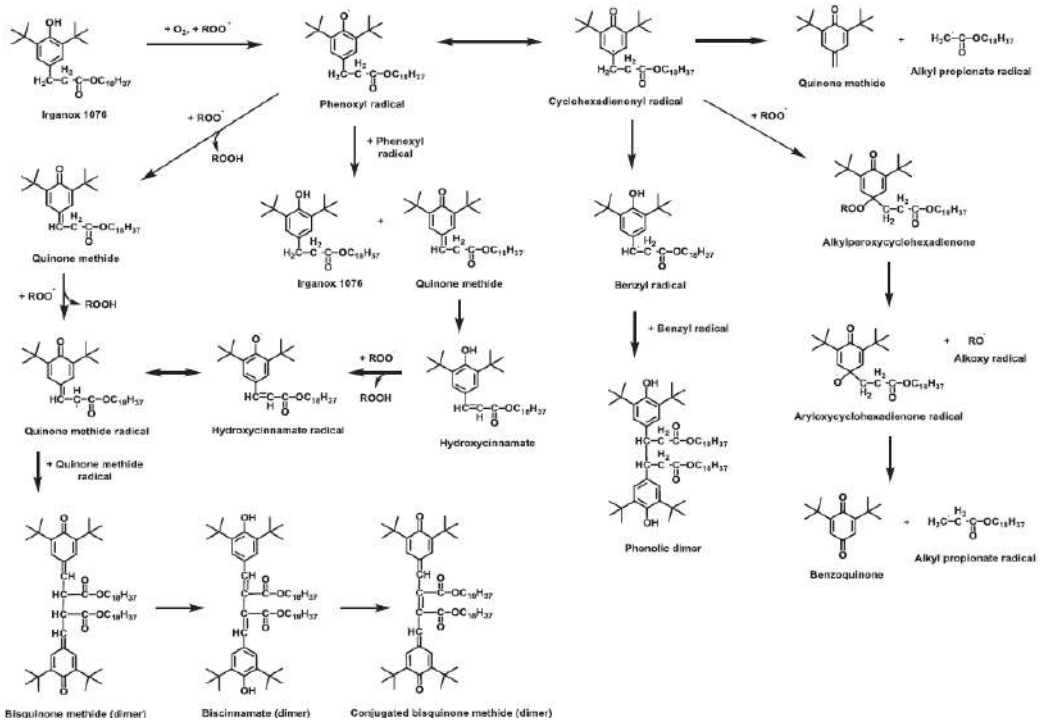

Figure 2.15: Schematics of the reaction pathways proposed for the thermal degradation of pure phenolic AO or polyolefins stabilized with phenolic AO [63].

into the outer layers over the course of ageing. Furthermore, the detection of quinone groups in the spectra of unaged samples indicated the presence of a minor amount of AO oxidation products prior to the ageing tests.

The primary findings from the PCA analysis after the ageing tests included a decrease in the band at 3650 cm^{-1}, attributed to the chemical consumption of antioxidants, and an increase in the bands around 1650 and 1590 cm^{-1}, associated with the formation of AO ageing products.

2.4 Morphological parameters: effect on thermo-mechanical properties

The practical properties of materials are intrinsically linked to their morphology. In the case of semicrystalline polymers such as PE, the mechanical and viscoelastic properties are largely governed by the relative proportions of the rigid crystalline phase, the mobile amorphous phase, and the interphase region that connects them. For PEX, the morphological changes introduced by the crosslinking process also significantly affect the thermo-mechanical behavior. The following subsections review the literature on how different morphological parameters influence the macroscopic properties of PE and PEX materials.

2.4.1 Phase distribution, molecular mobility and molecular weight

As previously mentioned, PE is a semicrystalline polymer composed of phases with very different chain mobilities, which significantly influence its behavior at both the micro- and macroscopic levels. In the crystalline phase, polymer chains are highly ordered, typically forming chain-folded lamellae with very limited mobility. In contrast, the amorphous phase consists of highly mobile and disorganized polymer chains. Between these two phases lies an interphase, composed of polymer chains with restricted motion compared to the amorphous phase. This restriction is due to their proximity to the crystalline regions, as well as the presence of chain entanglements and crosslinks [64, 65].

The dense packing of chains in the crystalline phase limits the diffusion of oxygen and stabilizing agents, which predominantly occurs within the amorphous region [11, 66]. Consequently, the phase proportion plays an important role in the oxidative degradation process, influencing the bulk material's stability.

Ageing can alter the crystallinity degree and molecular mobility, which, in turn, impacts macroscopic performance over time. Thus, a quantitative assessment of phase proportion and molecular mobility is essential for optimizing material development and evaluating degradation mechanisms.

Solid-state proton NMR is a highly effective tool for quantifying phase proportion and chain mobility in polymers [9, 67–69]. Shi et al. [70] utilized this technique, combined with tensile testing, to investigate the effects of thermo-oxidative ageing on the chain mobility, phase proportion, and mechanical behavior of HDPE films. The ageing experiments were conducted in air at 100 °C. The NMR signal was deconvoluted into three components corresponding to the crystalline phase, interphase, and amorphous phase. The signal was fitted by Equation 2-6, which is a linear combination of the Abragam function and two exponential functions [70].

$$I = I(0)^c \, exp\left[-\left(\frac{t}{T_2^c}\right)^2\right] \frac{sin(Rt)}{Rt} + I(0)^i \, exp\left(\frac{-t}{T_2^i}\right) + I(0)^a \, exp\left(\frac{-t}{T_2^a}\right) \quad (2\text{-}6)$$

In Equation 2-6, I is the normalized magnetization intensity, R is a fitting parameter, t is the decay time and T_2^c, T_2^i, T_2^a are the effective transverse relation times of the crystalline, interphase and amorphous phases, respectively. T_2 is related to chain mobility. Figure 2.16 shows the evolution of the phase proportion and T_2 over ageing time for the HDPE samples.

Analysis of the phase content and T_2 relaxation times revealed a two-stage

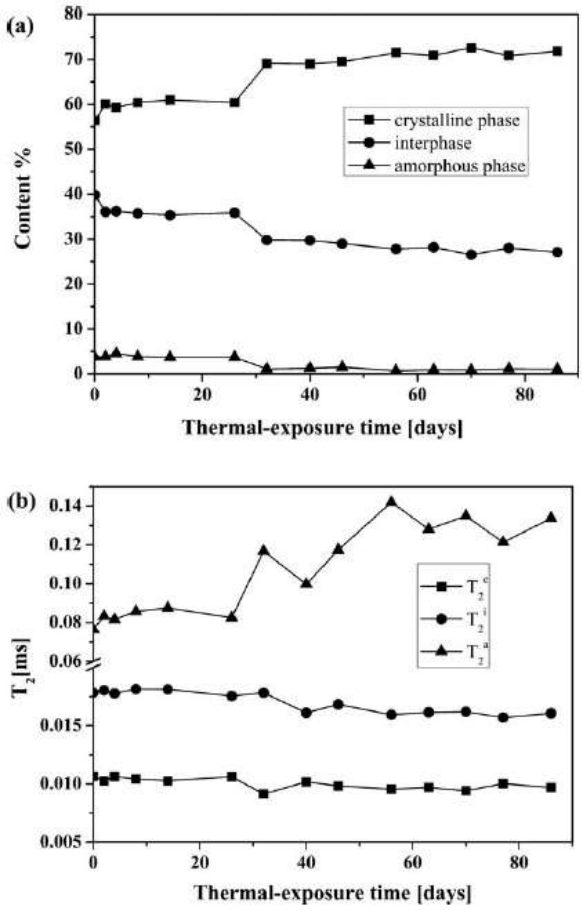

Figure 2.16: (a) Evolution of the relative phase content of HDPE films over ageing time. (b) The effect of ageing on molecular mobility determined by the T_2-relaxation time for the different phases of HDPE. Larger the amplitudes of molecular motions are, longer the T_2 value [70].

evolution during thermal exposure. In the first stage (up to approximately 26 days), a slight increase in the crystalline phase was observed at the expense of the interphase and amorphous phases. This behavior was attributed to annealing and recrystallization, commonly referred to as physical ageing. In the second stage of ageing (beyond 26 days), the crystalline phase increased abruptly, while the interphase and amorphous phases decreased simultaneously [70]. This was attributed to chain scission of tie molecules traversing the amorphous regions, followed by re-arrangement of released segments into the crystalline phase [70, 71].

Significant chain scission was confirmed through gel permeation chromatography (GPC) and FTIR spectroscopy. GPC analysis further indicated that degradation-induced crosslinking was not significant in the aged samples, with chain scission identified as the primary degradation mechanism affecting the morphology of the aged films. Figure 2.17 provides a schematic representation of the phase structure changes observed during ageing [70].

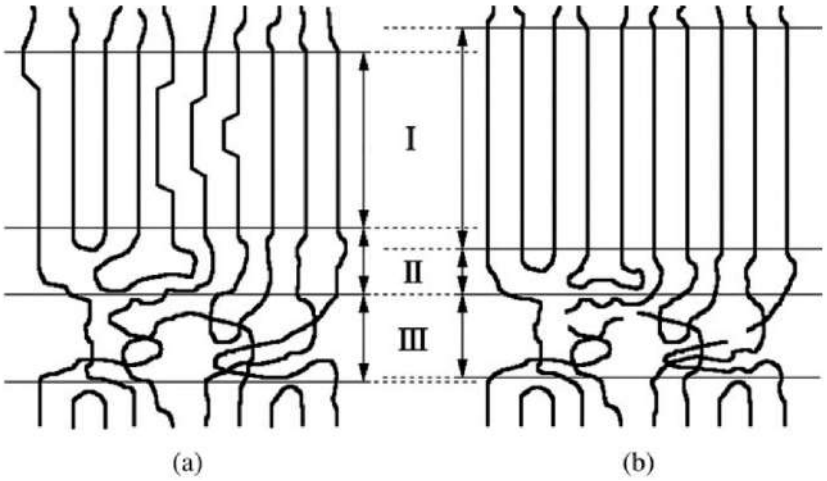

Figure 2.17: Suggested changes of phase structure (a) before and (b) after ageing. I, II and III represent the crystalline, interphase and amorphous regions, respectively [70].

The evolution of tensile strength during thermal exposure is shown in Figure 2.18 [70]. Initially, a slight increase in tensile strength was observed, which was attributed to the restraints imposed by the increased crystallinity degree. After 30 days of ageing, a pronounced drop in tensile strength and elongation at break occurred due to the embrittlement of the material. Correlations were identified between the loss of ductility and the decrease in molecular weight caused by chain scission [70].

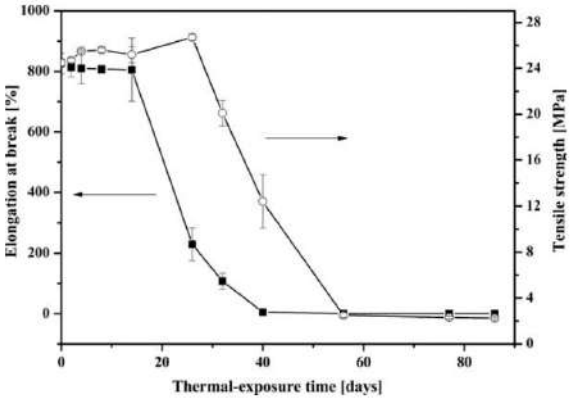

Figure 2.18: Effect of thermo-oxidative ageing on mechanical properties for HDPE samples: elongation at break and tensile strength [70].

Overall, it was concluded that the loss of mechanical performance in HDPE following degradation was primarily driven by changes in microstructure. These changes include a reduction in molecular weight, a decrease in the density of chain entanglements, a reduction in chain mobility, and an increase in crystallinity [70].

Li et al. [71] employed differential scanning calorimetry (DSC) and X-ray diffraction (XRD) to monitor changes in the crystal structure of PEX during thermal ageing. Antioxidant depletion was assessed using oxidation induction time (OIT) measurements. Samples were retrieved from the PEX insulation of a high-voltage cable. Ageing tests were conducted in air at 100, 120, 140, and 160 °C. Figures 2.19 and 2.20 illustrate the evolution of crystallinity and OIT values over ageing time, respectively. The analysis identified two distinct stages of degradation. The first stage, referred to as the physical ageing stage, was characterized by re-crystallization processes that lead to increased crystallinity. The second stage, the chemical ageing stage, involved significant thermo-oxidative degradation, resulting in drastic chain scission and deterioration of the crystal structure. It was observed that the critical ageing time, at which the crystal structure of the PEX samples began to deteriorate rapidly, corresponded to the complete depletion of antioxidants, i.e., when OIT reached zero.

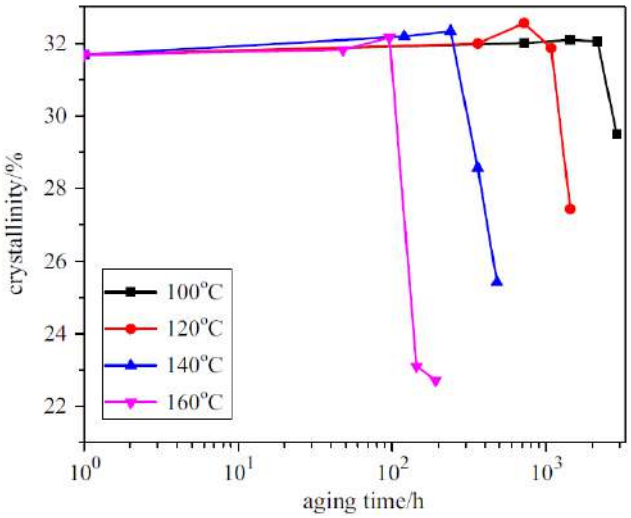

Figure 2.19: Evolution of crystallinity of PEX insulation over ageing time [71].

2.4.2 Crosslink morphology

The mechanical and viscoelastic properties of polymers are critically dependent on the structures and dynamics at the chain segments scale at different temperatures. At temperatures below the T_g (glass transition temperature) the material's behavior is dominated by the stiffness of the crystalline phase. At temperatures in the range between T_g and T_m (melting temperature), the crosslinked network significantly affects the storage modulus by restricting the mobility of polymer chains in the interphase. The crosslink constraints imposed

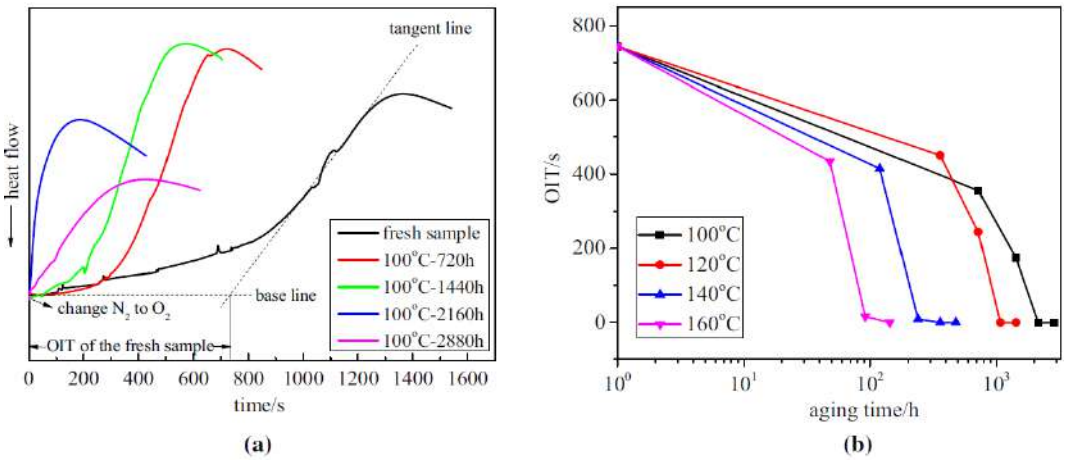

Figure 2.20: OIT measurement of PEX insulation samples at different ageing times. (a) OIT curves for samples aged at 100 °C. (b) OIT values [71].

by network junctions reduce the chain dynamic mobility and the stored elastic entropy [72]. At temperatures above the melting point, the material becomes entirely amorphous and the mechanical response is solely governed by the crosslinked structure. At this point the storage modulus reaches a minimum, referred to as the rubbery plateau, as shown in Figure 2.21 [73].

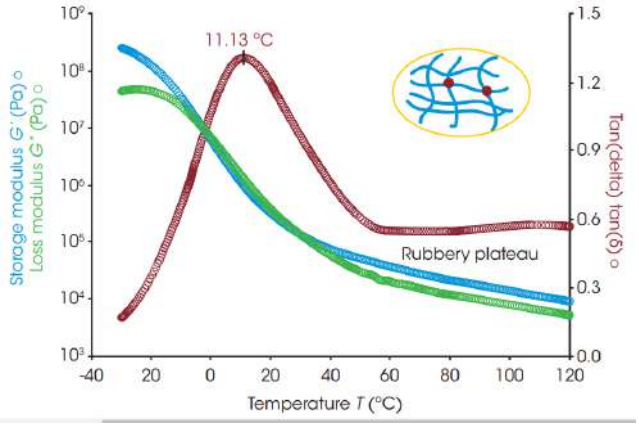

Figure 2.21: Dynamic mechanical analysis curves of a crosslinked adhesive highlighting the rubbery plateau [73].

For polyethylene, this plateau typically occurs around 150 °C [74, 75]. A correlation has been found between the storage modulus at the rubbery plateau and the average molecular weight between crosslinks (M_c), according to Equation 2-7 [74, 75]:

$$M_c = \frac{2(1+\nu)\rho RT}{E'} \tag{2-7}$$

where E' is the storage modulus at the rubbery plateau, ν is the Poisson ratio, ρ is the density of the amorphous polymer, R is the gas constant and T is

the absolute temperature. Similarly the effective crosslinking density can be calculated as per Equation 2-8 [75]:

$$\nu_c = \frac{\rho}{M_c} \tag{2-8}$$

.

Figure 2.22 exemplifies the relationship between crosslink density and the viscoelastic response measured by dynamic mechanical analysis (DMA) [73]. As can be seen the storage modulus at the rubbery plateau increased with increasing crosslink density.

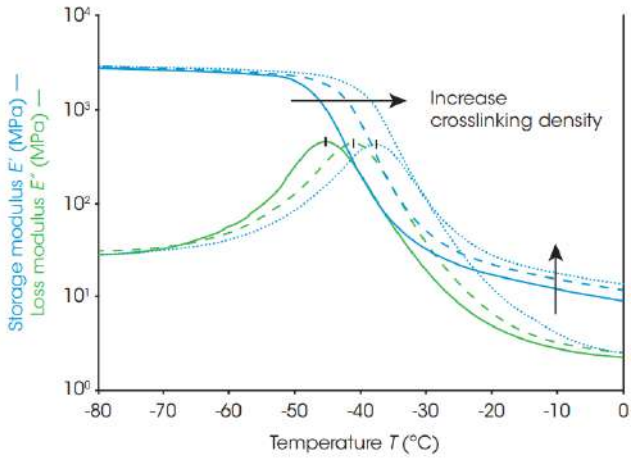

Figure 2.22: Dynamic mechanical analysis curves of a series of rubber elastomers with different crosslinking densities [73].

Shen et al. [72] employed molecular dynamics simulations to investigate the effects of crosslink density and distribution on the viscoelastic properties of chemically crosslinked polymers. Figure 2.23 illustrates the relationship between the viscoelastic properties in the rubbery plateau region and the crosslink density (n) as well as the degree of crosslink dispersion (B_2). A notable finding was that improving the crosslink dispersion state was essentially equivalent to increasing the effective crosslink density. The shear storage modulus, denoted as G', exhibited significant enhancement with increasing crosslink density and degree of crosslink dispersion. In contrast, the shear loss modulus G" demonstrated a comparatively moderate increase.

Important insights into the elastic effectiveness of the crosslinked network were derived from the tan δ values, as these are generally much higher for imperfectly crosslinked networks with low elasticity. The tan δ values were found to decrease linearly with increasing crosslink density and exponentially with increasing crosslink dispersion, reflecting the improved crosslink effectiveness and enhanced elastic response of polymer network [72].

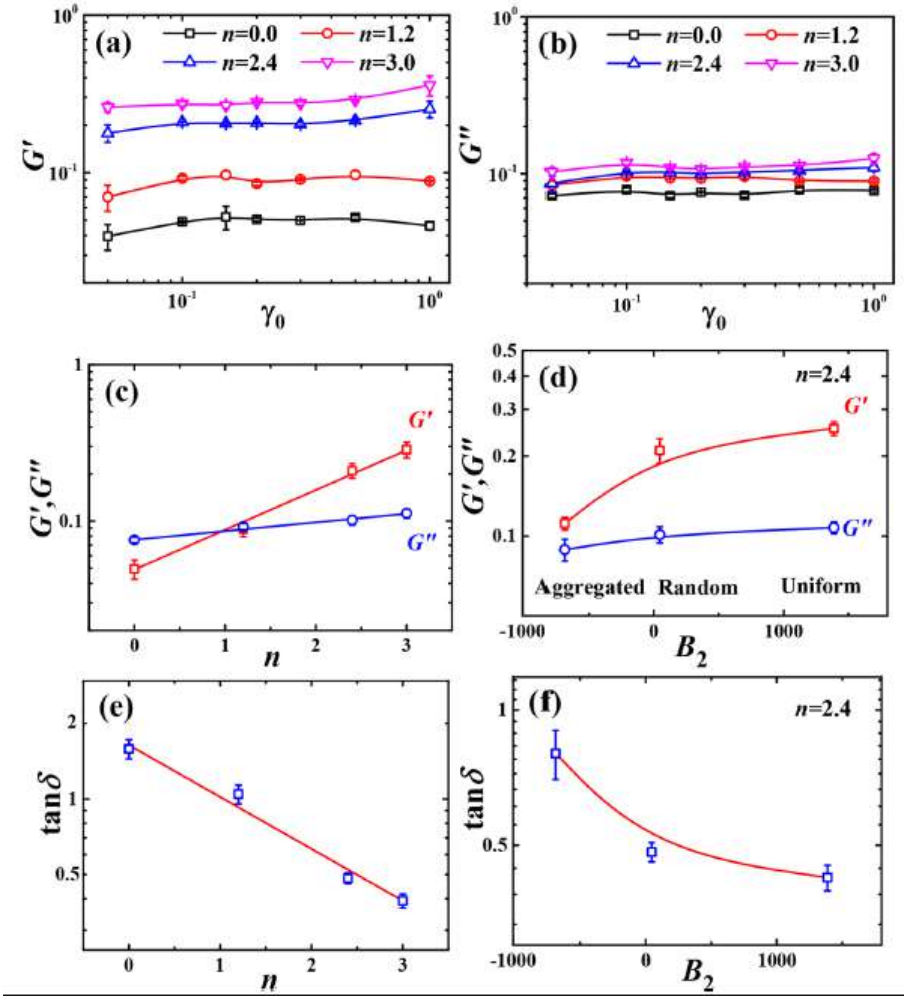

Figure 2.23: (a) Storage modulus G' and (b) loss modulus G" plotted against the shear amplitude. (c-f) Storage modulus G', the loss modulus G" , and the loss tangent tan δ as a function of the crosslink density n and the degree of crosslink dispersion B_2, respectively [72].

The authors emphasized that while their results closely aligned with experimental data, their model did not account for certain factors such as the type of crosslink, properties of the crosslinking agents, and the polydispersity in crosslink functionality. As pointed out, these factors might play an important role on the structure and dynamics of polymer networks [72].

A thorough review of the existing literature revealed no relevant references specifically addressing the relationship between morphology and the macroscopic properties of PEX pipes. Moreover, no publications were found on the effect of ageing on crosslinking morphology and viscoelastic properties of PEX materials, further underscoring the importance of the present study.

3
Characterization of photo-crosslinked polyethylene pipes for geothermal energy storage

Article published January 3, 2025 in ACS Omega. Available at: https://doi.org/10.1021/acsomega.4c09896.

Abstract: This study investigates the morphology and thermo-mechanical properties of crosslinked polyethylene (PEX) pipes for potential use in high-temperature borehole thermal energy storage systems. Particular attention is given to a novel type of PEX pipe produced through photo-initiated crosslinking (PEX-e). Two formulations, PEX-e1 and PEX-e2, were analyzed and compared to peroxide-crosslinked polyethylene (PEX-a) and non-crosslinked bimodal polyethylene (PE100) pipes. The degree of crosslinking was evaluated via gel content, while crosslink density and molecular weight between crosslinks were determined using dynamic mechanical analysis (DMA). Phase composition and molecular mobility were explored through ^{1}H static nuclear magnetic resonance (NMR), and the melting and crystallization behavior was assessed by differential scanning calorimetry (DSC). Oxidative stability and degradation were examined using Fourier transform infrared (FTIR) spectroscopy, oxidation induction time (OIT) measurements, and thermogravimetric analysis (TGA). Both PEX-e formulations achieved satisfactory crosslinking degrees and exhibited remarkable OIT values. However, significant differences in crosslink distribution were noted, with PEX-e2 showing a less uniform dispersion of crosslinks, which resulted in a lower storage modulus. FTIR analysis indicated that oxidation products were formed in PEX-e1 during crosslinking, highlighting the need for further optimization of the formulation and processing conditions.

3.1
Introduction

In response to the ongoing climate and energy crisis, thermal energy storage (TES) systems have emerged as a promising solution for extending the time gap between energy production and energy consumption. Among the various approaches available, borehole thermal energy storage (BTES) is often preferred due to its relatively low initial costs and minimal environmental

impact [1]. In BTES systems, a network of borehole heat exchangers transfers heat to and from the surrounding rock or sediment mass, allowing heat to be stored during the summer for use in winter space heating, or vice versa [1, 2, 76]. High-temperature BTES systems have also been used to store waste heat from shopping malls, data centers and industrial facilities, repurposing it for district heating [2, 21].

Borehole heat exchangers (BHE) consist of heat exchange pipes through which a heat transfer fluid is circulated via pumping [2, 76]. BHE pipes are typically made from high-density polyethylene (HDPE) and crosslinked polyethylene (PEX), with the latter being often preferred for high temperature applications due to its superior thermal resistance [2, 3].

Crosslinking is a well established method to improve the durability and thermal resistance of PE pipes [9–12]. Several methodologies have been developed for crosslinking PE, typically involving free-radical reactions initiated by chemical agents or physical processes. Among these, the photo-crosslinking process has recently gained significant commercial interest for pipe manufacturing [17, 18] and is being explored as a potential material for high-temperature BTES systems.

Currently, PEX-a is the most widely used type of PEX for potable water transport and heating applications [13, 14]. This process involves the use of a peroxide crosslinking agent, such as di-tert-butyl cumyl peroxide (BCUP) or dicumyl peroxide (DCP) [35]. At temperatures above the melting point of polyethylene, the peroxide decomposes and abstracts hydrogen from the polymer chain, creating polyethylene radicals that form covalent bonds (crosslinks) with adjacent radicals. [37, 38]. However, this process has several drawbacks, including a low crosslinking rate, heat sensitivity, and the production of unwanted volatile by-products, which require extended degassing at high temperatures [16]. As a result, PEX-e is being explored as a promising alternative due to its higher crosslinking rate (enabling greater production efficiency), lower overall energy consumption, and lack of volatile chemical emissions [15].

In the PEX-e process, the PE formulation contains a photo-initiator additive, typically a benzophenone derivative, that absorbs UV light, undergoes photo-excitation and can abstract hydrogen atoms from the polymer backbone [15, 44]. This reaction takes place immediately after extrusion, while the polymer remains in its melted state and therefore, is transparent to visible and UV light. The addition of an auxiliary crosslinking agent (CA), such as triallylcyanurate (TAC), has been shown to significantly accelerate the crosslinking process, leading to higher degrees of crosslinking (over 70%) and a more uniform distribution of crosslinks [15, 44, 45]. In this case, three possible crosslink

configurations can be formed: PE-PE, PE-CA-PE, and PE[CA]-PE, where [CA] represents the copolymer segment of the crosslinking agent. The statistical probability of each configuration depends on reaction kinetics [15]. As a result, the crosslinks in PEX-e are not solely composed of carbon-carbon bonds, as they are in PEX-a, which may influence the properties of the pipe.

Photo-crosslinking of polyethylene has been extensively studied by Rånby et al. [44–51]. Several photo-initiators, crosslinking agents, and experimental conditions were explored for the photo-crosslinking of polyethylene films and continuous profiles. One key issue identified was pre-oxidation of the polymer during photo-crosslinking [48], which can negatively affect the polymer's durability. However, it was found that optimized stabilizer formulations could significantly reduce pre-oxidation. Specifically, a formulation containing the antioxidant Irganox B215, along with small amounts of the hindered amine photo-stabilizer (Tinuvin 770), proved effective in preventing oxidation during processing [48].

Fallani et al. [77] investigated the mechanical properties of photo-crosslinked polyethylene films, reporting improvements in thermal stability, elastic modulus, and barrier properties. Numerous studies [15, 52–54, 78, 79] have also explored the reaction mechanisms of the photo-crosslinking process with PE containing different photo-initiators and co-agents. Xue et al. [80] reviewed the application of photo-crosslinking in the production of shape-memory polymers, while other studies have focused on its use in industrial cable insulation [15, 81, 82]. However, there is a notable gap in the scientific literature regarding the use of photo-crosslinking for pipes and tubing.

Accordingly, the present study aims to assess the morphology and physical properties of PEX-e pipes produced using two different formulations. For comparison, PEX-a and non-crosslinked HDPE pipes were also analyzed. The degree of crosslinking was evaluated through gel content, while crosslink density and the molecular weight between crosslinks were determined using dynamic mechanical analysis (DMA). The phase composition and molecular mobility were explored via ^{1}H static nuclear magnetic resonance (NMR), and the melting and crystallization properties were studied using differential scanning calorimetry (DSC). Oxidative stability and degradation were investigated through Fourier transform infrared (FTIR) spectroscopy, oxidation induction time (OIT) measurements, and thermogravimetric analysis (TGA). Finally, the dynamic mechanical response of the materials over a wide temperature range was assessed using DMA.

3.2 Experimental

3.2.1 Materials

The four different pipes investigated in this study were supplied by MuoviTech International Group, Sweden. Their characteristics are listed in Table 3.1. Two PEX-e pipes, namely, PEX-e1 and PEX-e2, with different formulations were investigated. According to the supplier, Formulation I (PEX-e1) contains a higher percentage of antioxidant additives compared to standard commercial formulations for drinking water, with the aim of enhancing thermo-oxidative stability for high-temperature BTES application. Since BTES systems are closed and do not allow leakage into other water sources, there is no concern about additives leaching into drinking water over time. Additionally, Formulation IV contains 2.5% of carbon black additive for UV stabilization. The supplier also indicated that PEX-e1 and PEX-e2 were manufactured under slightly different processing conditions to account for the different thickness in the pipes. However, specific details regarding the processing conditions were not disclosed. Further details about the additive packages were also not provided.

Table 3.1: Pipes investigated in the study.

Designation	Crosslinking agents	Additive package	Outer diameter (mm)	Thickness (mm)
PEX-e1	UV-photoinitiator + co-agent	I	32	3
PEX-e2	UV-photoinitiator + co-agent	II	16	2
PEX-a	Peroxide	III	32	3
PE100	-	IV	40	4

Samples for characterization were cut from the pipes according to Figure 3.1 in "as received" condition. For FTIR spectroscopy, the samples were cut from the pipes using a pipe cutting tool. The cross-sectional rings were cut from the pipes using a microtome and smaller sections were cut with a knife and weighted accordingly. A computer numerical control (CNC) machine was used to cut specimens for DMA.

3.2.2 Characterization methods

3.2.2.1 Gel content

The degree of crosslinking was assessed by determination of the gel content by solvent extraction, according to the ISO 10147:2012 standard.

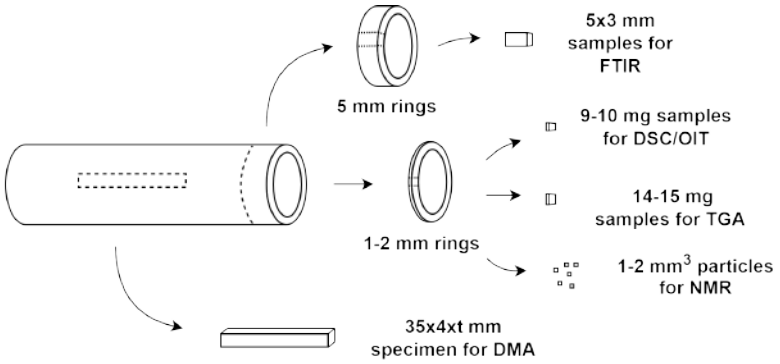

Figure 3.1: Schematics of sample preparation, where t stands for thickness of the pipe.

Samples were cut from the pipes using a microtome. Slices with thickness of (0.4 ± 0.1) mm were taken from the pipe cross-section. Two replicates of each pipe were made. The samples with mass ≥ 0.2 g were put in a cage made of stainless steel mesh with 120 μm pore size and the gel extraction was performed in xylene solvent at 138-140 °C for 8h. After extraction the samples were dried in a vacuum oven, kept at 90 °C at 0.85 bar for at least 3h before being weighted.

The degree of crosslinking (Gel) was calculated as per Equation 3-1:

$$Gel = \frac{m_3 - m_1}{m_2 - m_1} \tag{3-1}$$

where m_1 is the mass of the cage and lid; m_2 is the mass of the original test piece, the cage and the lid, and m_3 is the mass of the residue, cage and lid.

3.2.2.2 Solid-state proton NMR spectroscopy

^{1}H static (non-spinning sample) NMR was used to quantify the phase composition and molecular mobility of the different pipes. The experiments were carried out on a Bruker AVANCE-II spectrometer at 4.7 T magnetic field (^{1}H resonance at 200 MHz) using home-built NMR probe having strong rf pulse (90-degree pulse = 0.9 μs) and short dead time. The NMR data were acquired using the so-called solid echo pulse sequence (90x -τ-90y - τ - acquisition) [83]. This approach is used where the NMR free induction decay (FID) signal is very short, and the beginning of the decay signal can be lost in the *deadtime* of the NMR probe. The solid echo experiments were compared with the usual direct excitation experiment and the signals detected were similar.

The decay of the solid echo experiment was then decomposed into three components usually carried out for semi crystalline polymers [84, 85]. The decay components used were an Abragam function, a Weibullian function and

an exponential function. The fitting procedure was carried out using non-linear least squares regression in the "peak-o-mat" software (version 1.1.9).

The Abragam component is usually associated with rigid or crystalline areas and is represented by the combination of Gaussian and sine functions, as per Equation 3-2 [84–86]:

$$I = exp\left[-\left(\frac{t}{T_2^{short}}\right)^2\right]\frac{sin(Rt)}{Rt} \tag{3-2}$$

where I is the normalized magnetization intensity, R is a fitting parameter, t is the decay time and T_2^{short} is the fast decay rate.

The Weibullian function is associated with the interphase region between the crystalline and amorphous regions, where motion is restricted. This function ranges between a pure Lorentzian ($n = 1$) and a pure Gaussian ($n = 2$), as per Equation 3-3 [84–86]:

$$I = exp\left(\frac{-t}{T_2^{medium}}\right)^n \tag{3-3}$$

where T_2^{medium} is the intermediate decay rate. Finally, the contribution of amorphous phase is represented by a exponential function [85] as per Equation 3-4:

$$I = exp\left(\frac{-t}{T_2^{long}}\right) \tag{3-4}$$

where T_2^{long} in the long decay rate. The Abragam function can be rewritten in terms of two parameters a and b as shown in Equation 3-5 [87]:

$$I = exp\left[-0.5(at)^2\right]\frac{sin(bt)}{bt} \tag{3-5}$$

From the parameters a and b the theoretical second moment can be calculated as per Equation 3-6 [87]:

$$M_2 = a^2 + \frac{1}{3}b^2 \tag{3-6}$$

The second moment is a measure of the dipolar coupling between the H's in the system and is higher the closer the H's are to each other. If the experimental second moment is less than the expected value for a rigid lattice it can also provide information on any motion present within that system since the value is reduced due to motional averaging.

3.2.2.3 Differential Scanning Calorimetry

Melting and crystallization analysis of the materials were performed on TA Q2000 DSC equipment. Samples with 9-10 mg weight were heated in aluminum pans under a nitrogen flow (50 mL/min) for two heating and

one cooling cycles. First, the samples were heated from 30°C to 230°C at 10 °C/min and maintained isothermally for 3 min to erase any previous thermal history. Then, the samples were cooled down to 30°C at 10°/min, maintained at isothermal conditions for 3 min and heated to 230°C at 10 °/min for a second time. The degree of crystallinity (X_c) was calculated according to Equation 3-7 :

$$X_c = \frac{\Delta H_m}{\Delta H_0} \times 100 \tag{3-7}$$

where ΔH_m is the fusion enthalpy of the sample and ΔH_0 is the equilibrium fusion enthalpy of PE crystals (281 ± 6 J/g) [88, 89]. Three replicates measurements were performed for each material and the standard deviation (S) of X_c was calculated taking into account the error propagation, as shown in Equation 3-8 [90].

$$S_{Xc} = \sqrt{\left(\frac{S_{\Delta H_m}}{\Delta H_m}\right)^2 + \left(\frac{S_{\Delta H_0}}{\Delta H_0}\right)^2} \times X_c \tag{3-8}$$

3.2.2.4 FTIR spectroscopy

The infrared spectra were recorded in the 4000–400 cm^{-1} range with a Thermo Fisher Nicolet iS50 Spectrometer in ATR mode, with 32 scans per spectrum (4 cm^{-1}). The spectra were recorded using the "OMNIC software Advanced ATR correction" that normalizes the spectrum for a penetration depth of $\ln(10) \approx 2.3$ μm and gives more consistent results, that are comparable to transmission mode spectra [91]. The measurements were performed on the surface corresponding to the inside wall of the pipes. The spectra of three random samples were measured for each material to ensure the reproducibility of the results.

The data pre-processing was performed separately for each absorbance spectra using Python. The baseline correction was done by asymmetric least squares (ALS) [92] using the *irfpy* library [93]. The IR absorbance band at 2915 cm^{-1}, characteristic of CH_2 asymmetric stretching, was used as an internal reference to account for sample-to-sample intensity variations arising from differences in sample thickness and curvature effects. Further information on the pre-processing and quantification of FTIR data with Python is provided in Section A.2.

The carbonyl index has been used extensively in polymer studies as a comparative method to monitor the hydrolysis of stabilizing additives and oxidation processes. In the literature, there are different trends for calculating the carbonyl index either using normalized peak height or area [91]. In this

work the carbonyl index was calculated according to Hiles [94] as the integrated area of the spectral region from 1775-1675 cm^{-1}, as per Equation 3-9 [94]:

$$CI = \int_{1675}^{1765} A_x \, dx \tag{3-9}$$

where A_x is the normalized absorbance at wavenumber x after baseline correction. The area was calculated using numerical integration with the composite trapezoidal rule, implemented via the "trapz" function in the NumPy Python library.

3.2.2.5 Oxidation Induction Time

Oxidation induction time (OIT) tests were performed on a TA Q2000 DSC equipment to assess the thermo-oxidative stability of the pipe samples. Samples with 9-10 mg were heated up in aluminum pans to 200°C at 20 °C/min and kept isothermal for 5 min. Then, the gas was switched from nitrogen to oxygen. The temperature was maintained at 200 °C until the maximum exothermic peak was reached. The OIT is defined as the time between the gas switching and the onset of the oxidative reaction peak [95]. Five replicates were analyzed for each material.

3.2.2.6 Thermogravimetric analysis

Thermogravimetric analysis was performed on a TA Q500 TGA equipment. Samples with 14-15 mg weight were heated from 30 °C to 650 °C at 20 °C/min in both nitrogen and air purge stream, and the weight change as a function of temperature was recorded. The parameters obtained from the thermogravimetric (TG) and derivative (DTG) curves were T_5, T_{50}, T_{95} and T_{max}. T_5 is the onset temperature of decomposition, determined as the temperature at which the weight loss reaches 5%, while T_{50} and T_{95} are the temperature at which the weight loss reaches 50% and 95%, respectively. T_{max} is the temperature of the maximum decomposition peak in the DTG curve.

3.2.2.7 Dynamical mechanical analysis

Dynamic mechanical thermal analysis (DMA) was performed in a TA Q800 DMA equipment. PEX and PE specimens were cut from the pipes and deformed under flexure using a single cantilever arrangement, at a frequency of 1 Hz. Transitions were studied in a thermal scanning mode from -50 °C to 170 °C at a 3 °C/min rate. Three replicates were run for each material.

The average molecular weight between crosslinks (M_c) was determined according to Equation 3-10 [74, 75].

$$M_c = \frac{2(1+\nu)\rho RT}{E'} \tag{3-10}$$

where E' is the storage modulus at the rubbery plateau, ν is the Poisson ratio ($\nu = 0.41$) [96], ρ is the density of the amorphous polymer ($\rho = 0.850$ g/cm^3) [50, 97], R is the gas constant and T is the absolute temperature.

Equation 3-10 was derived from the statistical theory of rubber elasticity for lightly crosslinked rubber system in very small strains. It can also be applied to semicrystalline polymers, provided that the modulus contribution from crosslinks is isolated from the crystalline phase contribution [75]. For semicrystalline polymers at temperatures above their melting point, the material becomes entirely amorphous, and the storage modulus reaches a minimum or a plateau. In this plateau region, the storage modulus is a function of the molecular weight between physically effective crosslinks, which includes both entanglements and chemical crosslinks [74]. For polyethylene, this plateau typically occurs around 150 °C to 160 °C. This was confirmed by calculating the temperature derivative of the storage modulus, which was less than 0.1 at 160 °C for all materials. Therefore the E' at 160 °C was used to calculate M_c for all samples. The effective crosslinking density was calculated as per Equation 3-11 [75].

$$\nu_c = \frac{\rho}{M_c} = \frac{E'}{2(1+\nu)RT} \tag{3-11}$$

3.3 Results and discussion

3.3.1 Crosslinking morphology

The degree of crosslinking, as determined by gel content, is summarized in Table 3.2. Additionally, the table includes the average molecular weight between crosslinks (M_c) and the crosslinking density (ν_c), both calculated from the DMA data using Equations 3-10 and 3-11, respectively. The storage modulus at 160 °C (Table 3.8), where the material reaches the rubbery plateau, was used for determining the M_c and ν_c values. The PE100 pipe was also analyzed as a control. Since this pipe was not crosslinked, the gel content of 0.8% indicates that the experimental conditions were sufficient to dissolve the non-crosslinked portions of the PEX samples, with an experimental accuracy exceeding 99%. In general, PEX samples with higher gel content exhibited also a higher crosslinking density and a lower molecular weight between crosslinks,

which is in line with other studies for PEX pipes [48, 50, 98, 99]. In the case of PE100, the values of M_c and ν_c are a measure of molecular weight between chain entanglements only.

Table 3.2: Degree of crosslinking (Gel), molecular weight between crosslinks (M_c) and crosslinking density (ν_c) of the pipes. Uncertainties represent the standard deviation.

Material	Gel (%)	M_c $\times 10^3$ (g/mol)	ν_c $\times 10^2$ (mol/m^3)
PEX-e1	77.1 ± 1.5	2.3 ± 0.1	3.8 ± 0.2
PEX-e2	81.0 ± 0.0	1.4 ± 0.2	6.3 ± 1.2
PEX-a	90.7 ± 0.5	0.7 ± 0.1	11.6 ± 1.4
PE100	0.8 ± 0.0	15.2 ± 0.8	0.6 ± 0.0

The three PEX pipes exhibited different degrees of crosslinking, with PEX-a having the highest and PEX-e1 the lowest. Nevertheless, all three types met the required gel content threshold of over 70%, as specified by the standard for "Plastics piping systems for hot and cold water installations" (ISO 15875-2). The gel content in PEX-e2 was only slightly higher than in PEX-e1. However, PEX-e2 exhibited a significantly greater crosslinking density, suggesting that crosslinks are less dispersed in PEX-e2. The differences between PEX-e1 and PEX-e2 may stem from variations in processing conditions [100] and potentially from differences in additive formulations [48].

3.3.2 Molecular dynamics and quantitative phase composition

PE is a semicrystalline polymer, consisting of phases with significantly different chain mobilities [9]. The crystalline phase typically consists of chain-folded lamellae, which, under standard processing conditions, are arranged in an orthorhombic lattice [27, 101]. In this phase, the polymer chains are highly ordered, resulting in very limited mobility. Only methyl branches and a small proportion of ethyl branches can be incorporated into the crystalline phase, while the remaining branches form an intermediate or interphase region that is more ordered than the amorphous phase [9]. It is believed that this interphase consists of polymer chains with restricted motion compared to the amorphous phase, not only due to their proximity to the crystalline regions, but also due to chain entanglements and, in the case of PEX, crosslinks [64, 65].

Quantitative assessment of phase composition and molecular mobility is crucial in material development, as these phases exhibit vastly different morphology and, consequently, have different contributions to the material's properties. Static ^{1}H NMR was used to quantify the phase composition and molecular mobility of the different pipes investigated in this study. The solid echo decay (Figure 3.2) was decomposed into three components, as demonstrated in Figure 3.3 for PEX-e2. The fitting results for all samples, presented

in Figure 3.4 and Table 3.3, reveal the proportions of rigid, intermediate and mobile components, along with their corresponding T_2 relaxation times.

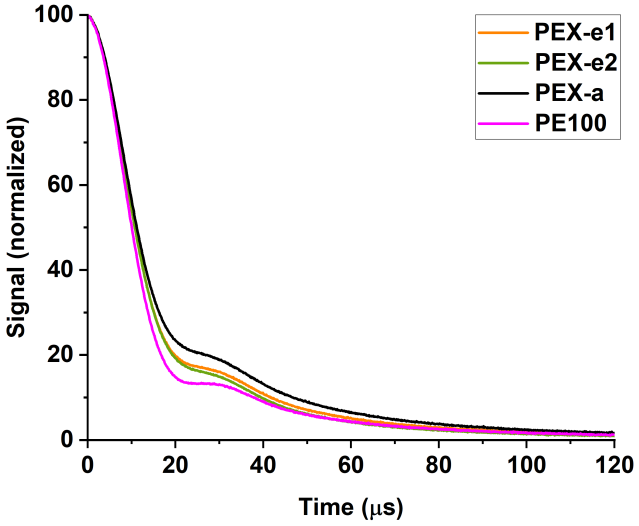

Figure 3.2: ^{1}H NMR solid echo decay acquired for PEX and PE pipes samples.

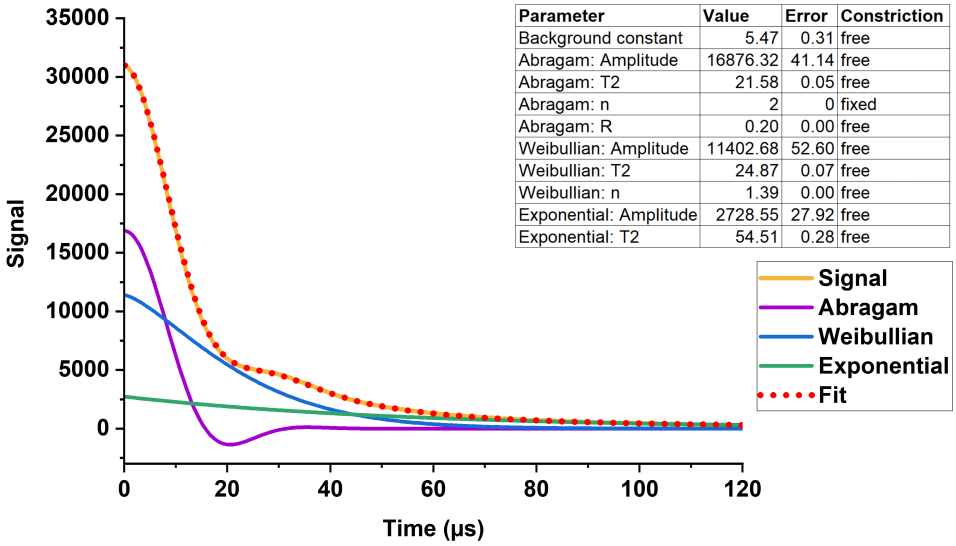

Figure 3.3: Example showing the fitting of the Abragam, Weibullian, and exponential functions to ^{1}H NMR signal of PEX-e2.

Table 3.3: Results of the ^{1}H NMR echo decay fitting.

	Rigid component (Equation 3-2)			Intermediate component (Equation 3-3)			Mobile component (Equation 3-4)	
Material	Total (%)	T_2 (μs)	R (-)	Total (%)	T_2 (μs)	n (-)	Total (%)	T_2 (μs)
PEX-e1	54.5	21.7	0.20	36.0	25.5	1.35	9.5	60.2
PEX-e2	54.4	21.6	0.20	36.8	24.9	1.39	8.8	54.5
PEX-a	50.7	21.7	0.21	36.8	26.7	1.35	12.5	59.2
PE100	60.0	21.7	0.21	32.7	23.7	1.24	7.3	65.8

As previously discussed, the second moment (M_2) is a measure of the relative proximity of the neighbouring H's in the lattice. The calculated second

moment for rigid polyethylene is 25.5 G^2 [86] and the experimental second moment at 84 K was found to be 26.3 G^2 [102]. The observed values shown in Table 3.4 vary between 25.2 G^2 and 25.6 G^2, indicating that the resulting Abragam component is, in fact, due to the rigid part of the polymer and can be assigned to the crystalline region. As expected for the crystalline domains, the mobility within this area does not change between samples, as the measurements were performed below the crystalline melting point.

Table 3.4: Additional parameters of the ^{1}H NMR echo decay fitting.

Material	Rigid component (%) (Equation 3-5)	M_2 (G^2) (Equation 3-6)
PEX-e1	54.5	25.4
PEX-e2	54.4	25.2
PEX-a	50.7	25.6
PE100	60.0	25.6

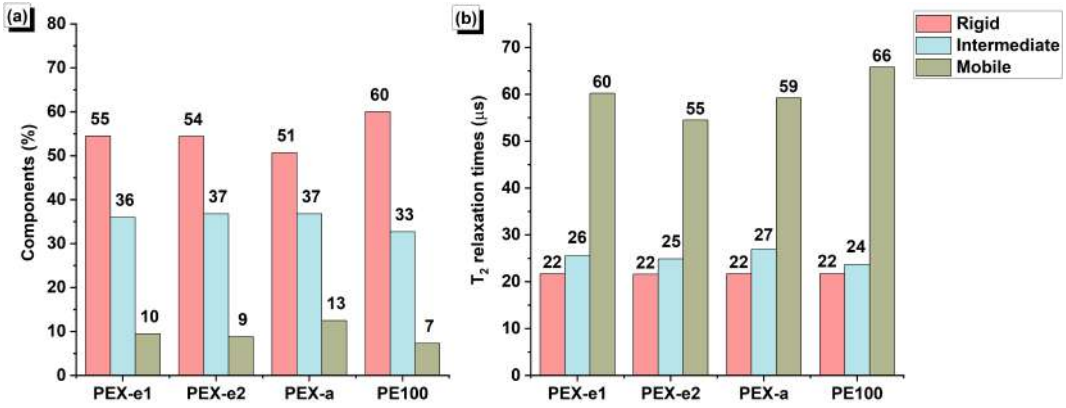

Figure 3.4: Results of the fittings for the ^{1}H NMR decay showing (a) the amount of rigid (crystalline), intermediate (interphase) and mobile (amorphous) components and (b) their corresponding T_2 relaxation times. (The color legend applies to both graphs.)

PEX-a has the lowest amount of rigid component (lowest degree of crystallinity) and the highest amount of mobile component. This reduced crystallinity is likely due to its higher degree of crosslinking. In both the peroxide- and photo-initiated processes, crosslinking occurs at temperatures above the melting point, which directly influences subsequent crystallization. During cooling, the presence of crosslinks hinders chain folding and close packing, leading to a lower degree of crystallinity [10, 50, 99, 103, 104]. Accordingly, the non-crosslinked PE100 exhibits a higher proportion of rigid component compared to the other samples.

The amount of interphase material in PEX-a is roughly the same as in PEX-e1 and PEX-e2. However, if the degree of crosslinking is higher, the mobility of the interphase region was expected to be reduced. Surprisingly, it is slightly more mobile (longer T_2^{inter}) compared to PEX-e1 and PEX-e2. This

could be attributed to the nature of the crosslinks. As previously discussed, the crosslinks in PEX-e are not solely composed of carbon-carbon bonds [15], as they are in PEX-a, which may influence the mobility of the network and, consequently, the mobility of the interphase.

Although PEX-e2 exhibited a significantly greater crosslinking density compared to PEX-e1, their phase proportions and interphase mobility are rather similar. However, the amorphous phase in PEX-e1 showed greater mobility compared to PEX-e2. These findings support the assumption that the crosslinks are more evenly dispersed in PEX-e1 compared to PEX-e2. A more uniform distribution of crosslinks within the interphase region of PEX-e1 would allow for slightly more free PE chains in the amorphous region, resulting in higher T_2^{long} relaxation times.

3.3.3 Melting and crystallization behavior

Differential scanning calorimetry was used to asses the melting and crystallization behavior of the pipe samples. The heating and cooling curves of PEX and PE are shown in Figure 3.5, while the average values for the melting temperature (T_m), crystallization temperature (T_c), melt enthalpy (ΔH_m) and crystallinity degree (X_c) are listed in Table 3.5. All materials exhibited distinct endothermic melting peaks and well-defined crystallization peaks.

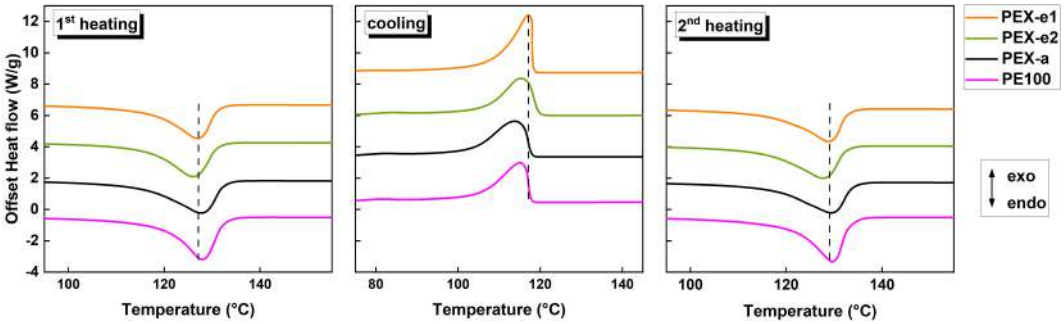

Figure 3.5: DSC curves showing first heating, cooling and secondary heating cycles for pipe PEX and PE pipe samples.

Table 3.5: Parameters obtained from the DSC curves of PEX and PE pipes. The superscripts 1 and 2 stand for first and second heating, respectively. (Average and standard deviation for three replicate runs).

Material	T_m^1 (°C)	T_m^2 (°C)	T_c (°C)	ΔH_m^1 (J/g)	X_c^1 (%)	ΔH_m^2 (J/g)	X_c^2 (%)
PEX-e1	127 ± 1	129 ± 0	115 ± 0	153 ± 6	54.4 ± 2.4	176 ± 3	62.7 ± 1.7
PEX-e2	126 ± 0	129 ± 1	113 ± 0	180 ± 6	63.9 ± 2.5	183 ± 3	65.1 ± 1.7
PEX-a	128 ± 1	130 ± 1	114 ± 2	169 ± 3	60.0 ± 1.6	173 ± 2	61.4 ± 1.5
PE100	128 ± 1	130 ± 0	117 ± 1	203 ± 3	72.1 ± 1.9	212 ± 4	75.4 ± 2.1

The first heating curve is typically performed to erase the samples' thermal history. However, in this study, the first melt peak is of particular interest, as it provides information on the effect of the crosslinking process on the properties of the pipes. During the first heating, PEX-e2 displayed a slightly lower melting temperature compared to the other materials, indicating differences in the crystalline phase morphology. In general, lower lamellae thickness and lower crystal regularity result in lower melting temperatures [103, 105].

Notable differences in melt enthalpy, and consequently in crystallinity degree, were observed between the first and second heating cycles. In general, all materials showed lower crystallinity (X_c^1) during the first heating compared to the second (X_c^2), suggesting that the processing conditions negatively impacted crystallization. This effect was more pronounced in PEX-e1, which exhibited a considerably lower value of X_c^1. Once the thermal history was erased and the chains were allowed to reorganize and recrystallize, the melt enthalpy increased for all samples. In the second heating, the differences in melting temperature between the materials were statistically insignificant.

The crystallinity results obtained from DSC are generally inconsistent with the phase composition determined by NMR (see Section: Molecular dynamics and quantitative phase composition). While both methods consistently indicate that PE100 has a higher crystallinity than the PEX samples, the crystallinity values determined by DSC are generally higher than those measured by NMR. Additionally, NMR indicated that both PEX-e pipes had similar phase compositions, whereas DSC indicated higher crystallinity for PEX-e2, compared to PEX-e1. This discrepancy between DSC and NMR was also observed by Posadas et al. [9] and it is likely due to differences in how each method measures crystallinity. DSC measures thermal properties, quantifying crystallinity based on the heat required to induce the melt transition. Proton NMR, on the other hand, measures the physical structure of the polymer at a molecular level, by examining the mobility and arrangement of hydrogen nuclei, distinguishing between the highly ordered crystalline region, a slightly ordered interphase and the more mobile amorphous region.

The crystallization temperature was similar between the PEX variants. However, as shown in Figure 3.5, the shape of the crystallization and melting peaks varies slightly among them. PEX-e1 displays a sharper crystallization peak and a slightly narrower melting peak compared to PEX-e2 and PEX-a. These observations indicate slight differences in crystallization kinetics and crystallite size distribution [106]. Broader peaks are often associated with the presence of imperfect crystals with wider lamellae thickness distribution [107].

As highlighted by Qing et al. [47], when some segments between adjacent crosslinks are long enough to fold, certain crosslinks may become embedded within the crystal phase, having little effect on the crystallinity degree, but acting as defects and reducing crystal regularity.

This crystal irregularity may also contribute to the disparity between DSC and NMR crystallinity measurements. Crystalline regions containing defects likely exhibit different mobility, leading them to be more accurately detected as interphase by NMR. Further investigation into the morphology of the crystalline phase would be valuable to confirm this assumption. While conventional DSC provides limited insight into crystal regularity, more detailed analysis using modulated DSC [105, 107] appears to be a promising direction for future research.

3.3.4 Antioxidant content and degradation products

During their manufacturing, installation and service, PE and PEX pipes can undergo thermo-oxidative and photo-oxidative degradation reactions that can lead to premature failure [8, 13]. Accordingly, antioxidant (AO) additives are incorporated into their formulations in order to prevent oxidative degradation and extend their service time.

FTIR spectroscopy was used to analyze antioxidant additive content and identify chemical species that play an important role in polymer degradation. Figure 3.6 shows the average spectrum for each pipe material. The main absorbance peaks observed are characteristic of PE molecular vibrations. The CH_2 asymmetric (ν_a) and symmetric (ν_s) stretching modes were observed at 2915 cm^{-1} and 2847 cm^{-1}, respectively. The doublet characteristic of CH_2 scissoring mode (δ) was observed at 1472 cm^{-1} and 1462 cm^{-1}, while the rocking mode (γ_r) peaks were identified at 730 cm^{-1} and 719 cm^{-1}. The maximum variation in peak position amongst materials was of ± 1 cm^{-1}, which is lower than the experimental resolution.

The carbonyl region, featured in Figure 3.6.b, is of specific interest for analysis of additive content and degradation products in polyolefins [8, 91]. Particularly, the most commonly used hindered phenolic antioxidant additives for stabilization of PEX and PE, such as Irganox 1010 and Irganox 1076, contain ester linkages with characteristic absorbance peak reported at 1738-1740 cm^{-1} [5, 8, 11, 56]. Accordingly, the carbonyl peaks located at 1739 cm^{-1} in PEX-e1 and 1738 cm^{-1} in the other pipes were assigned as ester. Additional peaks located approximately at 1733 cm^{-1}, 1718 cm^{-1} and 1699 cm^{-1} were assigned as aldehyde [108, 109], ketone [14, 108, 109] and carboxylic acid [13,

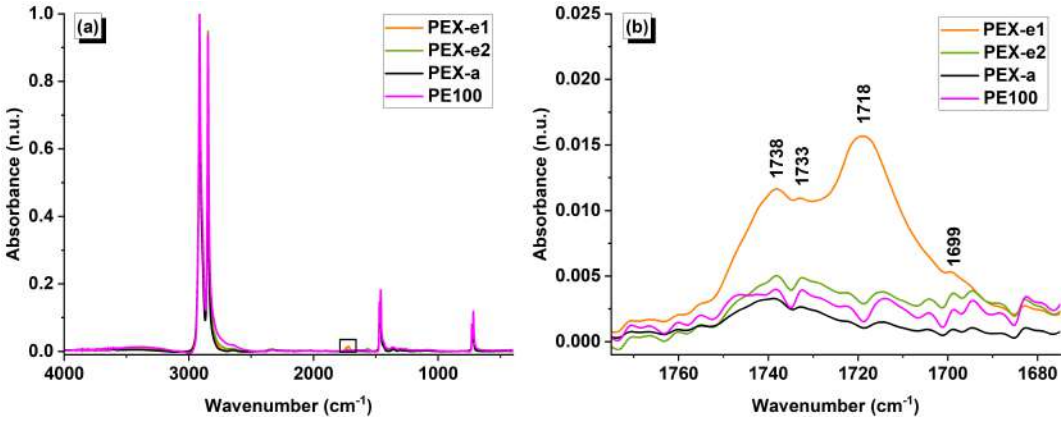

Figure 3.6: FTIR spectrum of PEX and PE pipe samples: (a) 4000–400 cm^{-1} range and (b) carbonyl region (1775–1675 cm^{-1}).

14, 108], respectively.

Although precise quantification of additive concentration with FTIR cannot be done without a calibration curve [5, 91], quantification of the carbonyl index and ester absorbances can provide valuable insight into the additive content amongst different pipes. The carbonyl index and average normalized absorbance of the carbonyl peaks detected in the spectra of the pipes are listed in Table 3.6, with the latter also shown in Figure 3.7.a for clearer visualization. PEX-e1 samples presented significantly higher carbonyl index compared to the other pipe materials. Notably, the ester absorbance in PEX-e1 was more than twice that of the other pipes. This result confirmed the higher percentage of AO additives in Formulation I informed by the supplier.

Comparatively, PEX-a samples contained fewer ester groups, suggesting that a portion of the additives might have been consumed during processing. The PEX-a method is known for its potential to over-consume antioxidant (AO) stabilizers [30], as crosslinking occurs at elevated temperatures (170-190 °C [110]) in the presence of organic peroxides. In contrast, the PEX-e process occurs at lower temperatures (around 135 °C) and does not involve peroxide agents. However, oxidation has been reported to occur during photo-crosslinking [48]. In fact, as evidenced in Figure 3.7.a, the absorbance of ketones, aldehydes and carboxylic acids, which are known oxidation products [5, 94], was also comparatively higher in the PEX-e1 samples. These findings indicate that despite the increased amount of AO additives, the PEX-e1 pipe underwent some level of degradation during processing.

Although the extrusion of polyolefins occurs in a oxygen-poor environment, it has been proven that numerous degradation reactions can take place during high-temperature processing of polyethylene [111–113]. Various factors influence the extent of these reactions, including the chemical structure of the

Table 3.6: Carbonyl index (CI) and normalized absorbance of carbonyl groups in the FTIR spectra of the pipes.

Material	CI	Ester	Aldehyde	Ketone	Carboxylic acid
	$\times 10^{-2}$ (cm^{-1})	$\times 10^{-3}$ (n.u.)	$\times 10^{-3}$ (n.u.)	$\times$ 10^{-3} (n.u.)	$\times 10^{-3}$ (n.u.)
PEX-e1	65.2 ± 1.9	11.7 ± 0.3	11.0 ± 0.3	15.7 ± 0.8	5.3 ± 0.1
PEX-e2	26.9 ± 1.5	5.0 ± 0.2	4.9 ± 0.2	3.8 ± 0.2	3.7 ± 0.2
PEX-a	13.2 ± 0.8	3.3 ± 0.1	2.7 ± 0.1	1.5 ± 0.1	0.9 ± 0.1
PE100	23.4 ± 0.9	4.1 ± 0.7	4.1 ± 0.5	3.3 ± 0.2	2.4 ± 0.1

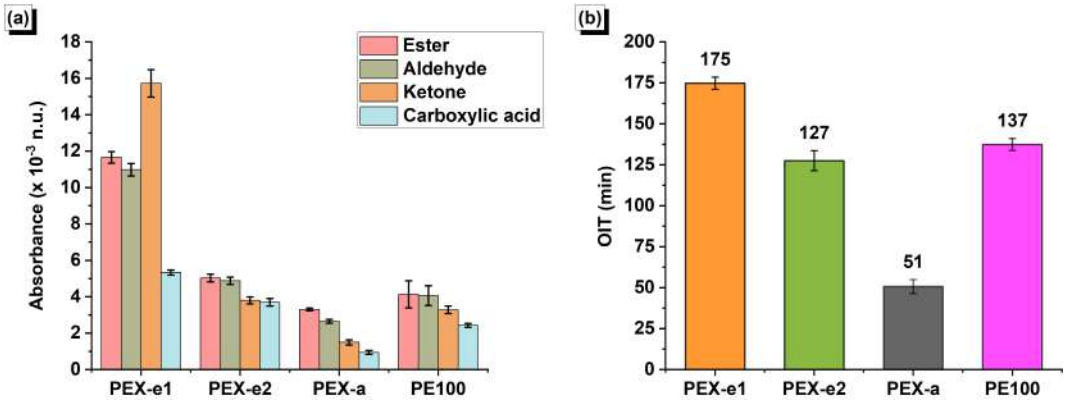

Figure 3.7: (a) Normalized absorbance of carbonyl groups and (b) OIT values for the PEX and PE pipes. (Error bars represent the standard deviation).

polymer, type and amount of catalyst residues, composition of the additive package, as well as the processing conditions, such as temperature, concentration of oxygen diffused into the sample, intensity of shear forces, etc [111, 112]. In the case of PEX, the crosslinking process can also play an important role on degradation [30]. For PEX-e, the presence of a certain amount of unreacted residual photo-initiator and its photolytic products may also influence the stability of the crosslinked polymer [46].

Oxidation induction time (OIT) is one of the most frequently used methods for assessing the oxidative stability and the performance of AOs in polyolefins pipes [8, 114]. The OIT values for all pipe samples were measured and are presented in Figure 3.7.b. Notably, PEX-e1 exhibited significantly higher OIT values compared to the other materials, which can be expalined by its higher AO content. In contrast, the average OIT value obtained for PEX-a was considerably lower than that of the other materials, which is consistent with the FTIR observations.

Previous studies have reported correlations between OIT values and concentration of primary AO additives [8, 115]. However, this correlation was not observed in some of the pipes. Although the carbonyl index and ester absorbance detected in the FTIR spectrum of PE100 and PEX-e2 were relatively low, the OIT values measured for these materials were significantly high (above 120 min). These findings underline that OIT values are influenced

not only by the concentration of primary AOs but also by the effectiveness of the entire additive package. Certain combinations of primary and secondary AOs have been shown to produce a synergistic effect, reducing the total amount of primary AOs required for stabilization [6, 56, 111].

3.3.5 Thermal degradation

Thermogravimetric studies were conducted under nitrogen and air atmospheres to evaluate the thermal degradation of the pipes. Figure 3.8 shows the TG curves for the PEX and PE pipes in nitrogen and air atmospheres. A final residue of 2.3 wt% was observed for PE100, which was attributed to the carbon black additive. All other samples reached less than 0.1 wt% residue at 650 °C. The relative thermal stability of the materials can be analyzed using the parameters listed in Table 3.7.

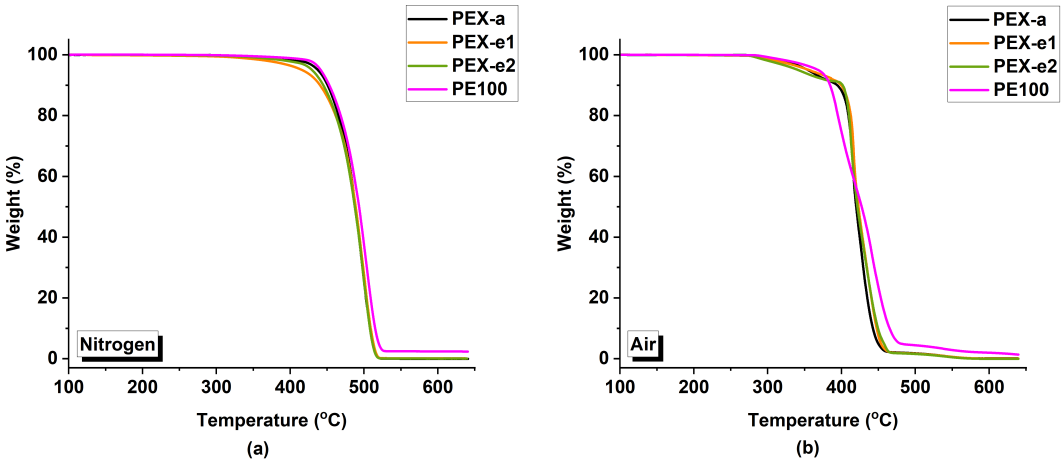

Figure 3.8: TG curves of pipe samples under (a) nitrogen and (b) air atmospheres. (One representative curve was chosen for each material based on the median values from three replicate tests).

Table 3.7: Thermal degradation parameters for pipes obtained from the TG curves.

Purge gas	Material	T_5 (°C)	T_{50} (°C)	T_{95} (°C)	T_{max} (°C)
Nitrogen					
	PEX-e1	416 ± 3	490 ± 4	514 ± 2	499 ± 3
	PEX-e2	433 ± 6	491 ± 6	514 ± 3	501 ± 4
	PEX-a	445 ± 10	492 ± 5	514 ± 3	499 ± 5
	PE100	451 ± 15	497 ± 5	519 ± 1	506 ± 1
Air					
	PEX-e1	354 ± 2	424 ± 1	451 ± 2	419 ± 2
	PEX-e2	340 ± 2	425 ± 3	457 ± 2	418 ± 4
	PEX-a	351 ± 3	421 ± 1	452 ± 2	418 ± 2
	PE100	360 ± 6	425 ± 3	487 ± 8	425 ± 17

Under a nitrogen atmosphere, the materials degraded in a single step beginning around 430°C and reaching 95% of weight loss at approximately

515 °C. Surprisingly, the degradation of PE100 occurred at a slightly higher temperature range, indicating higher thermal resistance when compared to the PEX samples. Among the PEX pipes, PEX-a had the highest average T_5 value at 445 °C, while PEX-e1 had the lowest at 416 °C, indicating that PEX-a can withstand higher temperatures under inert conditions. However, this disparity was less prominent under atmospheric conditions.

As expected, the degradation range shifts to lower temperatures under air atmosphere, generally occurring between 350°C and 420°C approximately. Additional effects of the purge gas can be observed in the DTG curves shown in Figure 3.9. Under nitrogen flow, a single degradation peak was observed for all materials. According to Peterson et al. [116], in an inert atmosphere, the degradation mechanism of PE involves both chain scission and chain branching, which occur simultaneously, leading to a single mass loss step. Findings reported by Du et al. [117] indicate that crosslinking and chain scission are two competitive reactions that occur concurrently within a single degradation stage during the pyrolysis of PEX.

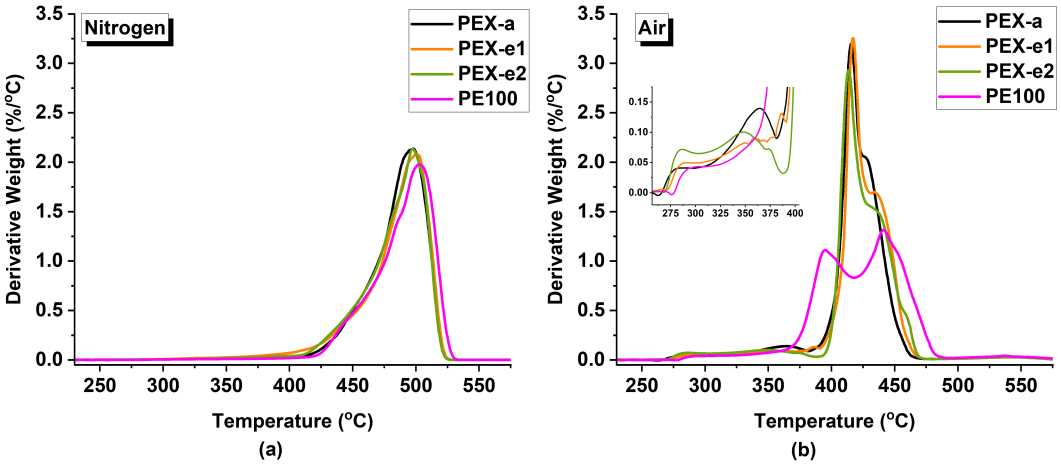

Figure 3.9: DTG curves of pipe samples under (a) nitrogen and (b) air atmospheres. (One representative curve was chosen for each material based on the median values from three replicate tests).

Conversely, under air atmosphere, the degradation of PE and PEX occurs through numerous degradation steps due to the presence of oxygen and high temperatures. This leads to various thermo-oxidative degradation reactions with chain radicals that accelerate the degradation process [95, 116, 118]. At least three degradation stages were observed for PE and PEX in air: the first stage consisted of small irregular degradation peaks in the 270-400 °C region, as highlighted in Figure 3.9.b. The second stage consisted of a well defined degradation peak at 395 °C for PE100 and 418 °C for PEX. The third stage

consisted of another peak, which appeared as a shoulder between 420-430 °C for PEX, while for PE100 it involved a defined peak around 440 °C.

The differences observed in Figure 3.9 indicate that the kinetics of PE degradation in air changes in the presence of crosslinks. For PEX, the main degradation occurred in stage two, with a very intense and sharp peak, indicating faster degradation when compared to PE100. For the latter, the degradation transpired over a wider temperature range, throughout stages two and three. A possible explanation for the faster degradation in PEX might be the presence of weak link sites, such as peroxides, carbonyl groups and unsaturated structures, induced by the crosslinking process [116, 118]. Further investigations on the chain morphology and degradation kinetics could better elucidate these differences.

3.3.6 Thermo-mechanical properties

The dynamic mechanical properties of the PEX and PE pipes over the temperature range of -50 °C to 170 °C are shown in Figure 3.10. Significant differences in storage modulus (*E'*) were observed among the pipes, with these differences being more pronounced at lower temperatures, as detailed in Table 3.8. Below the melting point, the storage modulus is strongly influenced by the crystalline morphology [74, 75]. In general, higher crystallinity leads to higher mobility restriction and, consequently higher storage modulus. Accordingly, the higher *E'* values exhibited by PE100 below the melting point can be attributed to its higher degree of crystallinity. In general, crosslinked PE exhibits lower stiffness compared to non-crosslinked PE due to the negative impact of the crosslinked network on crystallinity [106]. However, the differences observed among the PEX pipes suggest that the morphology of the crosslink network also plays a critical role in determining their mechanical properties.

As shown in Figure 3.10.a, PEX-a and PEX-e1 exhibited similar stiffness overall, with PEX-a having a slightly lower storage modulus at around -50°C. This difference can be attributed to the lower proportion of the rigid phase, i.e., reduced crystallinity, as identified by NMR analysis. As the temperature increases, molecular motion becomes more pronounced, leading to a continuous decrease in storage modulus for all materials. However, PEX-a showed a slower decrease in *E'* with temperature, compared to PEX-e1, maintaining slightly higher *E'* values above -5°C. This more gradual decline is likely due to the higher crosslinking density in PEX-a. In general, shorter chain segments between crosslinks, as evidenced by the lower M_c values, inhibit chain

movement, contributing to a stiffer network [74].

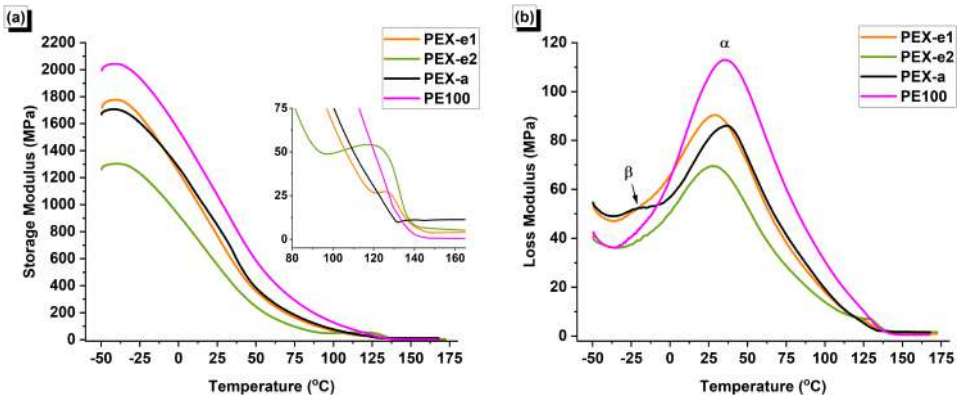

Figure 3.10: (a) Storage modulus and (b) loss modulus of PEX and PE pipe samples. (One representative curve was chosen for each material based on the median values from three replicate tests).

Table 3.8: Parameters obtained from the DMA curves of PEX and PE pipes. (Average and standard deviation for three replicate runs).

Material	E' at 0°C (MPa)	E' at 23°C (MPa)	E' at 90°C (MPa)	E' at 160°C (MPa)	T_α (°C)	E" at T_α (MPa)
PEX-e1	1213 ± 44	791 ± 42	90 ± 7	4 ± 0	29 ± 2	88 ± 2
PEX-e2	920 ± 27	584 ± 21	54 ± 5	6 ± 1	27 ± 1	68 ± 1
PEX-a	1251 ± 40	868 ± 15	111 ± 0	12 ± 1	35 ± 2	85 ± 2
PE100	1510 ± 65	1098 ± 78	192 ± 25	1 ± 0	38 ± 4	110 ± 4

Despite having a similar amount of rigid phase as PEX-e1, PEX-e2 unexpectedly exhibited a significantly lower storage modulus below melting. This suggests that other morphological factors, such as the dispersion of crosslinks, are crucial in determining mechanical properties. Indeed, Shen et al. [72] found that improving crosslink dispersion can have a similar effect on the elastic modulus as increasing the crosslink density. For polymers with the same crosslink density, greater crosslink dispersion resulted in a notably higher storage modulus, while more aggregated networks led to reduced stiffness [72]. Thus, the lower stiffness observed in PEX-e2 could be explained by a less uniform distribution of crosslinks in this material.

Once the material surpasses its melting point, it becomes fully amorphous, and the storage modulus reaches a minimum and stabilizes at a plateau. This plateau, known as the rubbery region, is proportional to the density of crosslinks and molecular entanglements [74, 75]. As shown in the zoomed-in section of Figure 3.10.a, the storage modulus of the PEX pipes does not exhibit a continuous decrease at melting, as seen with non-crosslinked PE. Instead, a step occurs before the modulus stabilizes at the plateau, with this effect being more pronounced in PEX-e2 and less pronounced at PEX-a. Xie and Li [75] observed a similar phenomenon in ultrahigh molecular weight polyethylene,

attributing it to a highly entangled network. In the case of PEX, this behavior could be related to the crosslinked network structure. It can be speculated that the larger step observed in PEX-e2 compared to the other PEX pipes is due to higher chain entanglement and aggregation of crosslinks in this material.

The loss modulus (E") is a measure of the energy dissipated as heat during the deformation cycle. The loss modulus curves reveal relevant information about the mechanical relaxations occurring over different temperature ranges. Polyethylene displays three transitions conventionally designated as α, β and γ relaxations [119]. The γ transition is usually observed in the range -150 °C to -120 °C, the β transition in the range -30 °C to 10 °C and the α transition is usually found between 30 °C and 120 °C [119, 120].

The α-relaxation is assigned to motion or deformation of chain units within the crystalline regions [121, 122]. In the E" curve, this transition was observed at lower temperatures for both PEX-e, compared to PEX-a and PE100, respectively. Differences in the shape of the α peak were also evident. The main factor governing T_α in linear polyethylene has been found to be lamellar thickness [119, 121]. Popli et al. [119] also noted that the morphology of the spherulites and the interfacial structure might have a significant effect on the α transition. Unfortunately, no literature regarding the effect of crosslinks on the α transition was found. However, the values obtained in the present study suggest that the different morphology formed in the PEX-e crosslinking process shifts the α relaxation to lower temperatures.

A weak β transition peak was observed around -22 °C for PEX-a. This transition was not resolved for the other materials. The β relaxation has been attributed to the relaxation of chain units located at the amorphous and interfacial regions and is usually hardly resolved for linear PE [119].

3.4 Conclusions

The PEX pipes produced using a novel photo-crosslinking method (PEX-e) were characterized in detail. Two formulations, PEX-e1 and PEX-e2, were analyzed and compared to peroxide-crosslinked polyethylene (PEX-a) and non-crosslinked bimodal polyethylene (PE100) pipes. Both PEX-e formulations achieved high crosslinking degrees (above 70%). However, significant differences in crosslink density and molecular weight between crosslinks were noted, suggesting PEX-e2 had a more aggregated crosslinked network.

Static ^{1}H NMR provided insights into the phase composition and molecular mobility of the different pipes. A three-component model was used to fit the solid echo decay data, distinguishing contributions from the crystalline

phase, interphase, and amorphous region. As expected, the PEX samples exhibited a lower degree of crystallinity compared to PE100. Among the PEX variants, the PEX-e samples showed a slightly higher proportion of the rigid component compared to PEX-a, which was attributed to the higher gel content in PEX-a. Differences in the interphase relaxation times suggested that the bonds formed in the PEX-e process create a more rigid network with reduced molecular mobility compared to the carbon-carbon bonds formed in the PEX-a process.

FTIR analysis revealed a lower antioxidant (AO) content in PEX-a, suggesting over-consumption of stabilizers during processing. This was supported by the significantly low oxidation induction time (OIT) values observed in PEX-a. Both FTIR and OIT analysis indicated higher AO content in PEX-e1 compared to the other pipes. However, the PEX-e1 spectrum also showed signs of oxidation, with increased absorbance of ketones, aldehydes, and carboxylic acids. This suggests that, despite the higher AO content, some oxidation occurred during processing. Interestingly, both PEX-e2 and PE100 also showed high OIT values, despite having relatively low primary AO content, suggesting potential synergistic effects from their additive package formulations.

Differential scanning calorimetry (DSC) revealed that PEX-e2 had a slightly lower melting temperature, indicating reduced crystal regularity, which was further supported by broader crystallization and melting peaks. The thermal degradation of the materials, as assessed by TGA, followed similar trends in an inert atmosphere but showed significant differences in air. Under a nitrogen atmosphere, all materials degraded in a single step, whereas, in air, degradation occurred in multiple steps. Among the PEX samples, PEX-a had the highest onset temperature under nitrogen (445°C), while PEX-e1 had the lowest (416°C), suggesting that PEX-a can withstand higher temperatures under inert conditions. However, this disparity was less prominent under atmospheric conditions.

Dynamic mechanical analysis (DMA) revealed significant differences in thermo-mechanical behavior. Below the melting point, PE100 exhibited a significantly higher storage modulus, attributed to its higher degree of crystallinity. However, the differences observed among the PEX pipes suggested that crystallinity alone was not the only factor influencing dynamic mechanical properties; the morphology of the crosslink network also played a critical role. The higher crosslinking degree in PEX-a resulted in a less steep decline in storage modulus (E') with temperature. Additionally, the lower storage modulus observed in PEX-e2 below the melting point further supported the

idea of crosslink aggregation in this pipe.

In conclusion, PEX-e pipes show promise for high-temperature borehole thermal energy storage systems, as both formulations investigated exhibited high degrees of crosslinking and robust OIT values. For PEX-e1, the storage modulus was comparable in magnitude to that of the commercially established PEX-a. However, the presence of oxidation products in PEX-e1 highlights the importance of refining the formulation, particularly in the selection and concentration of stabilizing additives. This optimization is a critical direction for future work to enhance long-term stability. Additionally, further investigation into processing conditions, photo-initiators, and crosslinking co-agents could play an important role in achieving PEX-e pipes with properties comparable to, or exceeding, those of PEX-a.

4
Thermo-oxidative ageing of photo-crosslinked polyethylene pipes for thermal energy storage

Article under review at the *Journal of Polymer Degradation and Stability* (Submitted January 2025). Tracking available at: https://track.authorhub.elsevier.com/?uuid=0d0e0ee0-73d1-45ab-99ed-746e9932548c

This study presents a comprehensive evaluation of the thermo-oxidative stability of crosslinked polyethylene (PEX) pipes designed for borehole thermal energy storage (BTES) systems, with a particular focus on a novel PEX type produced via a photo-initiated crosslinking process (PEX-e). Two formulations, PEX-e1 and PEX-e2, were assessed and compared to commercial peroxide-crosslinked polyethylene (PEX-a) and bimodal polyethylene (PE100) pipes. The pipes were aged in water at the intended BTES service temperature for 210 days, with periodic analyses conducted to monitor antioxidant (AO) depletion and the formation of degradation products. Advanced analytical techniques were employed, including Fourier transform infrared (FTIR) and nuclear magnetic resonance (NMR) spectroscopy, gel content analysis, colorimetry, differential scanning calorimetry (DSC), oxidation induction time (OIT), and dynamic mechanical analysis (DMA). FTIR analysis revealed the presence of degradation-related peaks on the pipe surfaces, while the formation of oxidation products in the bulk material was limited. Phase composition analysis showed that physical ageing dominated during the first 30 days, leading to increased crystallinity and enhanced lamellar thickness. Over time, chain scission emerged as the primary degradation mechanism, resulting in molecular weight reductions, with PEX-a being the most severely affected. No abrupt changes in phase composition or mechanical properties were observed after 210 days of ageing, indicating that the pipes remained in the induction phase of degradation. Interestingly, despite their high OIT levels, both PEX-e formulations exhibited accelerated AO depletion during prolonged exposure, suggesting the need for further optimization of PEX-e formulations to ensure long-term stability under demanding BTES conditions.

4.1 Introduction

In the face of current energy and environmental crises, borehole thermal energy storage (BTES) systems have emerged as a cost-effective solution to balance energy production with consumption. Renewable energy sources like solar power, while valuable, are subject to significant fluctuations and often do not align with energy demand. BTES systems address this mismatch by storing heat generated during high-production periods to be used in other periods, such as storing summer heat for winter use or capturing industrial waste heat for district heating purposes [1, 2, 21].

A typical BTES system consists of several densely packed closed-loop borehole heat exchangers (BHEs), that transfer heat to and from surrounding rock or sediment, making it particularly efficient for seasonal heat storage [1, 2, 4, 76]. These systems are usually made from high-density polyethylene (HDPE) or crosslinked polyethylene (PEX) and operate within temperature ranges of approximately 5 °C to 90 °C [2, 4].

For high-temperature applications, PEX is often preferred over HDPE due to its enhanced thermal stability [9–12]. PEX types are classified by crosslinking method, with PEX-a (peroxide crosslinked) being the most commonly used for water and heating applications [13, 14]. Recently, photo-crosslinked polyethylene (PEX-e) has emerged as a promising alternative to PEX-a, attracting particular interest from the pipe industry due to its higher production efficiency, reduced energy consumption, and absence of volatile chemical emissions [15, 16, 33]. Although the foundational photo-crosslinking process was developed in the 1990s by Rånby et al. [44–51], its application in PEX pipe production is a more recent innovation that still requires further optimizations [17, 18, 33].

In a recent study [33], we examined the morphology and thermal properties of two PEX-e formulations, PEX-e1 and PEX-e2, produced using different additive compositions and slightly varied processing conditions. Both formulations achieved a high degree of crosslinking and elevated oxidation induction time (OIT) values, surpassing those of a commercial PEX-a pipe. Particularly, the PEX-e1 formulation exhibited a uniform distribution of crosslinks and mechanical properties comparable in magnitude to those of PEX-a [33]. These results highlight the potential of PEX-e materials for BTES applications. Building on these findings, the next step in assessing the suitability of PEX-e pipes for this application is to investigate their long-term stability under typical operating conditions.

Long-term stability is a critical consideration for BTES applications, as

the pipes are subjected to elevated temperatures and oxygen during operation. These conditions can accelerate thermo-oxidative degradation, leading to a loss of physical properties and potentially causing premature failure. Accordingly, antioxidants (AOs) additives are incorporated into the PEX formulation to inhibit or delay the formation of hydroperoxides, the key species driving degradation [123]. There are two main types of AOs commonly used: free radical scavengers (primary AOs) and hydroperoxide decomposers (secondary AOs) [63]. Among the primary AOs, sterically hindered phenols—such as octadecyl-3-(3,5-di-tert-butyl-4-hydroxyphenyl)propionate, known as Irganox 1076—are frequently used [62, 63]. Their stabilization mechanism relies on the H-donor nature of the phenol group, which can induce the termination of peroxyl radicals and prevent the formation of hydroperoxides [63]. However, during prolonged exposure to high temperatures, the active antioxidant molecules are gradually depleted, leaving the polymer susceptible to degradation [8].

This study investigates the thermo-oxidative degradation and stability of PEX-e pipes specifically designed for BTES applications. As documented in the literature, hot water, rather than hot air or pressure, is the primary factor driving AO depletion in PEX pipes used in hot-water applications [59]. Consequently, long-term ageing tests were conducted in water at the intended BTES service temperature of 90 °C. Two formulations, PEX-e1 and PEX-e2, were investigated alongside a commercial peroxide-crosslinked polyethylene (PEX-a) and non-crosslinked bimodal polyethylene (PE100) pipes to establish their relative performance. During the ageing protocol, samples were periodically removed and subjected to a comprehensive series of characterization techniques to evaluate AO content and elucidate degradation mechanisms at different stages. Surface changes were monitored using colorimetry, optical microscopy and Fourier-transform infrared (FTIR) spectroscopy, while cross-sectional slices from aged pipes were analyzed using both FTIR and nuclear magnetic resonance (NMR) spectroscopy. Additional characterizations included gel content analysis, differential scanning calorimetry (DSC), and OIT measurements. Dynamic mechanical analysis (DMA) was used to assess changes in mechanical properties.

4.2 Experimental

4.2.1 Materials

The four pipes analyzed in this study were provided by MuoviTech AB, Sweden. These comprised two experimental formulations of PEX-e, designated as PEX-e1 and PEX-e2; one commercial formulation of PEX-a; and a commercial bimodal HDPE pipe, PE100, which included a 2.5 wt% carbon black additive for UV stabilization. Different additive formulations and processing conditions were used to manufacture PEX-e1 and PEX-e2, although specific details were not disclosed. According to the supplier, PEX-e1 contained a higher concentration of primary AO compared to the other pipes. The dimensions and properties of these pipes in 'as received' condition were reported in our previous publication [33].

4.2.2 Ageing Protocol

Multiple pipe segments with 10-15 cm were immersed in distilled water at 90°C for 210 days in a Grant OLS Aqua Pro water bath. The water was refilled every 15 days to account for evaporation and to guarantee that the pipes remained completely immersed during the entire protocol. Samples were removed from the pipes periodically (0, 30, 60, 90, 150 and 210 days) and analyzed.

4.2.3 Characterization methods

The characterization methodology was divided into surface and bulk analyses, as illustrated in Figure 4.1. For surface analysis, small pipe segments were prepared using a pipe cutting tool. Cross-sectional rings were sectioned with a microtome, and smaller portions of these rings were trimmed with a knife as needed. After 210 days of the ageing protocol, rectangular specimens for DMA analysis were cut from the remaining pipe segments using a computer numerical control (CNC) machine. Details of the characterization methodologies and sample dimensions are provided in the following subsections.

4.2.3.1 Colorimetry

Color changes were measured using a Datacolor 500 Spectrophotometer equipped with a D65 illumination source, UV filter, and USAV aperture plates (6.5 mm illuminated, 2.5 mm measured). Samples with 8 × 4 cm (length × width) were analyzed. The measured spectral reflectance in the 400-

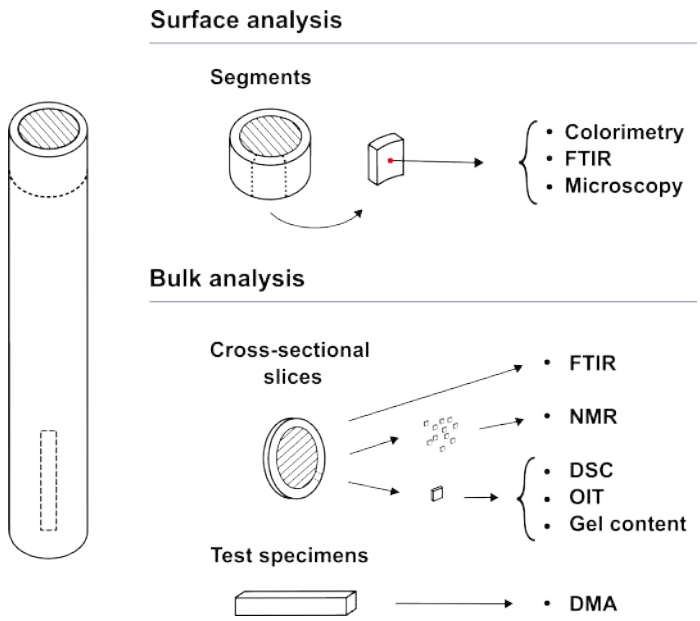

Figure 4.1: Schematics illustrating the sample preparation for surface and bulk analysis. (Drawings are not to scale).

700 nm range were reported using the three-dimensional CIE (International Commission on Illumination) color coordinate system, which quantifies color perception through three parameters: L (lightness), a (position on the red-green axis), and b (position on the blue-yellow axis). The values given by the software represented the average of five replicate measurements. The 'as received' samples (0 days) served as reference standards, against which other samples of the same pipe at varying ages were compared. The yellowness index (YI), that is often used to measure color development in polyolefins, was calculated from the L, a, b coordinates as per Equation 4-1 [124, 125]:

$$YI = 100\left(\frac{0.72a + 1.79b}{L}\right) \tag{4-1}$$

4.2.3.2 FTIR Spectroscopy

FTIR spectroscopy was employed to evaluate antioxidant additive content and identify chemical species generated during degradation. Measurements were taken from the inner surface of the pipe walls with three random samples analyzed per material to ensure reproducibility. Complementary analysis was performed on the center of cross-sectional slices (∼2 mm thickness) to evaluate potential additive diffusion from the bulk to the surface.

Spectra were recorded using a Thermo Fisher Nicolet iS50 spectrometer in ATR mode, covering the 4000–400 cm^{-1} range with 32 scans per spectrum at a resolution of 4 cm^{-1}. The background was collected between every

measurement to improve accuracy. For quantitative analysis, the FTIR data were pre-processed using baseline correction and normalization with an internal standard. The baseline correction was carried out in Python, following the procedure outlined in the previous publication [33]. The spectra was normalized by the absorbance of the crystal phase CH_2 scissoring vibrations at 1472 cm^{-1}, according to Xu et al. [63].

The carbonyl index (CI) was calculated by numerical integration of the area of the spectral region from 1775-1675 cm^{-1}, as per Equation 4-2 [33, 94]:

$$CI = \int_{1675}^{1765} A_x \, dx \tag{4-2}$$

where A_x is the normalized absorbance at wavenumber x after baseline correction. To isolate the effect of the ageing protocol, the relative carbonyl index was calculated by dividing the carbonyl index at a certain age (CI_t) by the carbonyl index of the unaged pipes CI_0 as per Equation 4-3.

$$relative\ CI = \frac{CI_t}{CI_0} \tag{4-3}$$

The standard deviation (SD) of the relative carbonyl index was calculated using the general formula for error propagation. When a property C is determined as the ratio of two variables, $C = A/B$, the standard deviation (SD_C) must account for the propagation of errors, as shown in Equation 4-4 [90].

$$SD_C = \sqrt{\left(\frac{SD_A}{A}\right)^2 + \left(\frac{SD_B}{B}\right)^2} \times C \tag{4-4}$$

4.2.3.3 Optical Microscopy

Optical microscopy was employed as a complementary method to FTIR spectroscopy, to confirm the presence or absence of AO crystals on the surface. The inside surface of the unaged pipes were analyzed in a Nikon Eclipse LV100ND with Nikon TU Plan Fluor 20X objective lenses. Images were obtained on reflection mode, with polarized light and in dark field mode.

4.2.3.4 Solid State Nuclear Magnetic Resonance

^{1}H static NMR was used to measure the chemical shift of the materials with ageing. The experiments were performed on a Bruker AVANCE-II spectrometer at 4.7 T magnetic field (^{1}H resonance at 200 MHz) using home-built NMR probe having strong rf pulse (90-degree pulse = 0.9 μs) and short dead

time. The NMR data were acquired using the a solid echo pulse sequence (90x -τ-90y - τ - acquisition), as detailed in our previous publication [33].

The experimental decay signal was decomposed into three components used for semicrystalline polymers: an Abragam function, a Weibullian function and an exponential function. This fitting procedure was performed in the "peak-o-mat" software (version 1.1.9) by using non-linear least squares regression.

The crystalline region is usually represented by the Abragam component, which is defined as combination of Gaussian and sine functions, as per Equation 4-5 [84–86]:

$$I = exp\left[-\left(\frac{t}{T_2^{short}}\right)^2\right]\frac{sin(Rt)}{Rt} \tag{4-5}$$

where I is the normalized magnetization intensity, R is a fitting parameter, t is the decay time and T_2^{short} is the fast decay rate.

The intermediate or interphase region between the crystalline and amorphous regions can be represented by a Weibullian function, ranging between a pure Lorentzian ($n = 1$) and a pure Gaussian ($n = 2$), as per Equation 4-6 [84–86]:

$$I = exp\left(\frac{-t}{T_2^{medium}}\right)^n \tag{4-6}$$

where T_2^{medium} is the intermediate decay rate. Lastly, the contribution of amorphous phase to the solid echo decay is represented by a exponential function [85], as per Equation 4-7:

$$I = exp\left(\frac{-t}{T_2^{long}}\right) \tag{4-7}$$

where T_2^{long} in the long decay rate.

^{13}C cross-polarization magic spinning angle (CPMAS) NMR was performed to identify formation of oxidation products and changes in molecular weight with ageing. The spectra were recorded on the same Bruker AVANCE-II spectrometer at 14.1 T magnetic field using a home built double resonance probe for magic-angle-spinning with 4×25 mm Si3N4 rotors. The spinning speed of the sample was 11.5 kHz. The duration of ramped CP pulse was 2 ms, the relaxation delay between accumulations was 5s and typically 16000 scans were accumulated. The spectra are given in TMS scale using the CH_2 peak of solid glycine at 43.63 ppm as external reference.

4.2.3.5 Gel Content

The degree of crosslinking in the aged samples was assessed by measuring the gel content through solvent extraction, following the procedure outlined in the ISO 10147:2012 standard. Samples were cut from (0.4 ± 0.1) cross-sectional slices. Two replicates were analyzed for each material at 210 days of ageing. To ensure a reliable comparison, the experimental procedure and apparatus were identical to those used for the unaged samples described in a previous publication [33].

4.2.3.6 Differential Scanning Calorimetry

DSC was performed to assess potential changes in melting and crystallization behavior of the materials with ageing. Samples with 9-10 mg weight were cut from approximately 2 mm cross-sectional slices and placed in aluminum pans. Two cycles were performed under a nitrogen flow of 50 mL/min on a TA Q2000 DSC equipment. In the first cycle, the samples were heated from 30°C to 230°C at 10 °C/min and maintained isothermal for 3 min. Then, for analysis of crystallization the samples were cooled down to 30°C at 10°/min, maintained at isothermal conditions for 3 min.

The analysis of the DSC data was performed on the TA Universal Analysis 2000 software. A macro script was created to automate and guarantee consistency in the choice of integration limits for the enthalpy calculations among the many samples analyzed. The degree of crystallinity (X_c) was calculated according to Equation 4-8:

$$X_c = \frac{\Delta H_m}{\Delta H_0} \times 100 \tag{4-8}$$

where ΔH_m is the fusion enthalpy of the sample and ΔH_0 is the equilibrium fusion enthalpy of PE crystals (281 ± 6 J/g) [88, 89]. Three replicates measurements were performed for each material/age and the standard deviation (SD) of X_c was calculated taking into account the error propagation, as per Equation 4-4.

The average lamellar thickness (l) was calculated based on Thompson-Gibbs equation [126, 127] as per Equation 4-9:

$$l = \frac{2\sigma_e T_{m0}}{\Delta H_{m0}.(T_{m0} - T_m)} \tag{4-9}$$

where σ_e is the surface free energy per unit area of basal face, ΔH_{m0} is the enthalpy of fusion per unit volume, T_{m0} is the equilibrium melting temperature of an infinitely thick crystal and T_m is the melting temperature of the sample

in Kelvin. The values used in the calculations were $\sigma_e = 60.9 \times 10^{-3}$ J/m^2, $\Delta H_{m0} = 2.88 \times 10^8$ J/m^3, and $T_{m0} = 414.6$ K [127, 128].

4.2.3.7 Oxidation Induction Time

Oxidation induction time (OIT) tests were were carried out using the same equipment as for the DSC analysis and followed the same sample preparation procedure. The samples at different ages were heated up to 200°C at 20 °C/min and kept isothermal for 5 min, when the gas was switched from nitrogen to oxygen. The temperature was maintained at 200 °C until the maximum exothermic peak was reached. The OIT values were determined as the time between the gas switch and the onset of oxidation.

4.2.3.8 Dynamic Mechanical Thermal Analysis

The mechanical properties of the pipes after 210 days of ageing were measured by dynamic mechanical thermal analysis (DMA) in a TA Q800 DMA equipment. Specimens with 35 mm length × 4 mm width × pipe thickness were cut from the pipes and deformed under flexure using a single cantilever arrangement, at a frequency of 1 Hz. Transitions were studied in a thermal scanning mode from -50 °C to 170 °C at a 3 °C/min rate. Three replicates were run for each material.

Consistent with our previous work [33], the average molecular weight between crosslinks (M_c) and effective crosslinking density (ν_c) were determined based on the storage modulus in the rubbery plateau region (at 160 °C). These calculations were performed using Equations 4-10 and 4-11, respectively [74, 75]:

$$M_c = \frac{2(1+\nu)\rho RT}{E'} \tag{4-10}$$

$$\nu_c = \frac{\rho}{M_c} = \frac{E'}{2(1+\nu)RT} \tag{4-11}$$

where E' is the storage modulus at the rubbery plateau, ν is the Poisson ratio ($\nu = 0.41$) [96], ρ is the density of the amorphous polymer ($\rho = 0.850$ g/cm^3) [50, 97], R is the gas constant and T is the absolute temperature.

At temperatures above their melting point, semicrystalline polymers become fully amorphous. In this state, the storage modulus decreases and stabilizes at a minimum value known as the rubbery plateau. The storage modulus in this region reflects the molecular weight between physically effective crosslinks, including both entanglements and chemical crosslinks [74]. For

polyethylene, this plateau typically appears above 150 °C. Consequently, E' measured at 160 °C was used to calculate M_c and ν_c for all samples.

4.3 Results and discussion

4.3.1 Surface analysis

4.3.1.1 FTIR: Antioxidant content and oxidation products

The oxidation process of polyethylene (PE) has been extensively studied and well-documented in the literature [5, 6, 8, 11, 56]. This process begins with the formation of alkyl radicals, initiated either by hydrogen abstraction or chain cleavage. These radicals react with oxygen to form peroxy radicals, which, in turn, abstract hydrogen atoms from the polyethylene backbone, leading to the formation of hydroperoxides [5, 11]. Due to their inherent instability, hydroperoxides decompose into alkoxy and hydroxyl radicals. These highly reactive species can further abstract hydrogen atoms from neighboring polymer chains, initiating branching reactions and resulting in the production of additional alkyl radicals that perpetuate the degradation process [5, 56]. Termination of occurs through recombination and disproportionation reactions, which can result in crosslinking, the formation of unsaturated vinyl groups, or the generation of carbonyl compounds such as ketones, aldehydes, and carboxylic acids [94, 129].

In polymers stabilized with antioxidant (AO) additives, the propagation of free-radical reactions is significantly slowed or almost entirely halted. During the initial stages of ageing, active AO molecules are chemically consumed and/or can leach from the pipe through hydrolysis and diffusion [59]. As long as active AO molecules are present, substantial polymer degradation is not expected in the bulk. However, surface oxidation has been reported before the complete depletion of active AO molecules [8, 33].

To monitor the consumption of AO additives and the formation of oxidation products in the pipes over time, FTIR-ATR spectroscopy was performed on the inner surface of the pipes. Figure 4.2 illustrates the main changes detected in the FTIR spectra of the PEX-e1 pipe with ageing time. In line with our previous findings [33], carbonyl peaks (C=O) at 1739 cm^{-1}, 1733 cm^{-1}, 1719 cm^{-1} and 1699 cm^{-1} were detected on the unaged PEX-e1 surface. These peaks were initially assigned as ester, aldehyde, ketone and carboxylic acid, respectively. The ester absorbance was linked to the presence of phenolic

AO additives and was particularly consistent with the spectra reported for Irganox 1076 [8, 62]. The remaining carbonyl groups were attributed to pre-oxidation during the pipe manufacturing process [33].

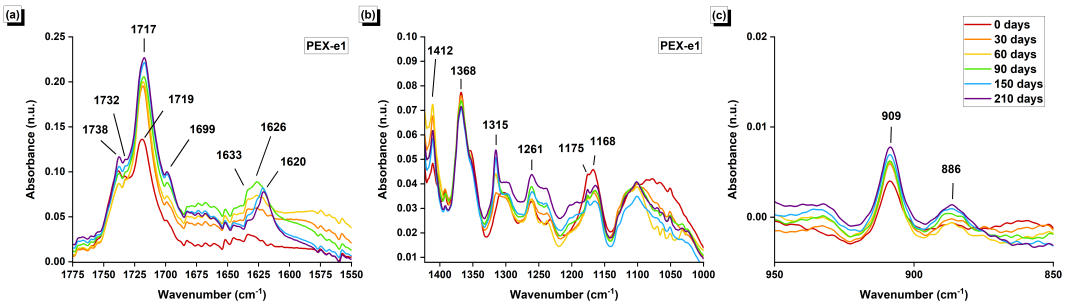

Figure 4.2: Evolution of the FTIR spectra of PEX-e1 surface during thermal-oxidative ageing: (a) between 1775 and 1550 cm^{-1}, (b) between 1420 and 1000 cm^{-1}, and (c) between 950 and 850 cm^{-1}. The color legend applies to all graphs.

Significant changes in the carbonyl region were observed following the ageing protocol, as shown in Figure 4.2.a. During the initial phase, a slight decrease was observed in the ester carbonyl absorbance at 1739 cm^{-1}, likely due to the chemical consumption of the primary antioxidant (AO) [8, 63] and/or hydrolysis of AO ester linkages by prolonged exposure to hot water [13, 59]. This reduction in AO content is further supported by the decreased intensity of the ester C-O symmetric stretching bands at 1175 and 1168 cm^{-1}, along with the asymmetric stretching band around 1060 cm^{-1}.

After 60 days, however, the ester absorbance began to gradually increase, with a minor peak shift to 1738 cm^{-1}. This increase might be attributed to either (1) ester formation from oxidative degradation of polyethylene or (2) to the diffusion of AOs from the bulk to the pipe surface. A similar trend was noted for the 1732 cm^{-1} peak, which decreased slightly over the first 30 days before showing a slight intensification. This behavior suggests that the 1732 cm^{-1} peak may be associated with ester groups from either a second ester-containing stabilizing additive [59] or crystallized AO on the pipe surface [62], rather than aldehyde groups resulting from polymer oxidation, as previously proposed.

Hindered phenols, due to their polarity, exhibit limited solubility in polyethylene, making supersaturation likely in industrially formulated polyolefins [63]. At processing temperatures (melt state), AOs are generally highly soluble in polyethylene. However, during cooling, as solubility decreases with temperature, the polymer can quickly become supersaturated with AOs. This excess AO content can lead to phase separation and surface segregation through exudation, resulting in the crystallization of AO on the polymer sur-

face [62]. This phenomenon has been documented in the literature for PEX-b films [62, 63], where phase separation was observed at ambient temperature above an AO concentration threshold of approximately 0.9 wt%. In these cases, excess AO formed crystals on the surface of the samples. Ester groups within these AO crystals were detected at 1733 cm^{-1}, while ester groups from dissolved AO were observed at 1740 cm^{-1} [62].

Although the exact AO concentration in the pipes investigated here is unknown, the presence of AO crystals was confirmed by optical microscopy. As shown in Figure 4.3, AO crystals were observed on the surface of all investigated pipes. Notably, the PEX-e1 surface exhibited a greater number and larger size of crystals, consistent with its comparatively higher concentration of AOs. In contrast, no crystals were found on the surface of the pipes after 210 days of ageing.

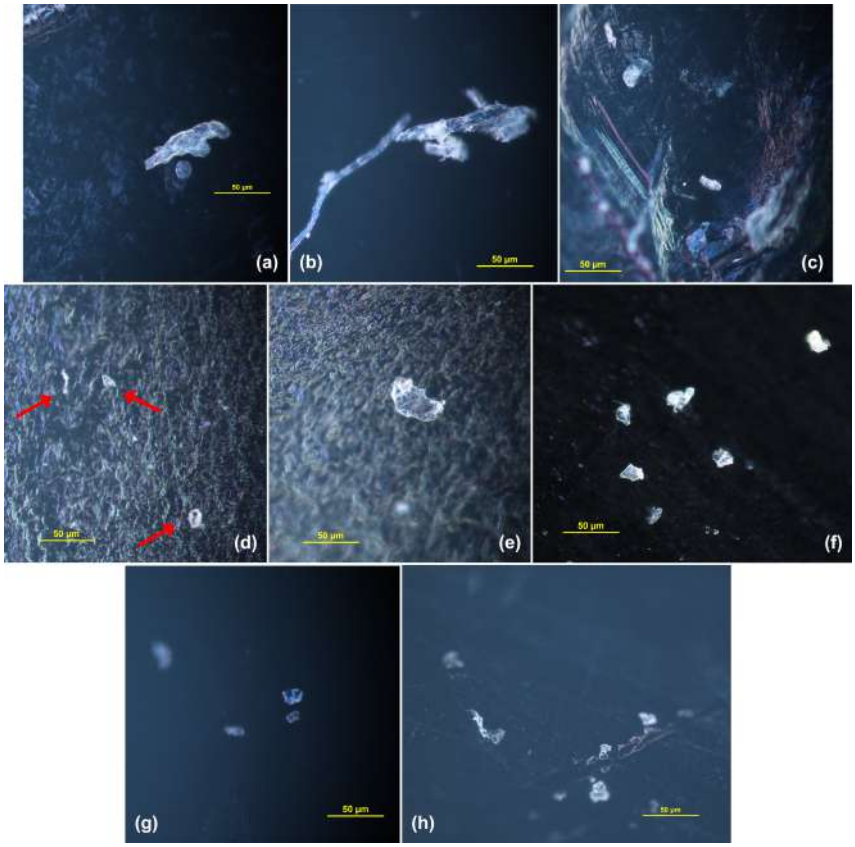

Figure 4.3: Micrographs of the surface of the unaged (a)-(c) PEX-e1; (d)-(e) PEX-e2; (f) PE100; and (g)-(h) PEX-a pipes. Images obtained in dark field with 20× objective lens.

The peaks at 1719 cm^{-1} and 1699 cm^{-1} increase consistently throughout the ageing period, with the 1719 cm^{-1} peak slightly shifting towards 1717 cm^{-1} by 150 days. This pattern aligns with the formation of oxidation products, specifically ketones and carboxylic acids, from oxidation reactions on the

polymer backbone [13, 94]. Additionally, the hydrolysis of AO ester linkages has also been associated to the formation of carboxylic acids [59]. It is noteworthy that, the ketone peak was detected at a slightly lower wavenumber in the other pipes (around 1714 cm^{-1}), thus the very intense 1717 cm^{-1} might be a result of overlapped absorptions.

During exposure to oxidative environments, carbonyl groups can be also generated as a consequence of the chemical consumption and ageing of phenolic AOs. The main products of phenolic AO oxidation are quinoidal compounds, which absorption peaks can be observed in the region between 1650 cm^{-1} and 1590 cm^{-1} [8]. Notably, a band characteristic of quinone methides have been reported to appear at 1633 cm^{-1} during thermal degradation of PEX-b stabilized with Irganox 1076 [63]. Similarly, a band at 1633 cm^{-1} was detected on the unaged PEX-e1 sample and continued to intensify up to 90 days, after which it diminished. The formation of quinone methides aligns with the yellowing effect reported in Section 4.3.1.2.

New bands appeared around 1626 cm^{-1} after 30 days of ageing, with their intensity steadily increasing up to 90 days. This indicates the formation of unsaturated (C=C) vinyl groups, which was confirmed by the increased in the absorbance of the 909 cm^{-1} and 886 cm^{-1}, attributed to the formation of vinyl and vinylidene groups, respectively [14, 60, 108, 129]. After 150 days, however, a shift was observed: the bands near 1626 cm^{-1} decreased, and a sharp peak emerged at 1620 cm^{-1} instead, suggesting further molecular changes occurred with prolonged ageing.

New bands also appeared/increased in the 1350-1240 cm^{-1} region, corresponding to C-O stretching of alcohols (1150-1050 cm^{-1}) and carboxylic acids (1320-1070 cm^{-1}) [63, 108]. A slight decrease was observed on the 1368 cm^{-1} peak, attributed to the -C-H bend vibrations.

Similar patterns were observed in the surface FTIR spectra of the PEX-e2 (Figure 4.4) and PEX-a (Figure 4.5) pipes, although the changes were less pronounced. Significant increases were noted in the peaks at 1722 cm^{-1} and 1714 cm^{-1}. The latter corresponds to the formation of ketone groups [108], while the band at 1722 cm^{-1} is attributed to cinnamate species resulting from the degradation of phenolic antioxidants. Xu et al. [63] similarly identified a hydroxycinnamate peak near 1720 cm^{-1} after the thermal ageing of PEX-b stabilized with Irganox 1076.

The evolution of carbonyl peaks on the surface of PE100 pipes over ageing time (Figure 4.6) showed a slightly different pattern compared to the PEX pipes. Multiple carbonyl peaks were present in unaged pipes, and all peaks increased steadily with ageing up to 150 days, after which a slight

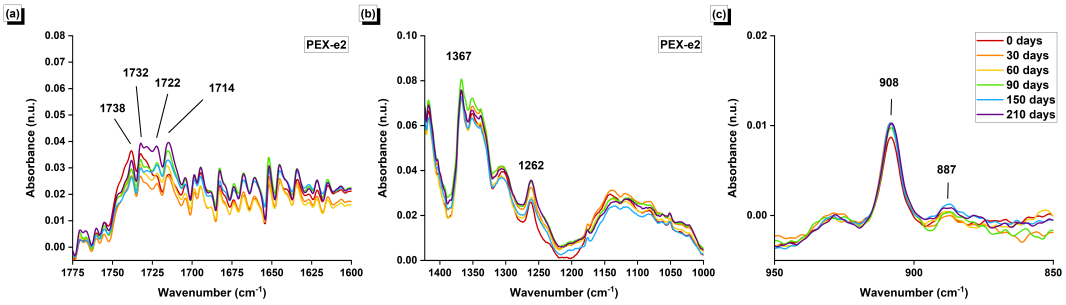

Figure 4.4: Evolution of the FTIR spectra of PEX-e2 surface during thermal-oxidative ageing: (a) between 1775 and 1600 cm^{-1}, (b) between 1420 and 1000 cm^{-1}, and (c) between 950 and 850 cm^{-1}.

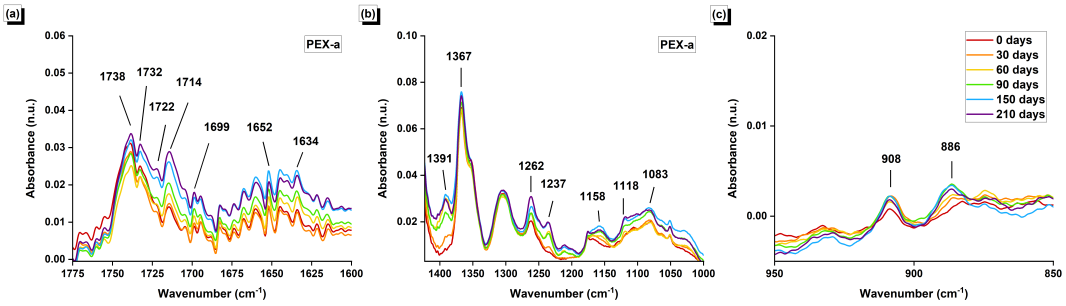

Figure 4.5: Evolution of the FTIR spectra of PEX-a surface during thermal-oxidative ageing: (a) between 1775 and 1600 cm^{-1}, (b) between 1420 and 1000 cm^{-1}, and (c) between 950 and 850 cm^{-1}.

decrease was observed. Among the pipes studied, PE100 exhibited the most significant changes in the 1400–1000 cm^{-1} region, with all peaks intensifying and new peaks emerging, suggesting the formation of esters, carboxylic acids, and alcohols [59, 63, 108]. In the 950–850 cm^{-1} region, substantial variation was observed across different ageing times. Overall, peaks at 933 cm^{-1}, 908 cm^{-1}, and 887 cm^{-1} increased, indicating the formation of vinyl groups.

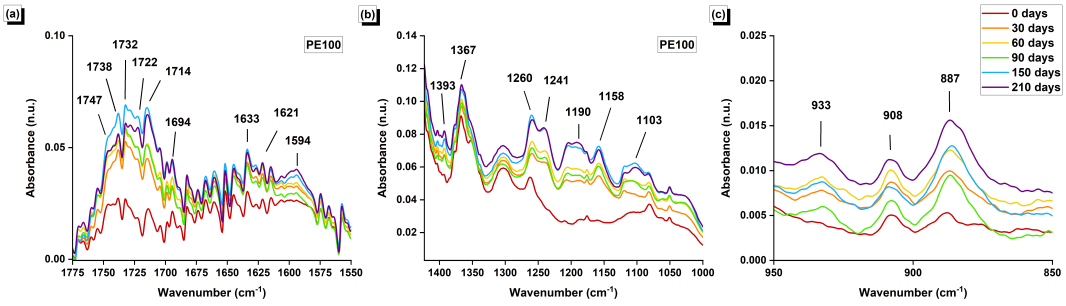

Figure 4.6: Evolution of the FTIR spectra of PE100 surface during thermal-oxidative ageing: (a) between 1775 and 1550 cm^{-1}, (b) between 1420 and 1000 cm^{-1}, and (c) between 950 and 850 cm^{-1}.

To compare changes in the carbonyl region across the different pipes, the carbonyl index was calculated using Equation 4-2, and the results are

presented in Figure 4.7.a. Notably, the carbonyl index of unaged PEX-e1 was significantly higher than that of the other pipes. this was consistent with our previous findings [33] and were attributed to the higher AO content and the presence of oxidation products generated during pipe manufacturing.

To isolate the effect of the ageing protocol on the carbonyl region, the relative carbonyl index was calculated using Equation 4-3. This index normalizes the carbonyl index at each ageing stage to the values of the unaged pipe (0 days). The results, shown in Figure 4.7.b, indicate that while the overall carbonyl index was higher for PEX-e1, the ageing protocol had a significantly greater impact on the surface of PE100. Among the PEX samples, PEX-e1 exhibited the highest formation of carbonyl groups during ageing, whereas PEX-e2 showed the least change on its inner surface.

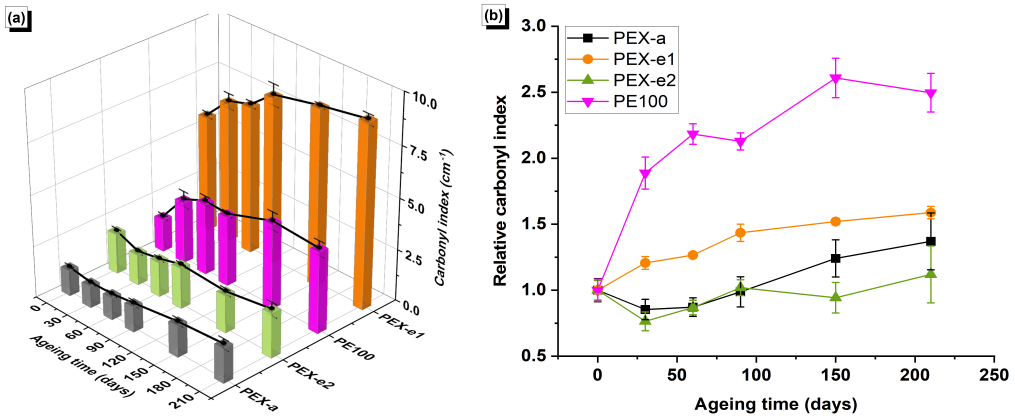

Figure 4.7: Changes in (a) total carbonyl index and (b) relative carbonyl index over ageing time for the four pipes. Uncertainties represent the standard deviation calculated from three replicate measurements.

4.3.1.2 Colorimetry: Yellowing effect

Polyolefin degradation is frequently associated with progressive color changes over ageing time [123, 124, 130–135]. In the present study, significant shifts towards the color yellow were observed as the PEX pipes aged, as illustrated by the samples shown in Figure 4.8. This color variation was quantified throughout the ageing process using colorimetry and the resulting yellowness index (Equation 4-1) is shown in Figure 4.9. The color maps for each pipe are provided in Section A.3.

The PE100 pipe demonstrated minimal changes in the yellowness index (less than 0.15) even after 210 days. This color stability may result from the presence of the carbon black additive in this pipe, which gives it a dark color, likely concealing any potential yellowing. In contrast, the PEX pipes,

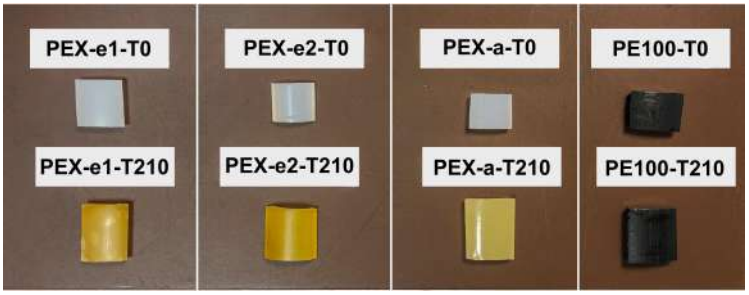

Figure 4.8: Comparison of the color difference between the unaged pipe samples (T0) and pipe samples after 210 days of ageing (T210).

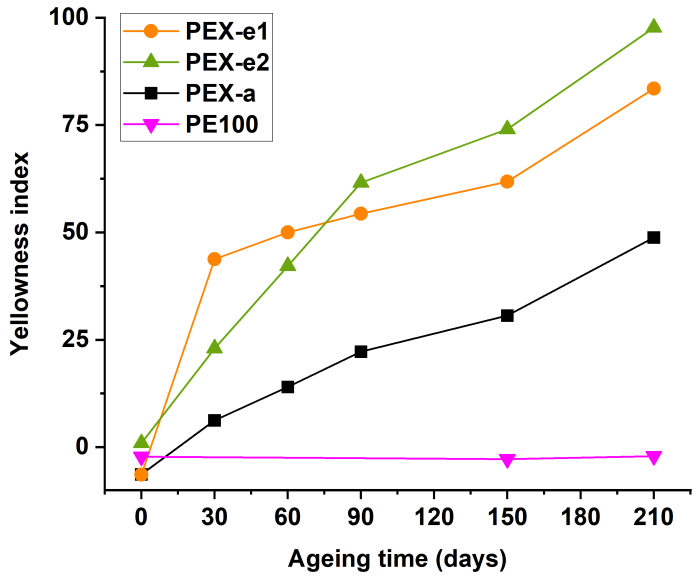

Figure 4.9: Yellowness index over ageing time for the pipes. Average values determined from five replicate measurements.

particularly PEX-e, showed a significant increase in yellowness index over time. Yellowing was more pronounced in PEX-e1 during the first 60 days but became more prominent in PEX-e2 after 90 days.

Two primary factors contribute to color development in polyolefins during ageing. The first is structural inhomogeneities and impurities that absorb UV-VIS light [131, 135]. The second is the formation of by-products from stabilization processes involving AO stabilizers [123, 135]. These by-products result from reactions of hindered phenolic AOs, which trap alkylperoxy radicals that would otherwise accelerate polymer oxidation. Certain transformation products, particularly conjugated and unconjugated quinoidal compounds such as quinone methides, can cause significant discoloration and yellowing in polyolefins [123, 135]. The degree of color variation depends on both the structure and concentration of these phenolic transformation products [135]. This explanation aligns with FTIR analysis, which detected peaks characteristic of quinone methides on the pipe surfaces.

4.3.2
Bulk analysis

4.3.2.1
OIT: Antioxidant performance and thermal-oxidative stability

Oxidation induction time (OIT) measurements were conducted on the aged samples to evaluate the AO performance and assess the oxidative stability of the pipes over the ageing period. Samples were cut from the cross-section of the aged pipes, following the schematics shown in Figure 4.1, to obtain an average OIT value representative of the pipe bulk. The evolution of OIT values over ageing time is presented in Figure 4.10.

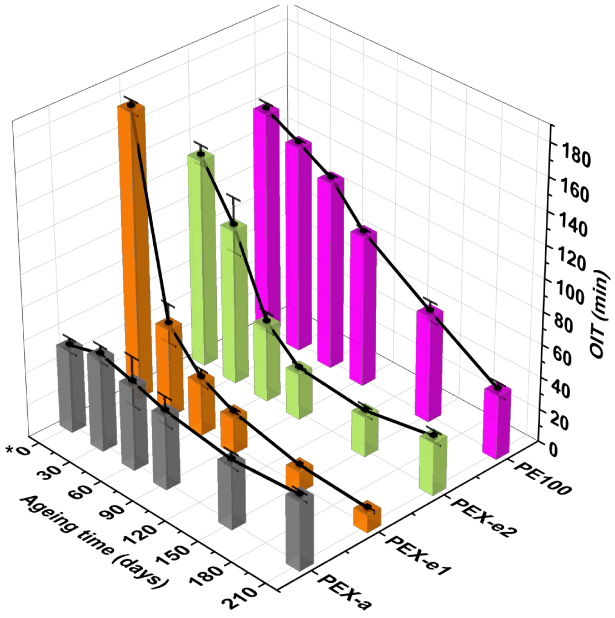

Figure 4.10: Evolution of OIT values for (a) PEX-e1, (b) PEX-e2, (c) PEX-a and (d) PE100 pipes over time. *Results for unaged pipes (0 days) were sourced from [33]. Average and standard deviation calculated from five replicate runs.

An intriguing trend was observed for PEX-e1: while this pipe initially exhibited the highest OIT, it experienced a exponential decline throughout the ageing protocol, with a 69% reduction after 30 days and reaching a 94% reduction by 210 days of ageing. A similar exponential decrease was observed for PEX-e2, although at a slower rate, showing a 25% decrease within the first 30 days and reaching a 75% reduction by 210 days. PE100 exhibited an approximately linear decrease throughout the ageing protocol, culminating in a 71% reduction of its initial value by 210 days. Remarkably, PEX-a, despite starting with a significantly lower initial OIT value, showed no statistically significant changes in OIT throughout the ageing protocol (p-value > 0.05), indicating superior thermal-oxidative stability compared to the other pipes.

Overall, the OIT results indicate that AO depletion occurred at a significantly faster rate in the PEX-e1 compared to the other pipes. This rapid AO depletion in PEX-e1 bulk was further corroborated by FTIR and NMR spectroscopy (see Sections 4.3.2.2 and 4.3.2.3) and it is likely due to a suboptimal stabilizer additive package. However, the similar pattern observed in both PEX-e pipes suggests that factors inherent to the photo-crosslinked morphology may also play a critical role in AO depletion.

4.3.2.2 FTIR: Antioxidant content

The surface analysis of the PEX pipes revealed a distinct pattern throughout the ageing process. In the early stages, the absorbance bands corresponding to ester groups decreased, likely due to AO depletion. However, after approximately 60 days of ageing, these bands began to gradually increase. As discussed, this subsequent increase can be attributed to either (1) the formation of esters as a result of the oxidative degradation of polyethylene or (2) the diffusion of antioxidants from the bulk material to the pipe surface.

To further explore the possibility of AO diffusion, FTIR-ATR spectra were measured on cross-sectional slices of the PEX and PE100 pipes. The evolution of the carbonyl peaks over ageing time is shown in Figure 4.11. In the cross-section of the unaged PEX-e1 sample (Figure 4.11.a), a single peak at 1740 cm^{-1} was observed, corresponding to the ester absorbance of dissolved Irganox 1076 AO. Over time, this peak steadily decreased, supporting the hypothesis of AO diffusion from the center of the pipe wall towards the surface.

An interesting comparison can be made between the surface (Figure 4.2) and cross-sectional (Figure 4.11) spectra of PEX-e1. While two ester absorbance peaks were detected on the surface, the presence of only a single ester peak in the cross-section suggests that the AO within the bulk material was fully dissolved and no second phase was formed in the bulk. Furthermore, the oxidation products observed on the surface of the unaged PEX-e1 sample were absent in the unaged cross-section. This suggests that the pre-oxidation that occurred during processing was confined to the surface layer.

After 90 days of the ageing protocol, a small peak emerged at 1715 cm^{-1} in the PEX-e1 cross-section, corresponding to the formation of ketone carbonyls. This indicates that oxidation had begun to occur at the pipe's center, although the extent of oxidation in the central region remained significantly lower than that observed on the surface.

Two ester absorbances were detected on the cross-section of PEX-e2 (Figure 4.11.b) at 1739 cm^{-1} and 1732 cm^{-1}. The latter suggest either a second

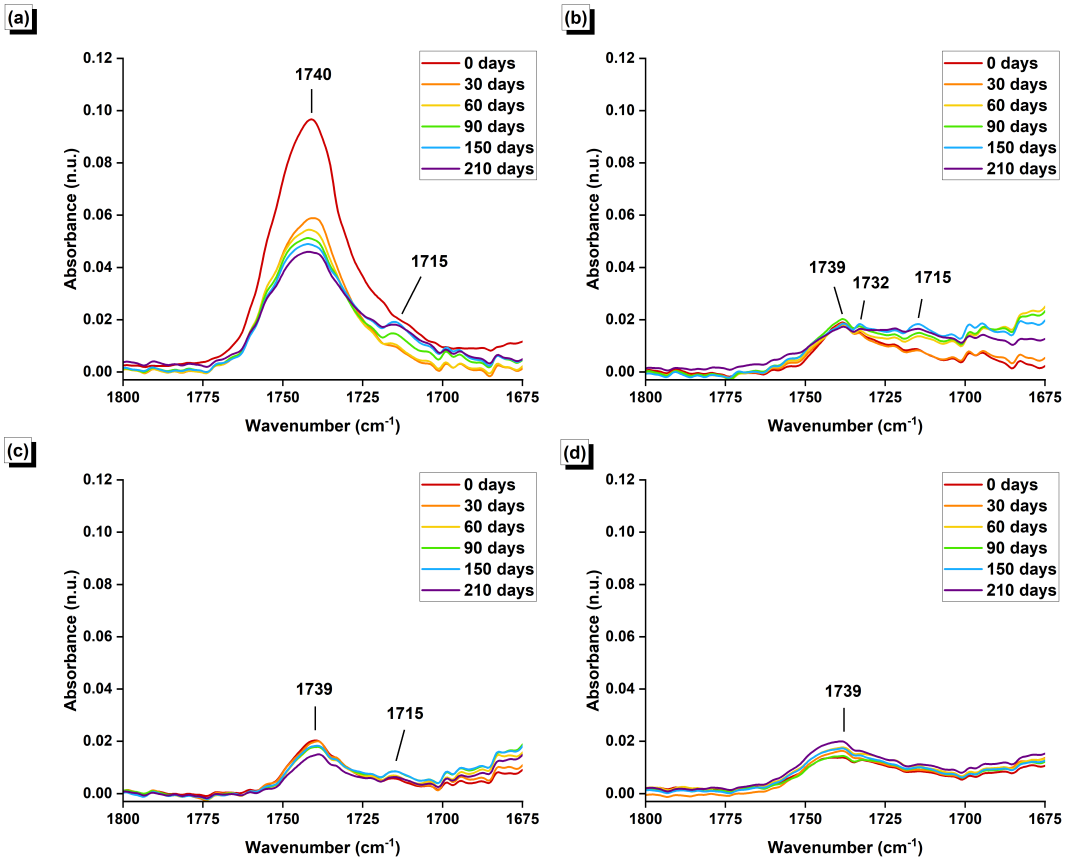

Figure 4.11: Evolution of the carbonyl region in FTIR spectra for the cross-sections of (a) PEX-e1, (b) PEX-e2, (c) PEX-a, and (d) PE100 during thermal-oxidative ageing. Average curve calculated from three replicate measurements.

ester-containing stabilizing additive [59] or the formation of a secondary phase due to AO supersaturation [62]. Additionally, an increase in the ketone peak at 1715 cm^{-1} after 60 days of ageing indicates the formation of oxidation products within the pipe bulk at this stage.

For PEX-a and PE100, a single ester peak at 1739 cm^{-1} was observed in the cross-section. However, changes in the carbonyl region during ageing were significantly less pronounced compared to PEX-e1. To get better insights into the evolution of AO concentration during ageing, Figure 4.12 presents a comparison of the normalized absorbance of ester peaks at the surface and the cross-section over time.

In PEX-e1, a significant reduction in bulk ester content was observed within the first 30 days of ageing, aligning closely with the exponential decrease in OIT measured in the bulk of this pipe (see Section 4.3.2.1). On the surface, however, the ester content exhibited a different pattern: it initially decreased but began to increase after 90 days. This behavior suggests the simultaneous occurrence of two processes during the ageing protocol: (1) depletion of primary AO due to chemical consumption and/or hydrolysis and (2) diffusion of AO

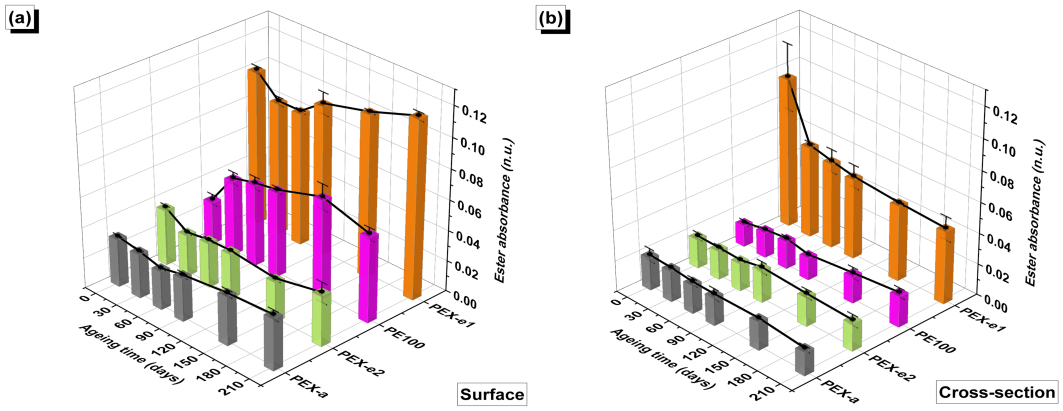

Figure 4.12: Comparison of the ester absorbance (detected at 1740-1738 cm^{-1}) in FTIR spectra of the (a) surface and (b) cross-section of the pipes during thermal-oxidative ageing. Uncertainties represent the standard deviation calculated from three replicate measurements.

from the pipe's bulk towards the surface.

Interestingly, this phenomenon was exclusive to PEX-e1. As shown in Figure 4.12.b, changes in ester absorbance across the cross-section of PEX-e2 were not statistically significant. Similar patterns were observed in the other pipes, with PEX-a showing only a minor decrease in cross-sectional ester content after 210 days of ageing.

For PE100, no significant changes were observed in the cross-section. However, a notable increase in ester groups on the surface suggests a distinct trend compared to PEX-e1. While changes in PEX-e1 were primarily driven by AO depletion/diffusion, the combined analysis of surface and bulk data indicates that the increase in ester absorbance for PE100 was primarily due to the formation of ester groups resulting from the oxidative degradation of polyethylene.

The stability of AO concentration in the cross-sections of PEX-a, inferred from the relatively unchanged normalized ester absorbance, is consistent with the OIT results reported in section 4.3.2.1. However, this is not the case for PEX-e2 and PE100, which showed significant reduction in OIT with ageing time, but relatively stable ester concentration in the bulk. Several factors may explain this discrepancy:

1. Measurement scope: The FTIR-ATR measurements were focused on the central region of the cross-sectional slices, while the OIT analysis considered samples spanning the entire cross-section. Consequently, OIT results represent an averaged measure of bulk stability, whereas FTIR-ATR provides a localized analysis of ester content. To complement this localized approach, the averaged bulk ester content was further analyzed

using ^{13}C NMR spectroscopy (see Section 4.3.2.3).

2. Measurement sensitivity: The concentration of primary AOs in these pipes is very low, likely on the order of 1 wt%. Consequently, the intensity of ester peaks is minimal compared to that of polyethylene peaks, reducing the sensitivity of FTIR-ATR in detecting potential changes. In contrast, PEX-e1, which has a higher AO concentration, exhibited more detectable changes in ester absorbance.

3. Additive interactions: OIT values are influenced not only by the concentration of primary AOs but also by the performance of the entire additive package [33]. The observed OIT decline in these pipes may therefore reflect the depletion of other stabilizing additives included in their formulations, rather than primary AO depletion alone.

4.3.2.3 ^{13}C NMR: Antioxidant content, oxidation products and molecular weight

To complement the FTIR analysis, ^{13}C CPMAS NMR spectroscopy was used to monitor the ester content and detect the potential formation of oxidation products within the bulk of the pipes. Furthermore, ^{13}C CPMAS NMR provided insights into changes in molecular weight associated with the ageing process. For this analysis, samples were prepared from cross-sectional slices of unaged pipes (0 days) and pipes aged for 150 and 210 days.

The ^{13}C CPMAS NMR spectrum of unaged PEX-e1 is shown in Figure 4.13.a. Upon vertical expansion of the spectrum, small peaks characteristic of carbonyl, vinyl, and methyl groups became visible and were identified as shown in Figure 4.13.b. The spectra for all pipes, both before and after ageing, are provided in Section A.3.

Three distinct peaks were observed in the 5–20 ppm region of the PEX-e1 spectra, corresponding to various carbon environments in the polymer. The peak at approximately 15 ppm was attributed to terminal methyl groups in the main chain, while the peak at 11 ppm was assigned to methyl groups in ethyl branches attached to secondary carbons [101, 136]. A third peak, located around 8 ppm, was associated with methyl groups in ethyl branches bonded to quaternary carbons.

Ester groups were also detected in the PEX-e1 spectra. The resonance of ester OCH_2 groups was detected around 67 ppm, while the ester carbonyl carbon appeared in the 170–175 ppm range [101]. Additionally, a peak corresponding to carboxylic acid carbonyl groups was observed in the same region [101]. Ketone groups were not detected in any of the pipes spectra, likely due

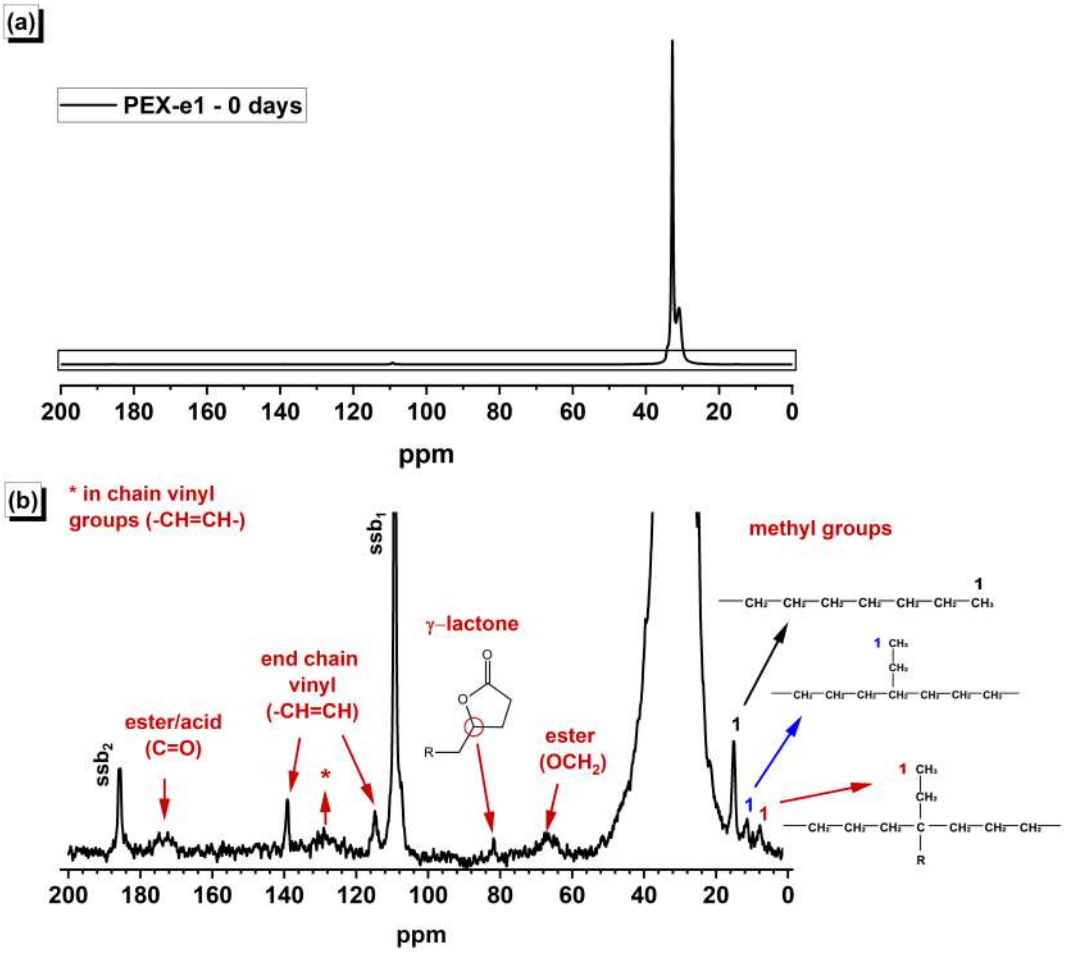

Figure 4.13: ^{13}C CPMAS NMR spectra of unaged PEX-e1 pipe: (a) full spectra and (b) vertical expansion of the spectra highlighting peak assignments for carbonyl, vinyl and methyl groups. ssb_1 and ssb_2 are spinning sidebands at ν_{MAS} and $2 \times \nu_{MAS}$ from the main chain CH_2 peak around 30 ppm.

to poor CP efficiency. A γ-lactone group was detected at approximately 82 ppm in PEX-e1 and PEX-e2 spectra. Since this group was hardly detected for the other pipes and its concentration did not vary significantly with ageing, it is likely due to a by-product of the photo-crosslinking process.

Peaks corresponding to unsaturated carbons were also identified. Small peaks assigned to main-chain vinyl groups ($-CH = CH-$) were detected around 129 ppm. End-vinyl groups ($-CH = CH$) produced more prominent peaks, with the CH_2 carbon resonating at 115 ppm and the CH carbon appearing at 139 ppm.

The groups identified in the spectra of all pipes were quantified by measuring their peak areas and normalizing these values against the main chain polyethylene (PE) area between 10 and 50 ppm. The resulting data were expressed as the number of groups per 1000 main chain carbons, as presented in Table 4.1. Although CP MAS NMR is not strictly quantitative it is assumed

that in similar types of materials, as examined here, the cross polarisation dynamics are similar for the different chemical groups between samples. This means that while the number of groups per 1000 main chain carbons may not be absolutely quantitative, the relative amounts per 1000 carbons between samples can be compared.

Table 4.1: Number of groups per 1000 main chain carbons calculated from the peak areas in the ^{13}C CPMAS NMR spectra of the pipes. (Values not specified were below detection threshold).

Material	Age (days)	Main chain vinyl	End vinyl	γ-lactone (OCH_2)	Ester branches	Ethyl
PEX-e1	0	0.24	0.37	0.16	0.78	0.26
	150	0.20	0.38	0.12	0.45	0.41
	210	0.25	0.38	0.17	0.50	0.36
PEX-e2	0	0.23	0.34	0.11	0.30	-
	150	0.27	0.39	0.12	0.28	-
	210	0.18	0.38	0.08	0.26	-
PEX-a	0	0.12	0.17	0.06	0.18	-
	150	0.12	0.18	-	0.22	-
	210	0.13	0.16	-	0.19	-
PE100	0	-	0.13	-	-	0.95
	150	-	0.07	-	-	0.70
	210	0.09	0.15	-	0.10	0.89

Analysis of the number of ester groups over ageing time indicated a significant decrease in AO in the bulk of PEX-e1 after 210 days. This finding aligns with the OIT and FTIR results. For PEX-e2, a very slight decrease in ester groups was observed, while for PEX-a the number of ester groups fluctuated among aged samples. However, caution must be taken when interpreting the small changes observed for PEX-e2 and PEX-a, as these variations can be due to experimental error and/or to a heterogeneous distribution of AO inherent of the pipes. For PE100, ester groups were not detectable in the unaged and 150 days aged samples, while a small amount of ester groups was detected in 210 days sample. These results corroborate to the FTIR analysis that revealed the formation of ester groups in PE100, resulting from the oxidative degradation of polyethylene.

Figure 4.14 shows the number average molecular weight (M_n) of the samples at different ages. As discussed above, the CPMAS NMR spectra are not strictly quantitative but peak areas between samples can be compared semi quantitatively. Since there is no long chain branching in the samples studied here, the methyl end group (peak 1 around 15 ppm) can be compared with the total main carbon chain area 0-50 ppm to calculate an approximate number average molecular weight (M_n). This calculated M_n may not be absolutely correct but the values obtained can be compared between the different samples. A comparison of CPMAS and direct excitation MAS NMR spectra (presented in Section A.3) showed that the amorphous component of the main chain CH_2 groups is somewhat underestimated in the CPMAS NMR spectra. Therefore

all the M_n values calculated here are most likely lower than the true values, but can be used comparatively.

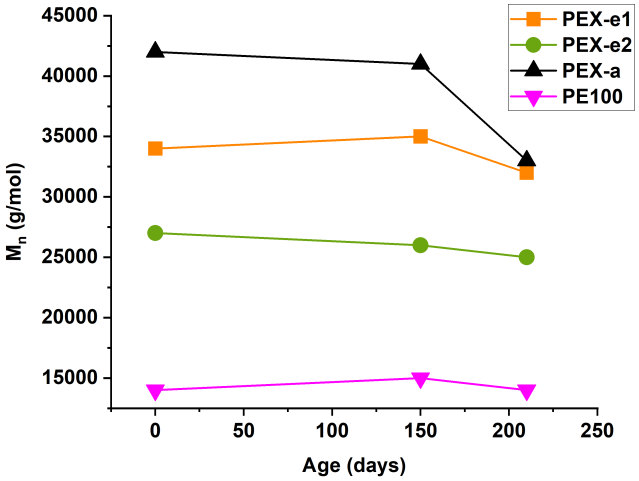

Figure 4.14: Evolution of the number average molecular weight (M_n) over ageing time.

Among the unaged pipes, a significant difference in molecular weight was observed, following the order: PEX-a > PEX-e1 > PEX-e2 > PE100. The substantially lower molecular weight of PE100 compared to the PEX pipes can be attributed to the HDPE base material used. The HDPE resin used for manufacturing PE100 pipes has a bimodal molecular weight distribution [95], whereas PEX pipes are typically manufactured from polyethylene with a narrower molecular weight distribution.

After 210 days of ageing, a decrease in molecular weight was observed for all PEX pipes, indicating that chain scission was the predominant degradation mechanism at this stage. This effect was more accentuated for PEX-a, with a 21% decrease from its initial value (unaged sample). While PEX-e1 and PEX-e2 exhibited a 6% and 7% reduction. This suggests that the morphology of PEX-e is less prone to chain scission compared to PEX-a.

4.3.2.4 ^{1}H NMR: Phase composition and molecular mobility

To further investigate the degradation mechanism, static ^{1}H NMR experiments were conducted on the aged pipe samples. The solid-echo decay was modeled using three components: rigid, intermediate, and mobile, which correspond to the crystalline phase, interphase, and amorphous phase, respectively. Analysis of the proportions of these components, along with the effective transverse relaxation times (T_2^{rigid}, T_2^{inter}, and T_2^{mobile}) provides valuable insights into potential changes in phase content and molecular mobility during ageing [70]. The solid-echo decay data for all samples, along with detailed tables of

the fitting parameters, are included in Section A.3. A summary of the fitting results is presented in Figure 4.15.

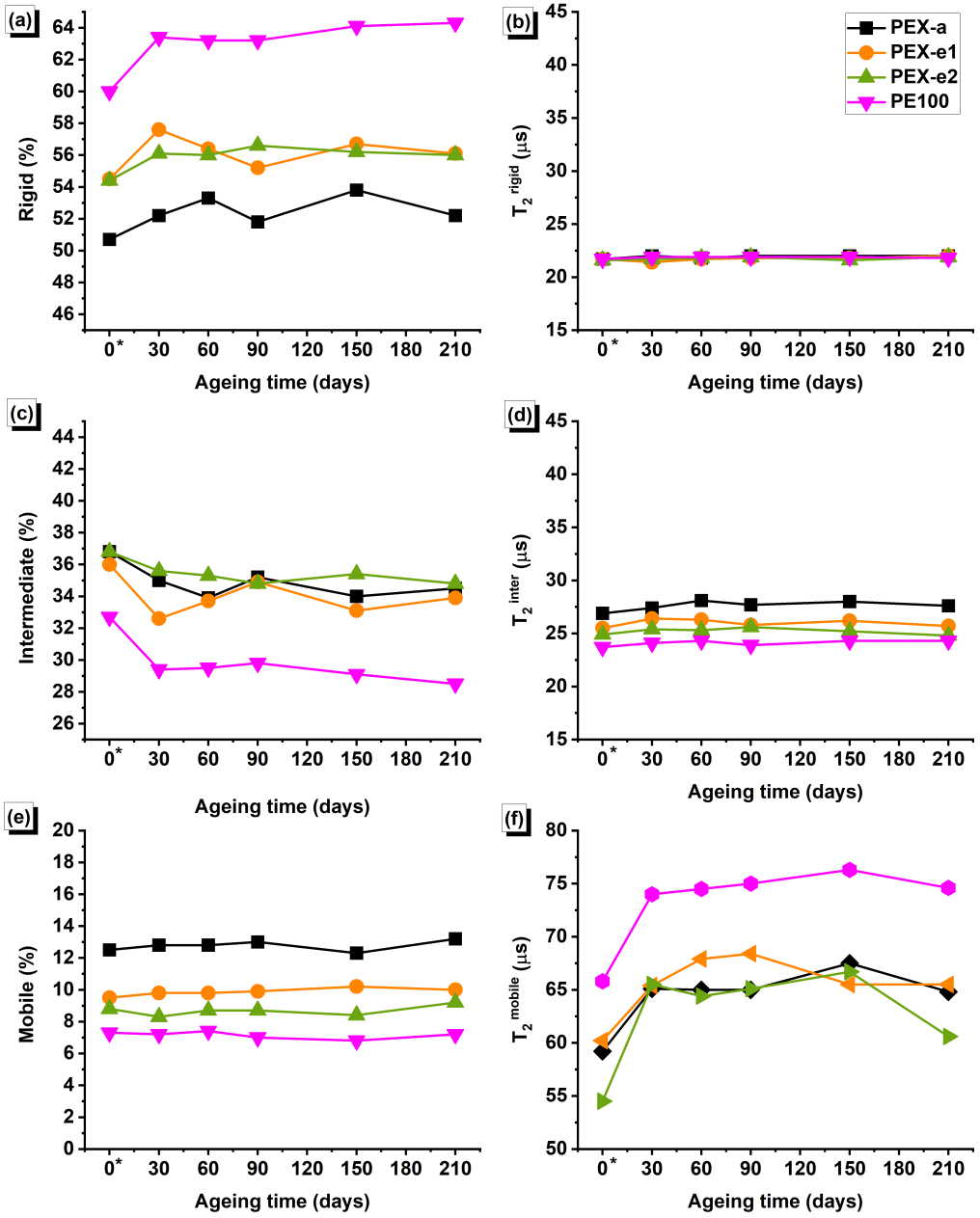

Figure 4.15: Summary of static ^{1}H NMR measurement results showing changes in the phase composition and molecular mobility (T_2 relaxation times) of (a) and (b) rigid; (c) and (d) intermediate; and (e) and (f) mobile components, respectively. *Results for unaged pipes (0 days) were sourced from [33].

Comparison with the results from the unaged samples, sourced from [33], revealed an increase in crystallinity (rigid component) for all samples in the first 30 days of the ageing protocol. This was accompanied by a decrease in the interphase component, while the percentage of amorphous component remained almost unchanged. These changes are characteristic of physical ageing, which is marked by annealing and re-crystallization effects.

This phenomenon has been previously reported in the literature for the initial phase of HDPE ageing in air [70], where prolonged exposure to high temperatures (below the melting point) allows the chains in the interphase to reorganize into the crystalline phase.

Although the overall amount of the amorphous component did not change with the ageing time, the mobility of the amorphous phase increased within the first 30 days of ageing (T_2^{mobile} increased) for all pipes. This is indicative of chain scission, as the broken chain segments gain higher mobility [70]. The mobility of the amorphous phase decreased after some ageing time, in PEX-e1 after 90 days and for the other pipes after 150 days. This decline was more pronounced for PEX-e2 compared to the other samples. Two possible hypothesis for the reduction of the mobility of the amorphous phase are: (1) the increase in crosslinking density and (2) decrease in the free-volume [137]. This was further investigated by analyzing the crosslink morphology after ageing (see Section 4.3.2.5).

4.3.2.5 Gel content and DMA: crosslink morphology

The degree of crosslinking in the 210-day aged samples, determined by gel content, is summarized in Table 3.2. The table also provides the average molecular weight between crosslinks (M_c) and the crosslinking density (ν_c), both calculated from the DMA data using Equations 4-10 and 4-11. The storage modulus at the rubbery plateau (160 °C), as listed in Table 3.8, was used to determine the M_c and ν_c values. It was not possible to perform DMA on the aged PEX-a pipe due to insufficient material, as the remaining pipe segment after the ageing protocol was too short to prepare DMA specimens. However, since the primary focus of the study is on the behavior of PEX-e pipes, this limitation was not considered critical.

Table 4.2: Comparison of the degree of crosslinking (Gel), molecular weight between crosslinks (M_c), and crosslinking density (ν_c) of the pipes before and after ageing. The data for the pipes at age 0 days is sourced from [33]. Uncertainties represent the standard deviation.

Material	Age (days)	Gel (%)	$M_c \times 10^3$ g/mol	$\nu_c \times 10^2$ mol/m^3	Ref.
PEX-e1	0	77.1 ± 1.5	2.3 ± 0.2	3.8 ± 0.2	[33]
	210	75.7 ± 0.5	3.0 ± 0.9	3.1 ± 1.0	
PEX-e2	0	81.0 ± 0.0	1.4 ± 0.2	6.3 ± 1.2	[33]
	210	78.4 ± 0.1	1.4 ± 0.1	5.9 ± 0.3	
PEX-a	0	90.7 ± 0.5	0.7 ± 0.1	11.6 ± 1.4	[33]
	210	91.2 ± 0.3	-	-	
PE100	0	0.8 ± 0.0	15.2 ± 0.8	0.6 ± 0.0	[33]
	210	0.2 ± 0.1	15.7 ± 0.6	0.5 ± 0.0	

For comparison, the values for unaged samples, sourced from our previous work [33], were also included in Table 3.2. A slight decrease in gel content was

observed for PEX-2, but the differences in crosslinking density between unaged and aged specimens across all pipe samples were statistically insignificant (p-values > 0.05 from the two-sample t-test). These results are consistent with previous findings that revealed that chain scission, rather than crosslinking, is the primary degradation mechanism during solid-state thermo-oxidation of high-density polyethylene [70].

In general, no significant changes were observed in the crosslink morphology of the pipes after 210 days of ageing. Therefore, the reduced mobility of the amorphous phase observed at the final stage of the ageing protocol by ^{1}H NMR (see Section 4.3.2.4) cannot be attributed to crosslinking. Accordingly, this reduction in mobility is likely due to a decrease in free-volume, driven by interactions between functional groups formed through hydrolysis and/or chain scission [137].

4.3.2.6 DSC: Melt and crystallization behavior

Differential scanning calorimetry (DSC) was employed to evaluate the melting and crystallization behavior of the pipe samples throughout the ageing process. Figure 4.16 illustrates the evolution of the melting peaks with ageing for all samples. Table 3.5 provides the average values for key thermal properties, including crystallization temperature (T_c), crystallization enthalpy (ΔH_c), melting temperature (T_m), melting enthalpy (ΔH_m), and the degree of crystallinity (X_c).

The melting peaks became narrower and shifted to slightly higher temperatures, with this effect being most pronounced in PEX-e1 during the first 30 days of ageing. This shift indicates improved crystal regularity, which was confirmed by the increase in average lamellar thickness, shown in Figure 4.17. These results are consistent with annealing and re-crystallization effects identified in the NMR analysis (see Section 4.3.2.4) and align with previous studies on PEX films aged in air [63, 71]. This phenomenon, often referred to as physical ageing, is recognized as the dominant process in PEX during the initial stages of thermal ageing [71, 128].

Figure 4.17 illustrates the evolution of crystallinity over time, calculated using Equation 4-8. While the general trends in DSC align with the phase composition identified via NMR (Section 4.3.2.4), some discrepancies exist due to differences in how each method measures crystallinity. DSC determines crystallinity based on heat absorption during the melting phase transition, whereas NMR quantifies the crystalline phase by analyzing chain mobility. The lower crystallinity values obtained from NMR reflect the presence of

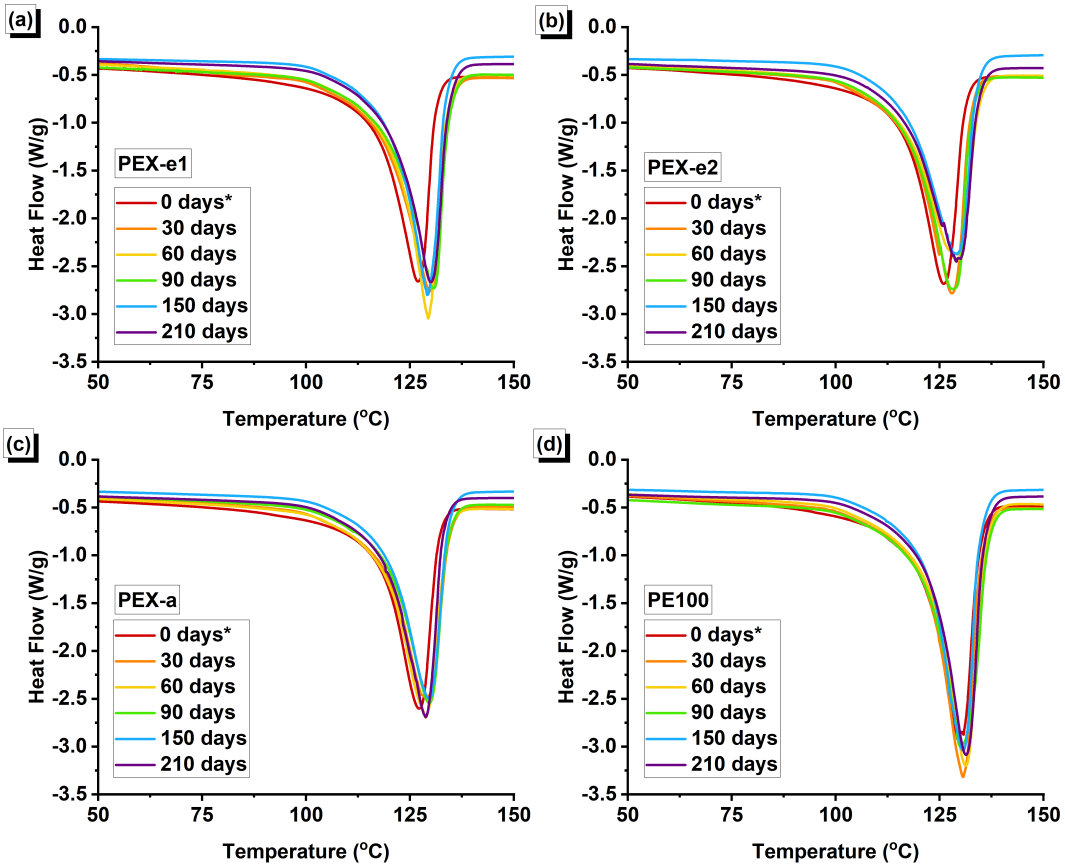

Figure 4.16: DSC curves showing the melting with ageing for (a) PEX-e1, (b) PEX-e2, (c) PEX-a and (d) PE100. *Results for unaged pipes (0 days) were sourced from [33].

an interphase, where polymer chains exhibit restricted motion due to the proximity to crystalline regions, crystallinity defects, chain entanglements, and crosslinks [33].

Despite these differences, both methods showed a notable increase in crystallinity for PEX-e1 during the first 30 days of ageing, attributed to physical ageing effects. For PEX-e2, DSC revealed a gradual decrease in crystallinity over the 210-day period, while NMR detected a slight increase in the initial stages, followed by a decline after 150 days.

Ageing also affected the crystallization kinetics, as evidenced by slight decreases in crystallization enthalpy (ΔH_c) reported in Table 3.5, particularly for PEX-a and PE100. Since ΔH_c strongly depends on the length of crystallizable sequences [138], these reductions are indicative of small-scale chain scission, consistent with early stages of chemical ageing [70, 71].

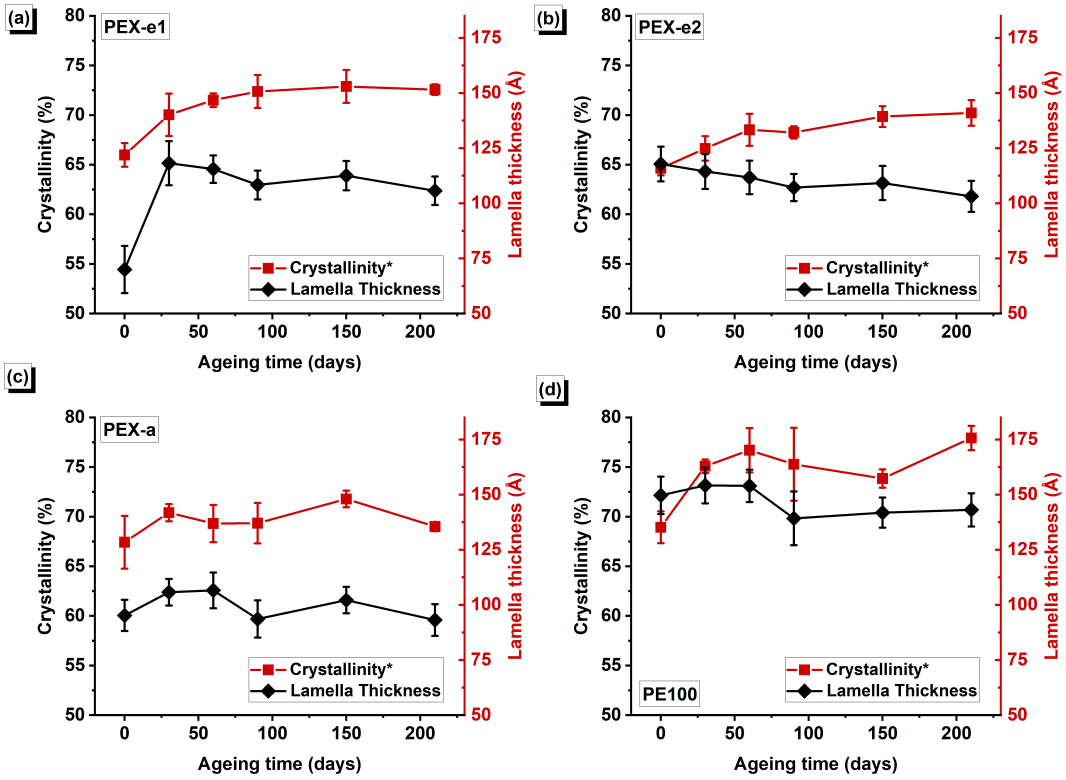

Figure 4.17: Evolution of crystallinity and average lamellar thickness, measured by DSC, of (a) PEX-e1, (b) PEX-e2, (c) PEX-a and (d) PE100 over ageing time. *Results for unaged pipes (0 days) were sourced from [33]. Average and standard deviation calculated from three replicate runs.

Table 4.3: Parameters obtained from the DSC curves of PEX and PE pipes. Average and standard deviation for at least three replicate runs.

Material	Age (days)	T_c (°C)	ΔH_c (J/g)	T_m (°C)	ΔH_m (J/g)	X_c (%)	Ref.
PEX-e1	0	115 ± 0	171 ± 3	127 ± 1	153 ± 6	54.4 ± 2.4	[33]
	30	114 ± 0	177 ± 2	129 ± 1	183 ± 5	65.2 ± 2.2	
	60	114 ± 0	175 ± 0	129 ± 0	181 ± 0	64.6 ± 1.4	
	90	115 ± 1	171 ± 2	130 ± 1	177 ± 2	63.0 ± 1.5	
	150	115 ± 0	172 ± 2	130 ± 1	180 ± 2	63.9 ± 1.5	
	210	115 ± 0	166 ± 1	130 ± 0	175 ± 1	62.4 ± 1.4	
PEX-e2	0	113 ± 0	179 ± 2	126 ± 0	180 ± 6	63.9 ± 2.5	[33]
	30	114 ± 1	176 ± 3	127 ± 1	180 ± 4	63.9 ± 1.9	
	60	113 ± 1	174 ± 3	128 ± 1	181 ± 4	64.3 ± 1.9	
	90	114 ± 0	171 ± 1	128 ± 0	177 ± 1	63.1 ± 1.4	
	150	117 ± 4	170 ± 3	129 ± 0	180 ± 3	63.9 ± 1.7	
	210	114 ± 1	169 ± 2	129 ± 1	174 ± 3	62.1 ± 1.8	
PEX-a	0	114 ± 2	169 ± 1	128 ± 1	169 ± 3	60.0 ± 1.6	[33]
	30	114 ± 2	171 ± 1	129 ± 0	175 ± 0	62.4 ± 1.3	
	60	113 ± 0	171 ± 3	129 ± 1	176 ± 3	62.6 ± 1.8	
	90	114 ± 1	162 ± 3	129 ± 1	168 ± 4	59.7 ± 1.9	
	150	114 ± 0	165 ± 1	130 ± 0	173 ± 1	61.6 ± 1.3	
	210	115 ± 1	162 ± 2	129 ± 0	167 ± 3	59.6 ± 1.6	
PE100	0	117 ± 1	205 ± 4	128 ± 1	203 ± 3	72.1 ± 1.9	[33]
	30	116 ± 0	202 ± 2	131 ± 0	206 ± 3	73.1 ± 1.8	
	60	116 ± 0	199 ± 2	131 ± 1	205 ± 1	73.1 ± 1.6	
	90	117 ± 1	191 ± 2	131 ± 1	196 ± 6	69.8 ± 2.7	
	150	117 ± 0	190 ± 0	130 ± 0	198 ± 1	70.4 ± 1.5	
	210	117 ± 0	189 ± 3	131 ± 0	199 ± 2	70.7 ± 1.7	

4.3.2.7
DMA: Thermo-mechanical properties

The thermo-mechanical properties of the PEX and PE pipes after 210 days of ageing were assessed using DMA over a temperature range of -50 °C to 170 °C. Samples were extracted from the aged pipes in the extrusion direction, following the same procedure described in a previous study for unaged pipes [33]. As explained in Section 4.3.2.5, DMA testing on the aged PEX-a pipe was not possible due to insufficient material. However, this limitation was not critical, as the primary focus of the study was on the behavior of PEX-e pipes, with PEX-a included mainly for comparison.

The parameters derived from the DMA curves of the aged specimens are detailed in Table 4.3.2.7. Comparisons of the storage modulus (E') before and after ageing are shown in Figure 4.18. An increase in the average E' was observed for all pipes, particularly at lower temperatures. However, these changes were statistically significant only for PEX-e2, as indicated by the confidence intervals. The increase in E' is likely attributed to morphological changes in the crystalline structure observed via DSC, including a slight increase in crystallinity and lamellar thickness, resulting in greater stiffness.

captionParameters obtained from the DMA curves of PEX and PE pipes after 210 days of ageing. Average and standard deviation for three replicate runs.

Material	E'at 0°C (MPa)	E' at 23°C (MPa)	E' at 90°C (MPa)	E' at 160°C (MPa)	T_α (°C)	E" at T_α (MPa)
PEX-e1	1189 ± 125	820 ± 54	113 ± 6	3.2 ± 1.0	35 ± 2	84 ± 5
PEX-e2	1159 ± 38	786 ± 42	82 ± 5	6.0 ± 0.3	34 ± 2	82 ± 2
PE100	1706 ± 54	1259 ± 40	250 ± 11	0.6 ± 0.0	41 ± 2	118 ± 3

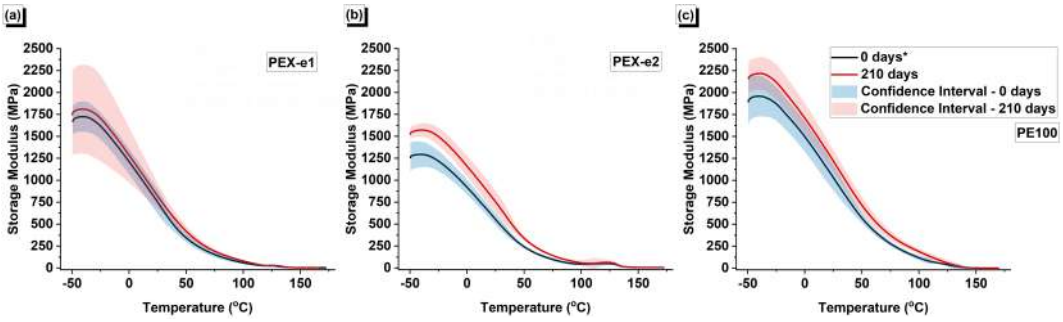

Figure 4.18: Comparison of the storage modulus of aged samples and unaged samples for (a) PEX-e1, (b) PEX-e2, and (c) PE100. *Results for unaged pipes (0 days) were sourced from [33]. Average curves and confidence intervals calculated from three replicate runs.

At temperatures exceeding the melting point, the material becomes fully amorphous, and E' reaches the rubbery plateau, where it is proportional to the density of crosslinks and molecular entanglements. At this plateau, the E'

values of unaged and aged samples were similar, indicating that the crosslinking network remained largely unchanged during the ageing protocol.

As shown in Figure 4.19, ageing also caused small changes in the loss modulus (E''), which were also only statistically significant for PEX-e2. E'' represents the energy dissipated as heat during deformation and provides insights into mechanical relaxations across different temperature ranges. For PEX-e2, the α transition peak, observed at 27 °C in the unaged sample [33], shifted to 41 °C after ageing. This shift can be attributed to the increase in lamellar thickness detected by DSC (see Section 4.3.2.6). The α transition reflects the motion and deformation of chains within the crystalline phase, and thicker lamellae are correlated with higher T_α values [119, 121, 122].

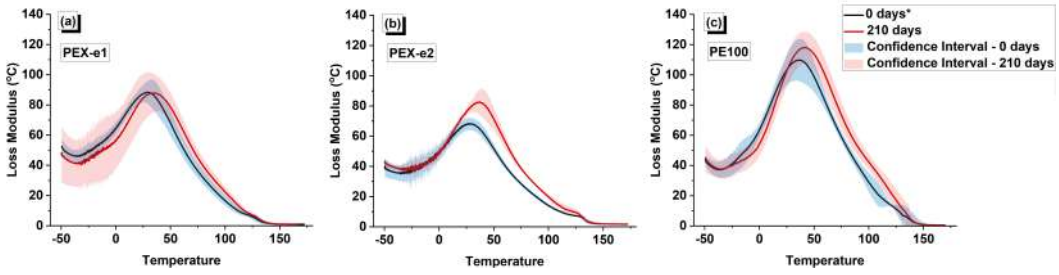

Figure 4.19: Comparison of the loss modulus of aged samples and unaged samples for (a) PEX-e1, (b) PEX-e2, and (c) PE100. *Results for unaged pipes (0 days) were sourced from [33]. Average curves and confidence intervals calculated from three replicate runs.

As expected, the 210 days ageing protocol did not result in substantial changes to the mechanical properties. As evidenced by OIT and FTIR results, antioxidant depletion was not complete, thus substantial polymer degradation was not expected within the bulk of the pipes.

4.4 Conclusions

This study investigated the thermo-oxidative degradation and stability of PEX-e pipes developed for BTES applications. Two formulations, PEX-e1 and PEX-e2, were compared to commercial PEX-a and non-crosslinked PE100 pipes. The pipes were aged in water at the target BTES service temperature for 210 days, with samples removed periodically to monitor antioxidant (AO) depletion and evaluate degradation mechanisms.

In the initial stage of the ageing protocol, physical ageing was identified as the primary degradation mechanism, characterized by increases in lamellar thickness and an expansion of the crystalline phase at the expense of the interphase. Across all PEX samples, chain scission was identified as the

predominant degradation mechanism throughout the ageing protocol. This was confirmed by reductions in molecular weight observed through ^{13}C CPMAS NMR, with the effects being more pronounced in PEX-a pipes.

The crosslink morphology of the pipes, assessed by gel content and DMA, was not significantly altered after 210 days of ageing. Additionally, DMA results indicated no abrupt changes in mechanical properties with ageing, suggesting that the pipes remained in the induction phase of degradation. This finding aligned with OIT and FTIR results, which identified the presence of active antioxidant additives in the pipes after 210 days. Since these additives were not entirely depleted during the ageing protocol, substantial polymer degradation was not expected. Indeed, FTIR analysis of the pipe cross-sections showed that the formation of degradation products in the bulk was still very limited after 210 days. However, surface analysis revealed significant signs of oxidation and AO depletion at the inner surface of the pipes.

OIT measurements highlighted a disparity in oxidative stability between the novel PEX-e pipes and the commercially established PEX-a pipes. Despite its lower initial AO concentration, PEX-a demonstrated remarkable stability in OIT values throughout the ageing protocol. In contrast, both PEX-e pipes exhibited an exponential decline in OIT, with PEX-e1 losing 94% of its initial OIT by 210 days. The non-crosslinked PE100 pipe showed a linear decline, reaching a 71% reduction over the same period.

Overall, these findings provide valuable insights into the degradation mechanisms and long-term stability of PEX pipes for heating and thermal energy storage applications. Although chain scission was less pronounced in the PEX-e formulations, the rapid AO depletion observed in both PEX-e1 and PEX-e2 underscores the need for further optimization of their additive formulations. Enhancing AO stabilization is essential to ensure long-term performance comparable to that of the commercial PEX-a pipes. Addressing these limitations will be critical for advancing the application of PEX-e materials in sustainable thermal energy storage systems.

5
Conclusions and future work suggestions

This thesis investigated the morphology, thermo-mechanical properties, and stability of novel photo-crosslinked polyethylene (PEX-e) pipes designed for borehole thermal energy storage (BTES) applications. Two formulations, PEX-e1 and PEX-e2, were evaluated and compared against established peroxide-crosslinked polyethylene (PEX-a) and non-crosslinked bimodal polyethylene (PE100) pipes.

Post-processing characterization revealed that both PEX-e formulations achieved a high degree of crosslinking, comparable to the 70-90% range typical of commercial PEX-a pipes used in heating applications. Notable differences in crosslink density and molecular morphology were observed between the two PEX-e formulations, significantly influencing their thermo-mechanical behavior. The PEX-e1 formulation exhibited a more uniform crosslink structure, resulting in mechanical properties comparable to PEX-a. In contrast, PEX-e2 exhibited a more aggregated crosslinked network, leading to a lower storage modulus compared to commercial pipes.

Both PEX-e pipes demonstrated very high oxidation induction times (OIT), indicating promising thermo-oxidative stability. However, ageing tests revealed accelerated antioxidant (AO) depletion in both formulations after prolonged exposure to hot water at 90°C. Significant color changes were observed during ageing, attributed to by-products formed through stabilization processes involving primary AO stabilizers. FTIR spectroscopy revealed the formation of carbonyl groups and unsaturations on the pipe surfaces, whereas oxidation in the bulk remained limited.

In-depth analysis during ageing tests provided insights into degradation mechanisms at different stages. In the initial stage (first 30 days), the primary degradation mechanism was physical ageing, marked by annealing and recrystallization effects. These changes led to slight increases in the crystalline phase at the expense of the interphase, as well as increased lamellar thickness. ^{1}H NMR analysis showed increased amorphous phase mobility early in the ageing protocol, consistent with chain scission. Across all PEX samples, chain scission was identified as the predominant degradation mechanism, confirmed by reductions in molecular weight observed through ^{13}C CPMAS NMR, with more

pronounced effects in PEX-a pipes.

Analysis of the degree of crosslinking and crosslink density revealed no significant alterations in the crosslink morphology of the pipes after 210 days of ageing. Additionally, dynamic mechanical analysis indicated no abrupt changes in mechanical properties with ageing, suggesting the pipes remained in the induction phase of degradation.

These findings highlight the critical role of additive formulations, processing conditions, and network morphology in ensuring the reliability and durability of PEX-e pipes. While the novel PEX-e materials show significant potential for application in BTES systems, further optimization is crucial to address the rapid depletion of antioxidants (AOs) and achieve performance that matches or surpasses that of PEX-a. Refining additive formulations and processing parameters will be key to enhancing long-term durability. Overcoming these challenges is essential for the application of PEX-e materials in sustainable thermal energy storage systems.

Based on this thesis findings, the following suggestions for future research are provided:

1. Optimization of additive formulations: studies on PEX-e pipes with different antioxidant types and concentrations to reach an optimal formulation and enhance the long-term stability of PEX-e pipes.

2. Investigation of processing parameters: investigation on optimal photo-crosslinking conditions, including light intensity, photo-initiator concentrations, and curing times, to improve the uniformity of crosslinking and reduce susceptibility to thermal degradation.

3. Long-term ageing studies: studies with extended ageing protocols to encompass the full service life of BTES applications. Incorporate real-world environmental factors such as fluctuating temperatures, moisture levels, and mechanical stresses to assess durability under operational conditions.

Bibliography

[1] H. Sadeghi, R. Jalali, and R. M. Singh, "A review of borehole thermal energy storage and its integration into district heating systems," *Renewable and Sustainable Energy Reviews*, vol. 192, p. 114 236, 2024.

[2] H. Skarphagen, D. Banks, B. S. Frengstad, and H. Gether, "Design considerations for borehole thermal energy storage (btes): A review with emphasis on convective heat transfer," *Geofluids*, vol. 2019, pp. 1–26, 2019.

[3] D. Mendrinos, S. Katsantonis, and C. Karytsas, "Review of alternative pipe materials for exploiting shallow geothermal energy," *Innovations in Corrosion and Materials Science*, vol. 7, pp. 13–29, 1 2017.

[4] R. K. Ramstad *et al.*, "The borehole thermal energy storage at emmaboda, sweden: First distributed temperature measurements," *Science and Technology for the Built Environment*, vol. 29, pp. 146–162, 2 2023.

[5] R. Maria, "Monitoring the degradation of PE pipes by ir-microscopy," PhD thesis, Technischen Universität Darmstadt, Darmstad, Germany, 2014.

[6] W. K. Wong, "Evaluation of the oxidative degradation mechanism of corrugated high density polyethylene pipe and the pipe resin," PhD Thesis, Drexel University, 2011.

[7] S. Zha, H. qing Lan, and H. Huang, "Review on lifetime predictions of polyethylene pipes: Limitations and trends," *Int. J. Pres Ves. Pip.*, vol. 198, p. 104 663, 2022.

[8] M. Bredács, E. Kanatschnig, A. Frank, G. Oreski, G. Pinter, and S. Gergely, "Identifying active and degraded phenolic antioxidants in aged pe with IR-microscopy," *Polym. Degrad. Stab.*, vol. 212, p. 110 345, 2023.

[9] P. Posadas *et al.*, "Crosslinked networks in electron beam irradiated polyethylenes evaluated by proton low-field NMR spectroscopy," *Radiat. Phys. Chem.*, vol. 204, p. 110 694, 2023.

[10] H. A. Khonakdar, J. Morshedian, U. Wagenknecht, and S. H. Jafari, "An investigation of chemical crosslinking effect on properties of high-density polyethylene," *Polymer*, vol. 44, pp. 4301–4309, 15 2003.

[11] M. Hiles, M. Grossutti, and J. R. Dutcher, "Classifying formulations of crosslinked polyethylene pipe by applying machine-learning concepts to infrared spectra," *J. Polym. Sci., Part B: Polym. Phys.*, vol. 57, pp. 1255–1262, 18 2019.

[12] H. Hirabayashi, A. Iguchi, K. Yamada, H. Nishimura, K. Ikawa, and H. Honma, "Study on the structure of peroxide cross-linked polyethylene pipes with several stabilizers," *Mater. Sci. Appl.*, vol. 04, pp. 497–503, 09 2013.

[13] M. Grossutti *et al.*, "Deep generative modeling of infrared images provides signature of cracking in cross-linked polyethylene pipe," *ACS Appl. Mater. Inter.*, vol. 15, pp. 22 532–22 542, 2023.

[14] S. Al-Malaika, S. Riasat, and C. Lewucha, "Reactive antioxidants for peroxide crosslinked polyethylene," *Polym. Degrad. Stab.*, vol. 145, pp. 11–24, 2017.

[15] Y. W. Fu, W. F. Sun, and X. Wang, "Uv-initiated crosslinking reaction mechanism and electrical breakdown performance of crosslinked polyethylene," *Polymers*, vol. 12, p. 420, 2 2020.

[16] R. Patterson, A. Kandelbauer, U. Müller, and H. Lammer, "Crosslinked thermoplastics," in *Crosslinked Thermoplastics. Handbook of Thermoset Plastics*, 3rd ed., Elsevier, 2014, pp. 697–737.

[17] J. Ericsson and T. Menssen, *Polyolefin pipe, WO2015162155*, Oct. 2015.

[18] J. Ericsson, A. Ortquist, T. Menssen, J. John, and J. Meeker, *Polyolefin pipe, US20180258255A1*, Sep. 2018.

[19] I. Kolo *et al.*, "A comprehensive review of deep borehole heat exchangers (dbhes): Subsurface modelling studies and applications," *Geothermal Energy*, vol. 12, p. 19, 1 2024.

[20] M. Janiszewski, "Techno-economic aspects of seasonal underground storage of solar thermal energy in hard crystalline rocks," PhD thesis, Aalto University, Helsinki, Finland, 2019.

[21] M. Reuss, "6 - the use of borehole thermal energy storage (btes) systems," in *Advances in Thermal Energy Storage Systems*, ser. Woodhead Publishing Series in Energy, L. F. Cabeza, Ed., Woodhead Publishing, 2015, pp. 117–147.

[22] A. K. Mehrjerdi, "Thermally conductive high-density polyethylene composites for ground heat exchangers," *Doctoral Thesis*, Högskolan i Borås, Borås, Sweden, 2020.

[23] J. H. Kupfernagel *et al.*, "Impact of operational temperature changes and freeze–thaw cycles on the hydraulic conductivity of borehole heat exchangers," *Geothermal Energy*, vol. 9, 1 2021.

[24] R. Bassiouny, M. R. Ali, and M. K. Hassan, "An idea to enhance the thermal performance of HDPE pipes used for ground-source applications," *Applied Thermal Engineering*, vol. 109, pp. 15–21, 2016.

[25] C. Shi, J. Yang, Y. Liu, *et al.*, "Thermally conductive study of polyethylene/al2o3 composite networks cross-linked pipes by electron beam irradiation," *Chemical Research in Chinese Universities*, vol. 36, pp. 940–945, 2020.

[26] R. Huang, B.-J. Kim, S. Lee, Z. Yang, and Q. Wu, "Co-extruded wood-plastic composites with talc-filled shells: Morphology, mechanical, and thermal expansion performance," *BioResources*, vol. 8, no. 2, pp. 2283–2299, 2013.

[27] G. S. de Sousa, A. K. Mehrjerdi, M. Skrifvars, and J. R. M. d'Almeida, "Thermo-mechanical properties of polyethylene composites filled with soapstone waste," *J. Appl. Polym. Sci.*, vol. 141, e55017, 9 2024.

[28] S. O. Han, D. W. Lee, and O. H. Han, "Thermal degradation of crosslinked high density polyethylene," *Polymer Degradation and Stability*, vol. 63, pp. 237–243, 2 1999.

[29] I. O. Salyer and J. E. Davison, "Thermal-energy storage in crosslinked pellets of high-density polythylene for home heating and cooling via off-peak electric power utilization," *Journal of Applied Polymer Science*, vol. 28, pp. 2903–2924, 9 1983.

[30] C. Munier, A. Tcharkhtchi, and J. Verdu, "Durability of cross-linked polyethylene pipes under pressure," *J. Mater. Sci*, vol. 37, pp. 4159–4163, 2002.

[31] H. Boneh, A. Marmur, and M. Narkis, "Thermal energy storage in columns packed with crosslinked polyethylene tubes," *Polymer Engineering & Science*, vol. 24, pp. 1227–1231, 16 1984.

[32] X. Dong *et al.*, "Mechanical characterizations, recyclability of thermoplastics through melt grafting a dynamic covalent network onto polyethylene," *Polym. Test.*, vol. 122, p. 108 005, 2023.

[33] G. Simão de Sousa, A. Root, I. Heinmaa, A. Kalantar Mehrjerdi, J. R. Moraes d'Almeida, and M. Skrifvars, "Characterization of photo-crosslinked polyethylene pipes for geothermal energy storage," *ACS Omega*, vol. 10, no. 1, pp. 1748–1760, 2025.

[34] M. Chanda and S. K. Roy, *Plastics Technology Handbook*. CRC Press, 2006.

[35] H. Ahmad and D. Rodrigue, "Crosslinked polyethylene: A review on the crosslinking techniques, manufacturing methods, applications, and recycling," *Polym. Eng. Sci.*, vol. 62, pp. 2376–2401, 8 2022.

[36] D. Akbarian *et al.*, "Atomistic-scale insights into the crosslinking of polyethylene induced by peroxides," *Polymer*, vol. 183, 2019.

[37] S. S. Sengupta, "XLPE manufacturing processes," in *XLPE Manufacturing Processes. Crosslinkable Polyethylene: Manufacture, Properties, Recycling, and Applications*, Springer, 2021, pp. 41–66.

[38] C. Meola, G. M. Carlomagno, and G. Giorleo, "Cross-linked polyethylene," in *Cross-Linked Polyethylene. Encyclopedia of Chemical Processing*, 1st ed., Taylor & Francis, 2005, pp. 577–588.

[39] J. Morshedian and P. M. Hoseinpour, "Polyethylene cross-linking by two-step silane method: A review," *Iranian Polymer Journal*, vol. 18, pp. 103–128, 2 2009.

[40] M. L. Sjeberg and E. Janjerbenkyla, *Method for heating and/or crosslinking polymers*, Issued by the Japanese Patent Office, 2008.

[41] J. C. M. Castano, *Systems and methods for forming piping or tubing*, Issued by the World Intellectual Property Organization, Jul. 2023.

[42] *Standard specification for crosslinked polyethylene (pex) tubing with oxygen barrier for hot-and cold-water hydronic distribution systems 1*, ASTM Standard F3253-23, West Conshohocken, PA, USA: ASTM International, 2023.

[43] N. Chandran, A. Sivadas, E. V. Anuja, D. K. Baby, and R. Ramdas, "XLPE: Crosslinking techniques and recycling process," in *Crosslinkable Polyethylene: Manufacture, Properties, Recycling, and Applications*, J. Thomas, S. Thomas, and Z. Ahmad, Eds. Singapore: Springer Singapore, 2021, pp. 167–188.

[44] Y. L. Chen and B. Rånby, "Photocrosslinking of polyethylene. I. photoinitiators, crosslinking agent, and reaction kinetics," *J. Polym. Sci., Part A: Polym. Chem.*, vol. 27, pp. 4051–4075, 12 1989.

[45] Y. L. Chen and B. Rånby, "Photocrosslinking of polyethylene. II. properties of photocrosslinked polyethylene," *J. Polym. Sci., Part A: Polym. Chem.*, vol. 27, pp. 4077–4086, 12 1989.

[46] Y. L. Chen and B. Rånby, "Photocrosslinking of polyethylene. III. thermal oxidative stability of photocrosslinked polyethylene," *J. Polym. Sci., Part A: Polym. Chem.*, vol. 28, pp. 1847–1859, 7 1990.

[47] Y. Qing, X. Wenying, and B. Rånby, "Photoinitiated crosslinking of low density polyethylene i: Reaction and kinetics," *Polym. Eng. Sci.*, vol. 31, pp. 1561–1566, 22 1991.

[48] Y. Qing and B. Rånby, "Photoinitiated crosslinking of low density polyethylene. iv: Continuous extrusion application," *Polym. Eng. Sci.*, vol. 32, pp. 831–835, 12 1992.

[49] B. J. Qu and B. Rånby, "Photocross-linking of low-density polyethylene. I. kinetics and reaction parameters," *J. Appl. Polym. Sci.*, vol. 48, pp. 701–709, 4 1993.

[50] B. J. Qu and B. Rånby, "Photocross-linking of low-density polyethylene. II. structure and morphology," *J. Appl. Polym. Sci.*, vol. 48, pp. 711–719, 4 1993.

[51] B. J. Qu and B. Rånby, "Photocross-linking of low-density polyethylene. III. supermolecular structure studied by sals," *J. Appl. Polym. Sci.*, vol. 49, pp. 1799–1807, 10 1993.

[52] H. Zhang, Y. Shang, M. Li, H. Zhao, X. Wang, and B. Han, "Theoretical study on the reaction mechanism in the uv radiation cross-linking process of polyethylene," *RSC Adv.*, vol. 6, pp. 110 831–110 839, 112 2016.

[53] H. Zhao *et al.*, "Theoretical study on the reaction of triallyl isocyanurate in the uv radiation cross-linking of polyethylene," *RSC Adv.*, vol. 7, pp. 37 095–37 104, 59 2017.

[54] H. Zhang, Y. Shang, H. Zhao, X. Wang, B. Han, and Z. Li, "Further discussion on the reaction behaviour of triallyl isocyanurate in the uv radiation cross-linking process of polyethylene: A theoretical study," *R. Soc. Open Sci.*, vol. 6, p. 182 196, 9 2019.

[55] P. Jackson and E. Wan, "Photo-crosslinkable polyolefin compositions," CA2908284C, Dec. 2017.

[56] M. Tolinski, "Antioxidants and heat stabilization," in *Additives for Polyolefins (Second Edition)*, M. Tolinski, Ed., Second Edition. Oxford: William Andrew Publishing, 2015, pp. 19–31.

[57] M. Tolinski, "Ultraviolet light protection and stabilization," in *Additives for Polyolefins (Second Edition)*, M. Tolinski, Ed., Second Edition. Oxford: William Andrew Publishing, 2015, pp. 19–31.

[58] C. Vasile and M. Pascu, *Practical Guide to Polyethylene*. Shawbury: Rapra Technology Limited, 2005.

[59] M. Grossutti *et al.*, "Quantifying stabilizing additive hydrolysis and kinetics through principal component analysis of infrared spectra of crosslinked polyethylene pipe," *Polym. Degrad. Stab.*, vol. 200, p. 109 963, 2022.

[60] U. W. Gedde and M. Ifwarson, "Molecular structure and morphology of crosslinked polyethylene in an aged hot-water pipe," *Polymer Engineering and Science*, vol. 30, pp. 202–210, 4 1990.

[61] W. K. Wong, S. Cheng, C. Y. Li, I. Ahmad, R. Cairncross, and Y. G. Hsuan, "Depletion mechanism of antioxidants in mdpe-clay nanocomposites under thermal aging," *Polymer Degradation and Stability*, vol. 97, pp. 192–199, 2 2012.

[62] A. Xu, S. Roland, and X. Colin, "Physico-chemical characterization of the blooming of irganox 1076® antioxidant onto the surface of a silane-crosslinked polyethylene," *Polymer Degradation and Stability*, vol. 171, 2020.

[63] A. Xu, S. Roland, and X. Colin, "Thermal ageing of a silane-crosslinked polyethylene stabilised with an excess of irganox 1076," *Polymer Degradation and Stability*, vol. 189, 2021.

[64] R. R. Eckman, P. M. Henrichs, and A. J. Peacock, "Study of polyethylene by solid state NMR relaxation and spin diffusion," *Macromolecules*, vol. 30, pp. 2474–2481, 8 1997.

[65] J. Paul, E. W. Hansen, and J. Roots, "Probing the molecular dynamics in XLPE aged at different temperatures by 1H NMR relaxation time measurements," *Polym. Degrad. Stab.*, vol. 97, pp. 2403–2411, 11 2012.

[66] M. Denberg, H. Mosbæk, O. Hassager, and E. Arvin, "Determination of the concentration profile and homogeneity of antioxidants and degradation products in a cross-linked polyethylene type a (pexa) pipe," *Polymer Testing*, vol. 28, pp. 378–385, 4 2009.

[67] M. Perera, U. Ishiaku, and Z. Ishak, "Thermal degradation of pvc/nbr and pvc/enr50 binary blends and pvc/enr50/nbr ternary blends studied by dma and solid state nmr," *Polymer Degradation and Stability*, vol. 68, pp. 393–402, 2000.

[68] D. Vanderhart and C. Snyder, "Proton NMR characterization of room-temperature aging after modest thermal cycling in isotactic polypropylenes," *Macromolecules*, vol. 36, pp. 4813–4826, 2003.

[69] D. Demco *et al.*, "Investigation of thermal aging of polyamide 4,6 by 1h solid-state nmr†," *Macromolecular Chemistry and Physics*, vol. 208, pp. 2085–2095, 2007.

[70] X. Shi, J. Wang, S. Stapf, C. Mattea, W. Li, and Y. Yang, "Effects of thermo-oxidative aging on chain mobility, phase composition, and mechanical behavior of high-density polyethylene," *Polym. Eng. Sci.*, vol. 51, pp. 2172–2177, 2011.

[71] H. Li, J. Li, Y. Ma, Q. Yan, and B. Ouyang, "The role of thermo-oxidative aging at different temperatures on the crystal structure of crosslinked polyethylene," *Journal of Materials Science: Materials in Electronics*, vol. 29, pp. 3696–3703, 5 2018.

[72] J. Shen, X. Lin, J. Liu, and X. Li, "Effects of cross-link density and distribution on static and dynamic properties of chemically cross-linked polymers," *Macromolecules*, vol. 52, pp. 121–134, 1 2019.

[73] T. T. Chen, *Quantifying polymer crosslinking density using rheology and dma*, `https://www.tainstruments.com/pdf/literature/RH102.pdf`, This paper was written by Dr. Tianhong Terri Chen, Senior Applications Support Scientist at TA Instruments., 2018.

[74] S. D. Reinitz, E. M. Carlson, R. A. Levine, K. J. Franklin, and D. W. V. Citters, "Dynamical mechanical analysis as an assay of cross-link density of orthopaedic ultra high molecular weight polyethylene," *Polym. Test.*, vol. 45, pp. 174–178, 2015.

[75] M. Xie and H. Li, "Viscosity reduction and disentanglement in ultrahigh molecular weight polyethylene melt: Effect of blending with polypropylene and poly(ethylene glycol)," *Eur. Polym. J.*, vol. 43, pp. 3480–3487, 8 2007.

[76] O. Kizilkan and I. Dincer, "Borehole thermal energy storage system for heating applications: Thermodynamic performance assessment," *Energy Conversion and Management*, vol. 90, pp. 53–61, 2015.

[77] F. Fallani, G. Ruggeri, S. Bronco, and M. Bertoldo, "Modification of surface and mechanical properties of polyethylene by photo-initiated reactions," *Polym. Degrad. Stab.*, vol. 82, pp. 257–261, 2 2003.

[78] H. Zhang, Y. Shang, H. Zhao, X. Wang, B. Han, and Z. Li, "Theoretical study on the reaction of maleic anhydride in the uv radiation cross-linking process of polyethylene," *Polymer*, vol. 133, pp. 232–239, 2017.

[79] Y. Wang *et al.*, "Theoretical study on the grafting reaction of maleimide and its derivatives to polyethylene in the uv radiation cross-linking process," *Struct. Chem.*, vol. 30, pp. 1033–1039, 3 2019.

[80] H. Xie, K. K. Yang, and Y. Z. Wang, "Photo-cross-linking: A powerful and versatile strategy to develop shape-memory polymers," *Prog. Polym. Sci.*, vol. 95, pp. 32–64, 2019.

[81] H. Zhao, C. Xi, X. D. Zhao, and W. F. Sun, "Elevated-temperature space charge characteristics and trapping mechanism of cross-linked polyethylene modified by uv-initiated grafting mah," *Molecules*, vol. 25, p. 3973, 17 2020.

[82] X. D. Zhao, H. Zhao, and W. F. Sun, "Significantly improved electrical properties of crosslinked polyethylene modified by uv-initiated grafting mah," *Polymers*, vol. 12, p. 62, 1 2020.

[83] J. G. Powles and J. H. Strange, "Zero time resolution nuclear magnetic resonance transient in solids," *Proceedings of the Physical Society*, vol. 82, pp. 6–15, 1 1963.

[84] H. Uehara, T. Aoike, T. Yamanobe, and T. Komoto, "Solid-state 1H NMR relaxation analysis of ultrahigh molecular weight polyethylene reactor powder," *Macromolecules*, vol. 35, pp. 2640–2647, 2002.

[85] E. W. Hansen, P. E. Kristiansen, and B. Pedersen, "Crystallinity of polyethylene derived from solid-state proton NMR free induction decay," *J. Phys. Chem. B*, vol. 102, pp. 5444–5450, 28 1998.

[86] D. Dadayli, R. K. Harris, A. M. Kenwright, B. J. Say, and M. M. Sünnetçioğlu, "Solid-state 1h n.m.r. studies of polypropylene," *Polymer*, vol. 35, pp. 4083–4087, 1994.

[87] A. Abragam, *The Principles of Nuclear Magnetism*. Oxford Univ. Press, 1961, p. 120.

[88] P. Cebe *et al.*, "Heat of fusion of polymer crystals by fast scanning calorimetry," *Polymer*, vol. 126, pp. 240–247, 2017.

[89] A. Bashirgonbadi, Y. Ureel, L. Delva, R. Fiorio, K. M. Van Geem, and K. Ragaert, "Accurate determination of polyethylene (pe) and polypropylene (pp) content in polyolefin blends using machine learning-assisted differential scanning calorimetry (dsc) analysis," *Polym. Test.*, vol. 131, p. 108 353, 2024.

[90] J. Kragten, "Tutorial review. calculating standard deviations and confidence intervals with a universally applicable spreadsheet technique," *The Analyst*, vol. 119, pp. 2161–2165, 10 1994.

[91] M. C. Celina, E. Linde, and E. Martinez, "Carbonyl identification and quantification uncertainties for oxidative polymer degradation," *Polym. Degrad. Stab.*, vol. 188, p. 109 550, 2021.

[92] P. H. Eilers and H. F. Boelens, "Baseline correction with asymmetric least squares smoothing," Leiden University Medical Centre, Report 1.1, 2005, p. 5.

[93] Y. Futaana, M. Wieser, and G. S. Wieser, *Python library, version 3.11.3*, version 3.11.3, Copyright 2007-2015 Swedish Institute of Space Physics, Swedish Institute of Space Physics, 2015.

[94] M. Hiles, "Classifying formulations and tracking accelerated aging of crosslinked polyethylene pipes by applying machine learning concepts to infrared spectra," Master Thesis, University of Guelph, Guelph, Canada, 2020.

[95] A. K. Mehrjerdi, D. Åkesson, and M. Skrifvars, "Influence of talc fillers on bimodal polyethylene composites for ground heat exchangers," *J. Appl. Polym. Sci.*, vol. 137, p. 49 290, 42 2020.

[96] F. Addiego, A. Dahoun, C. G'Sell, and J. M. Hiver, "Characterization of volume strain at large deformation under uniaxial tension in high-density polyethylene," *Polymer*, vol. 47, pp. 4387–4399, 12 2006.

[97] V. A. Beloshenko, A. V. Voznyak, Y. V. Voznyak, and G. V. Dudarenko, "Equal-channel multiple angular extrusion of polyethylene," *J. Appl. Polym. Sci.*, vol. 127, pp. 1377–1386, 2 2013.

[98] B. Rånby, "Photoinitiated modifications of polymers: Photocrosslinking, surface photografting and photolamination," *Mater. Res. Innov*, vol. 2, pp. 64–71, 2 1998.

[99] Y. Qing, X. Wenying, and B. Rånby, "Photoinitiated crosslinking of low density polyethylene: Ii. morphology and properties," *Polym. Eng. Sci.*, vol. 31, pp. 1567–1571, 22 1991.

[100] P. V. Zamotaev, "Photoinitiated crosslinking of polyethylene," *Makromol. Chem., Macromol. Symp*, vol. 28, pp. 287–304, 1 1989.

[101] O. Han, S. Chae, S. Han, and S. Woo, "High density polyethylene as a thermal storage material studied by mas 13C NMR spectroscopy," *Polymer*, vol. 40, pp. 6329–6336, 23 1999.

[102] A. Nishioka, H. Komatsu, and Y. Kakiuchi, "Nuclear magnetic resonance in some crystalline polymers," *J. Phys. Soc. Jpn.*, vol. 12, pp. 283–285, 1957.

[103] Y. Jia, Z. Mao, W. Huang, and J. Zhang, "Effect of temperature and crystallinity on the thermal conductivity of semi-crystalline polymers: A case study of polyethylene," *Mater. Chem. Phys.*, vol. 287, p. 126 325, 2022.

[104] A. Paajanen, J. Vaari, and T. Verho, "Crystallization of cross-linked polyethylene by molecular dynamics simulation," *Polymer*, vol. 171, pp. 80–86, 2019.

[105] Q. Liu *et al.*, "Photo-degradation of polyethylene under stress: A successive self-nucleation and annealing (ssa) study," *Polym. Degrad. Stab.*, vol. 172, 2020.

[106] M. C. Montoya-Ospina, H. Verhoogt, M. Ordner, X. Tan, and T. A. Osswald, "Effect of cross-linking on the mechanical properties, degree of crystallinity and thermal stability of polyethylene vitrimers," *Polym. Eng. Sci.*, vol. 62, pp. 4203–4213, 12 2022.

[107] C. J. Pérez, N. Villarreal, J. M. Pastor, M. D. Failla, E. M. Vallés, and J. M. Carella, "The use of ssa fractionation to detect changes in the molecular structure of model ethylene-butene copolymers modified by peroxide crosslinking," *Polym. Degrad. Stab.*, vol. 94, pp. 1639–1645, 10 2009.

[108] J. Coates, "Interpretation of infrared spectra, a practical approach," in *Interpretation of Infrared Spectra, A Practical Approach. Encyclopedia of Analytical Chemistry*, Wiley, 2000.

[109] A. L. Andrady, K. L. Law, J. Donohue, and B. Koongolla, "Accelerated degradation of low-density polyethylene in air and in sea water," *Sci. Total. Environ.*, vol. 811, p. 151 368, 2022.

[110] Y. Niu *et al.*, "Crosslinking kinetics of polyethylene with small amount of peroxide and its influence on the subsequent crystallization behaviors," *Chinese J. Polym. Sci. (English Edition)*, vol. 34, pp. 1117–1128, 9 2016.

[111] I. Kriston, Á. Orbán-Mester, G. Nagy, P. Staniek, E. Földes, and B. Pukánszky, "Melt stabilisation of phillips type polyethylene, part I: The role of phenolic and phosphorous antioxidants," *Polym. Degrad. Stab.*, vol. 94, pp. 719–729, 4 2009.

[112] E. Pock, C. Kiss, Á. Janecska, E. Epacher, and B. Pukánszky, "Effect of chain structure on the processing stability of high-density polyethylene," *Polym. Degrad. Stab.*, vol. 85, pp. 1015–1021, 3 SPEC. ISS. 2004.

[113] E. Epacher, E. Fekete, M. Gahleitner, and B. Pukánszky, "Chemical reactions during the processing of stabilized PE: 1. discolouration and stabilizer consumption," *Polym. Degrad. Stab.*, vol. 63, pp. 489–497, 3 1999.

[114] N. Byrne, R. D. Silva, and T. Hilditch, "Linking antioxidant depletion with material properties for polyethylene pipes resins," *Polym. Eng. Sci.*, vol. 60, pp. 323–329, 2 2020.

[115] F. Gugumus, "Aspects of the stabilization mechanisms of phenolic antioxidants in polyolefins," *Macromol. Mater. Eng.*, vol. 137, pp. 189–225, 1 1985.

[116] J. D. Peterson, S. Vyazovkin, and C. A. Wight, "Kinetics of the thermal and thermo-oxidative degradation of polystyrene, polyethylene and poly(propylene)," *Macromol. Chem. Phys.*, vol. 202, pp. 775–784, 6 2001.

[117] Y. Du *et al.*, "TG-DSC and FTIR study on pyrolysis of irradiation cross-linked polyethylene," *J. Mater. Cycles Waste Manag.*, vol. 19, pp. 1400–1404, 4 2017.

[118] S. Igarashi, I. Mita, and H. Kambe, "Thermogravimetric analysis of the effect of ionizing radiation on thermal stability of polyethylene," *J. Appl. Polym. Sci.*, vol. 8, pp. 1455–1464, 3 1964.

[119] R. Popli, M. Glotin, L. Mandelkern, and R. S. Benson, "Dynamic mechanical studies of alpha and beta relaxations of polyethylenes," *J. Polym. Sci., Polym. Phys. Ed.*, vol. 22, pp. 407–448, 3 1984.

[120] Y. Ren *et al.*, "Structures and impact strength variation of chemically crosslinked high-density polyethylene: Effect of crosslinking density," *RSC Adv.*, vol. 11, pp. 6791–6797, 12 2021.

[121] K. Nitta and A. Tanaka, "Dynamic mechanical properties of metallocene catalyzed linear polyethylenes," *Polym.*, vol. 42, pp. 1219–1226, 3 2001.

[122] Y. P. Khanna, E. A. Turi, T. J. Taylor, V. V. Vickroy, and R. F. Abbott, "Dynamic mechanical relaxations in polyethylene," *J. Polym. Sci., Polym. Phys. Ed*, vol. 18, p. 544, 14 1985.

[123] N. S. Allen, M. Edge, and S. Hussain, "Perspectives on yellowing in the degradation of polymer materials: Inter-relationship of structure, mechanisms and modes of stabilisation," *Polymer Degradation and Stability*, vol. 201, 2022.

[124] A. Kömmling *et al.*, "Discoloration effects of high-dose γ -irradiation and long-term thermal aging of (u)hmw-pe," *International Journal of Polymer Science*, vol. 2017, 2017.

[125] K. D. T. Sánchez, N. S. Allen, C. M. Liauw, and M. Edge, "Effect of polymerization catalyst technology on the melt processing stability of polyethylenes, part 3: Additives blends performance," *Journal of Vinyl and Additive Technology*, vol. 22, pp. 117–127, 2 2016.

[126] F. B. Meng, X. Chen, X. Xu, C. Dai, A. Paramane, and Y. Tanaka, "Effect of degassing treatment durations on physico-chemical and electrical properties of 500 kv extra HVDC XLPE cable insulation," *Polymer Degradation and Stability*, vol. 188, 2021.

[127] L. Contat-Rodrigo and A. R. Greus, "Biodegradation studies of LDPE filled with biodegradable additives: Morphological changes. i," *Journal of Applied Polymer Science*, vol. 83, pp. 1683–1691, 8 2002.

[128] L. Boukezzi, A. Boubakeur, C. Laurent, and M. Lallouani, "Observations on structural changes under thermal ageing of cross-linked polyethylene used as power cables insulation," *Iranian Polymer Journal*, vol. 17, pp. 611–624, 8 2008.

[129] Q. Wu, B. Qu, Y. Xu, and Q. Wu, "Surface photo-oxidation and photostabilization of photocross-linked polyethylene," *Polymer Degradation and Stability*, vol. 68, pp. 97–102, 1 2000.

[130] B. Abaroa-Pérez, S. Ortiz-Montosa, J. J. Hernández-Brito, and D. Vega-Moreno, "Yellowing, weathering and degradation of marine pellets and their influence on the adsorption of chemical pollutants," *Polymers*, vol. 14, 7 2022.

[131] M. M. Elmer-Dixon, L. P. Fawcett, B. R. Hinderliter, and M. A. Maurer-Jones, "Could superficial chiral nanostructures be the reason polyethylene yellows as it ages?" *ACS Applied Polymer Materials*, vol. 4, pp. 6458–6465, 9 2022.

[132] K. Grabmayer *et al.*, "Characterization of the aging behavior of polyethylene by photoluminescence spectroscopy," *Polymer Degradation and Stability*, vol. 107, pp. 28–36, 2014.

[133] A. A. Mendes, A. M. Cunha, and C. A. Bernardo, "Study of the degradation mechanisms of polyethylene during reprocessing," *Polymer Degradation and Stability*, vol. 96, pp. 1125–1133, 6 2011.

[134] S. M. Al-Salem, "Influence of natural and accelerated weathering on various formulations of linear low density polyethylene (LLDPE) films," *Materials and Design*, vol. 30, pp. 1729–1736, 5 2009.

[135] J. Pospíšil *et al.*, "Discoloration of polymers by phenolic antioxidants," *Polymer Degradation and Stability*, vol. 77, pp. 531–538, 3 2002.

[136] M. Pollard *et al.*, "Observation of chain branching in polyethylene in the solid state and melt via 13c nmr spectroscopy and melt nmr relaxation time measurements," *Macromolecules*, vol. 37, pp. 813–825, 3 2004.

[137] H. Hagihara, A. Oishi, M. Funabashi, M. Kunioka, and H. Suda, "Free-volume hole size evaluated by positron annihilation lifetime spectroscopy in the amorphous part of poly(ethylene terephthalate) degraded by a weathering test," *Polymer Degradation and Stability*, vol. 110, pp. 389–394, 2014.

[138] F. Bustos, P. Cassagnau, and R. Fulchiron, "Effect of molecular architecture on quiescent and shear-induced crystallization of polyethylene," *Journal of Polymer Science, Part B: Polymer Physics*, vol. 44, pp. 1597–1607, 11 2006.

A
Appendix

A.1
Publications and Scientific Contributions

The research presented in this thesis is based on the topic of crosslinked polyethylene (PE) pipes for geothermal applications, as outlined in two key publications and one conference presentation. Additionally, my academic journey includes significant contributions to the study of polyethylene composites reinforced with soapstone waste, a topic I explored during the early years of my PhD and my Master's degree. This section highlights all my scientific contributions, emphasizing both the research directly related to this thesis and work in related fields.

A.1.1
Publications and Contributions Related to the Thesis Topic

1. G. Simão de Sousa, A. Root, I. Heinmaa, A. Kalantar Mehrjerdi, J. R. Moraes d'Almeida, and M. Skrifvars, "Thermo-oxidative ageing of photo-crosslinked polyethylene pipes for thermal energy storage," Under review at *Journal of Polymer Degradation and Stability* (Submitted January 2025)

2. G. Simão de Sousa, A. Root, I. Heinmaa, A. Kalantar Mehrjerdi, J. R. Moraes d'Almeida, and M. Skrifvars, "Characterization of photo-crosslinked polyethylene pipes for geothermal energy storage," *ACS Omega*, vol. 10, no. 1, pp. 1748–1760, 2025.
   DOI: 10.1021/acsomega.4c09896.

3. G. Simão de Sousa, A. Kalantar Mehrjerdi, J. R. Moraes d'Almeida, and M. Skrifvars, "Evaluation of thermo-oxidative degradation of cross-linked polyethylene pipes," Presented at the Nordic Polymer Days, Helsinki, Finland, June 12–14, 2024.

A.1.2 Publications and Contributions on Related Topics

Prior to transitioning to the field of crosslinked PE for geothermal applications, I focused on developing and characterizing polyethylene composites reinforced with soapstone waste. This research addressed the potential of industrial waste as a reinforcing material for polymeric composites, contributing to the fields of materials science and sustainability, and also evaluating the possibility of using these composites as material for pipelines in the research area of this thesis. Key publications and conference contributions from this phase of my academic career include:

1. G. Simão de Sousa, A. Kalantar Mehrjerdi, M. Skrifvars, J. R. Moraes d'Almeida, "Thermo-mechanical properties of polyethylene composites filled with soapstone waste," *Journal of Applied Polymer Science*, 2023. DOI: 10.1002/app.55017.

2. G. Simão de Sousa, A. Kalantar Mehrjerdi, M. Skrifvars, J. R. Moraes d'Almeida, "Effects of soapstone waste on the mechanical and thermal properties of polyethylene composites," in *Proceedings of the 6th Brazilian Conference on Composite Materials*, Brazil, 2022. DOI: 10.29327/566492.

3. G. Simão de Sousa, G. da Silva, J. R. Moraes d'Almeida, "Influence of soapstone waste on the mechanical and rheological properties of high-density polyethylene," *Journal of Applied Polymer Science*, 2021. DOI: 10.1002/app.50966.

4. G. Simão de Sousa, C. G. P. de Souza, J. R. Moraes d'Almeida, "Microstructural characterization of soapstone-reinforced polyethylene composites and correlations with the macroscopic mechanical behavior," in *Proceedings of the 26th ABCM International Congress of Mechanical Engineering*, Virtual Conference, 2021.

5. G. Simão de Sousa, G. A. S. da Silva, J. R. Moraes d'Almeida, "Rheological characterization of HDPE and soapstone composites," in *Proceedings of the 5th Brazilian Conference on Composite Materials*, Virtual Conference, 2021.

6. G. Simão de Sousa, G. A. S. da Silva, J. R. Moraes d'Almeida, "Development of composites with soapstone waste," in *Proceedings of the 25th ABCM International Congress of Mechanical Engineering*, Uberlândia, Brazil, 2019.

A.2
FTIR spectroscopy data analysis: pre-processing and automation

This section provides supporting information on the processing of FTIR spectroscopy data. The first part discusses three different approaches to baseline correction. The second part includes the Python script developed for the pre-processing and quantitative analysis of FTIR data of the PEX pipes over ageing time.

A.2.1
FTIR baseline correction

Reliable quantitative analysis of FTIR spectra requires pre-processing of the spectral data, specifically through baseline correction. In this study, the spectra of the pipes were notably tilted due to curvature effects, as the ATR measurements were taken on the inner surface of the pipes. For example, Figure A.1 shows the spectra of three replicates from the unaged PEX-e2 pipe, demonstrating this effect and its variability among replicates of the same pipe.

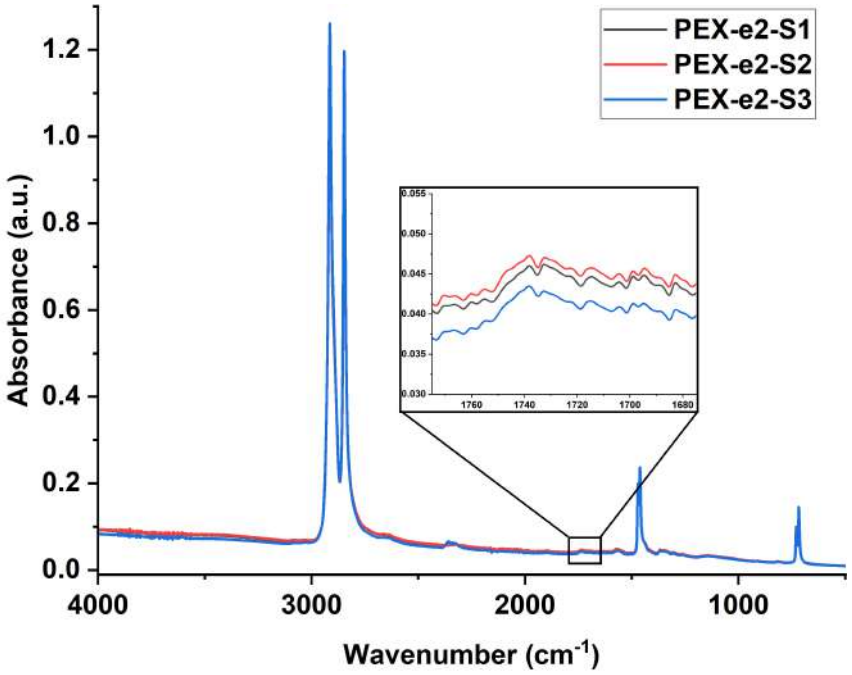

Figure A.1: FTIR spectra of three replicate samples of unaged pipe PEX-e2.

The spectra were recorded using OMNIC software, which includes an "Automatic Baseline Correction" option. However, this option does not provide control over the baseline correction parameters, and no documentation was found regarding the methodology behind this function. To ensure a more consistent baseline correction across all replicates and materials, the author chose to automate the analysis using Python.

Two approaches were tested: a polynomial fit [94] using the `baseline` function from the *Peakutils* library, and asymmetric least squares smoothing (ALSS) [92] using the `irfpy` library [93]. Figure A.2 presents a comparison of the spectra before and after baseline correction with OMNIC software, a 4^{th} order polynomial fit in Python, and the ALSS fit in Python. As shown in Figure A.2.b, the baseline correction method significantly affects peak intensity. Among the methods tested, the ALSS fit produced the most favorable results and was therefore adopted for processing the FTIR data reported in the thesis.

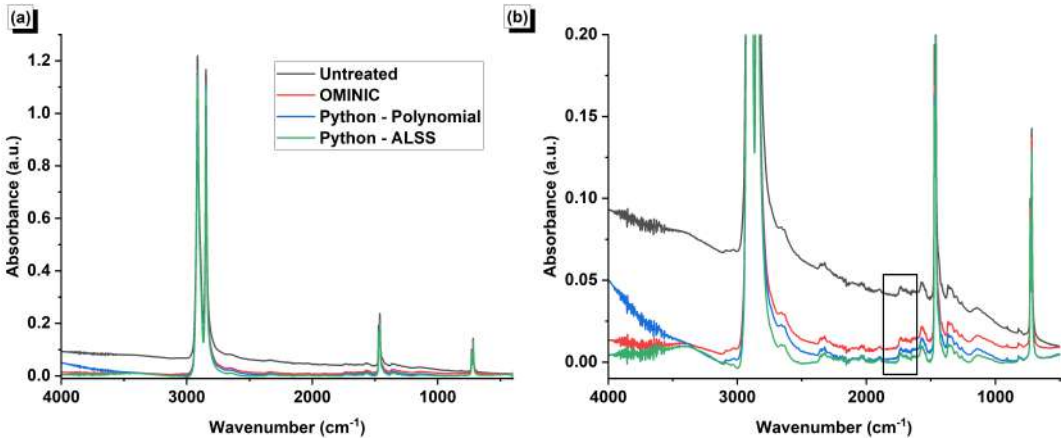

Figure A.2: (a) Full FTIR spectra and (b) zoom of a PEX-e2 sample highlighting the effect of the baseline correction on the carbonyl region. (The color legend applies for both graphs).

A.2.2 Python code for quantitative FTIR spectroscopy analysis

A Python script was developed to pre-process and analyze FTIR absorbance data from multiple spectra recorded at the same resolution and range. The pre-processing steps include baseline correction using ALSS and normalization with an internal standard. After pre-processing, the spectra are further analyzed by identifying peaks, calculating the area of the carbonyl region, and generating an average spectrum. The general schematic of the automation are shown in Figure A.3.

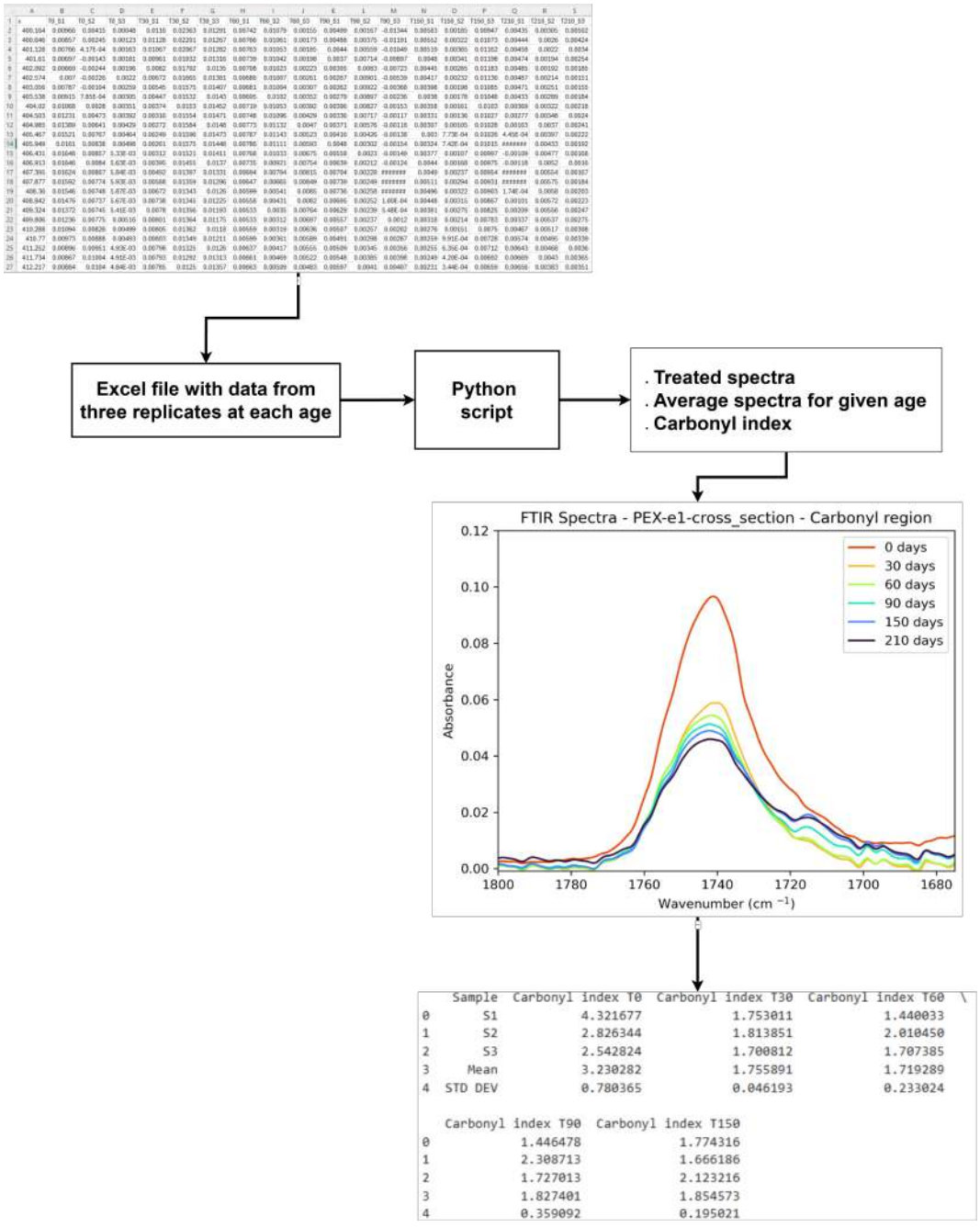

	Sample	Carbonyl index T0	Carbonyl index T30	Carbonyl index T60	Carbonyl index T90	Carbonyl index T150
0	S1	4.321677	1.753011	1.440033	1.446478	1.774316
1	S2	2.826344	1.813851	2.010450	2.308713	1.666186
2	S3	2.542824	1.700812	1.707385	1.727013	2.123216
3	Mean	3.230282	1.755891	1.719289	1.827401	1.854573
4	STD DEV	0.780365	0.046193	0.233024	0.359092	0.195021

Figure A.3: Schematic of the FTIR data analysis with Python with example of input and output.).

The script was written in Python 3 using the Jupyter Notebook environment and the main steps are exemplified below.

Importing:

The first part of the code imports all the necessary Python libraries and imports the Excel file for each material, containing data from three replicate spectra for each age. The files and figures were named in a consistent way to facilitate running the script for a new data set by simply replacing all the data files names with the *Find and Replace* function (ctrl+F).

The script given below was used for importing data from PEX-e1 cross-section spectra at ages 0, 30, 60, 90, 150 and 210 days, which were referred to as T0, T30... T210. The three replicates were referred to as S1, S2 and S3.

```
# Import all necessary python libraries
import numpy as np
import seaborn as sns
from matplotlib import cm
import matplotlib.pyplot as plt
import pandas as pd
import statistics
from scipy.stats import norm
from scipy import sparse
from scipy.sparse.linalg import spsolve
from scipy.linalg import cholesky
from peakutils import baseline, indexes
from scipy import integrate
from itertools import cycle, islice

# Importing the Excel files from Material at certain age. The
    name of the columns need to be modified according to the
    sample name
path="PEX-e1-cross_section.xlsx"  #-----> modify accordingly
curves_T0=pd.read_excel(path, usecols=['x','T0_S1','T0_S2','
    T0_S3']).rename(columns={'x':'Wavenumber', 'T0_S1': 'S1','
    T0_S2':'S2','T0_S3': 'S3'}).set_index('Wavenumber')
curves_T30=pd.read_excel(path, usecols=['x','T30_S1','T30_S2','
    T30_S3']).rename(columns={'x':'Wavenumber', 'T30_S1': 'S1','
    T30_S2':'S2','T30_S3': 'S3'}).set_index('Wavenumber')
curves_T60=pd.read_excel(path, usecols=['x','T60_S1','T60_S2','
    T60_S3']).rename(columns={'x':'Wavenumber', 'T60_S1': 'S1','
    T60_S2':'S2','T60_S3': 'S3'}).set_index('Wavenumber')
curves_T90=pd.read_excel(path, usecols=['x','T90_S1','T90_S2','
    T90_S3']).rename(columns={'x':'Wavenumber', 'T90_S1': 'S1','
    T90_S2':'S2','T90_S3': 'S3'}).set_index('Wavenumber')
curves_T150=pd.read_excel(path, usecols=['x','T150_S1','T150_S2
```

```
    ','T150_S3']).rename(columns={'x':'Wavenumber', 'T150_S1': '
    S1','T150_S2':'S2','T150_S3': 'S3'}).set_index('Wavenumber')
curves_T210=pd.read_excel(path, usecols=['x','T210_S1','T210_S2
    ','T210_S3']).rename(columns={'x':'Wavenumber', 'T210_S1': '
    S1','T210_S2':'S2','T210_S3': 'S3'}).set_index('Wavenumber')
```

Baseline correction:

The second part of the code calculates baseline and subtracts it from the data. The script below shows how this was done for the unaged spectra ("T0"). The same was also done for the other ages ("T30", "T60"... "T210").

```
# PRE-PROCESSING: BASELINE CORRECTION WITH POLYNOMIAL FIT

#function tha calculates baseline with Asymmetric Least Squares
    Smoothing
def als(y, lam, p, itermax):
    r"""
    Implements an Asymmetric Least Squares Smoothing
    baseline correction algorithm (P. Eilers, H. Boelens 2005)

    Baseline Correction with Asymmetric Least Squares Smoothing
    based on https://github.com/vicngtor/BaySpecPlots

    Baseline Correction with Asymmetric Least Squares Smoothing
    Paul H. C. Eilers and Hans F.M. Boelens
    October 21, 2005

    Description from the original documentation:

    Most baseline problems in instrumental methods are
    characterized by a smooth
    baseline and a superimposed signal that carries the
    analytical information: a series
    of peaks that are either all positive or all negative. We
    combine a smoother
    with asymmetric weighting of deviations from the (smooth)
    trend get an effective
    baseline estimator. It is easy to use, fast and keeps the
    analytical peak signal intact.
    No prior information about peak shapes or baseline (
    polynomial) is needed
    by the method. The performance is illustrated by simulation
    and applications to
    real data.

    Inputs:
```

```
        y:
            input data (i.e. chromatogram of spectrum)
        lam:
            parameter that can be adjusted by user. The larger lambda is,
            the smoother the resulting background, z
        p:
            wheighting deviations. 0.5 = symmetric, <0.5: negative
            deviations are stronger suppressed
        itermax:
            number of iterations to perform
    Output:
        the fitted background vector

    """
    L = len(y)
    D = sparse.csc_matrix(np.diff(np.eye(L), 2))
    w = np.ones(L)
    for i in range(itermax):
        W = sparse.spdiags(w, 0, L, L)
        Z = W + lam * D.dot(D.transpose())
        z = spsolve(Z, w*y)
        w = p * (y > z) + (1-p) * (y < z)
    return z

lam = 1e9
p = 0.005
itermax = 10

#creating baseline for each spectra
curves_T0_bsl = []
curves_T0_bsl_sub = []
for column in curves_T0: #Iterating over each column in excel file
    baseline = als(curves_T0[column], lam, p, itermax)  # calling function that calculates the baseline
    curves_T0_bsl.append(baseline)
    curve_sub = (curves_T0[column] - baseline) #subtracting raw spectra from baseline
    curves_T0_bsl_sub.append(curve_sub)

baselines_T0 = {'Wavenumber': curves_T0.index,
            'S1': curves_T0_bsl[0],
            'S2': curves_T0_bsl[1],
            'S3': curves_T0_bsl[2],
                  }
```

```
70
71 curves_baselines_T0  = pd.DataFrame(baselines_T0).set_index('
      Wavenumber')
72 print(curves_baselines_T0)
73
74 # Creating dataframe with the baseline-subtracted data
75 sub_T0 = {'Wavenumber': curves_T0.index,
76             'S1': curves_T0_bsl_sub[0],
77             'S2': curves_T0_bsl_sub[1],
78             'S3': curves_T0_bsl_sub[2],
79                    }
80
81 curves_sub_T0  = pd.DataFrame(sub_T0).set_index('Wavenumber')
82
83 #CREATING A AVERAGE SPECTRA OF S1, S2, S3
84 mean_sub_T0 =  curves_sub_T0.mean(axis=1, skipna=True)
85 curves_sub_T0.insert(3, "Mean", mean_sub_T0)
86 print(curves_sub_T0)
```

Normalization:

The baseline corrected spectra were normalized by a internal standard. In this case the absorbance of the crystal phase CH_2 scissoring vibrations at 1472 cm^{-1}.

```
1 # PRE-PROCESSING: NORMALIZATION
2
3 # Normalization of FTIR dta if often perfomed using a specific
      peak absorbance as an internal reference.
4 # Internal reference limits (as the values can vary a bit
      between spectra)
5 ref_lim_inf_1 = 1471 # -----> modify accordingly
6 ref_lim_sup_1 = 1473  # -----> modify accordingly
7
8
9
10 mdist=1
11 thres=0.1 # threshold for peak detection -----> modify
      accordingly
12
13 ref_peaks_T0 = []
14 curves_norm_T0 = []
15 for column in curves_sub_T0:  # interating over each spectra
16     p = indexes(curves_sub_T0[column].values, #finding peaks in
       spectra and returning the indexes (location of peaks in
      data frame)
17             min_dist=mdist,
```

```
            thres=thres
           )
    p
    print(curves_sub_T0[column].iloc[p])
    ref_peak = curves_sub_T0[column].iloc[p][curves_sub_T0[
   column].iloc[p].index > ref_lim_inf_1] #restricting to the
   limits of the reference peak
    ref_peak = ref_peak[ref_peak.index < ref_lim_sup_1] #
   restricting to the limits of the reference peak
    ref_peaks_T0.append(ref_peak)
    curve_norm = curves_sub_T0[column].values/ref_peak.values #
   normalizing all the y points in the spectra by the
   absorbance of the refernece peak
    curves_norm_T0.append(curve_norm)
print(ref_peaks_T0)

# Creating dataframe with the normalized data
norm_T0 = {'Wavenumber': curves_T0.index,
           'S1': curves_norm_T0[0],
           'S2': curves_norm_T0[1],
           'S3': curves_norm_T0[2],
           'Mean': curves_norm_T0[3],
                 }
curves_norm_T0  = pd.DataFrame(norm_T0).set_index('Wavenumber')
print(curves_norm_T0)
```

Plotting desired graphs:

Here there is an example on how to created a graph with the average spectra at each age. The plot limits can be changed to show the region of interest, e.g., carbonyl region.

```
# Plotting average spectra after pre-processing
colors = [plt.cm.turbo(i) for i in np.linspace(0, 1, 7)]
curves_norm_T0.Mean.plot(alpha=1, color=colors[5], legend="full
   ", label="0 days", ylabel="Absorbance", title="FTIR Spectra
   - PEX-e1-cross_section ") #-----> modify accordingly
curves_norm_T30.Mean.plot(alpha=1, color=colors[4], legend="
   full", label="30 days") #-----> modify accordingly
curves_norm_T60.Mean.plot(alpha=1, color=colors[3], legend="
   full", label="60 days") #-----> modify accordingly
curves_norm_T90.Mean.plot(alpha=1, color=colors[2], legend="
   full", label="90 days") #-----> modify accordingly
curves_norm_T150.Mean.plot(alpha=1, color=colors[1], legend="
   full", label="150 days") #-----> modify accordingly
curves_norm_T210.Mean.plot(alpha=1, color=colors[0], legend="
   full", label="210 days") #-----> modify accordingly
```

```

# control x and y limits  -----> modify accordingly
#plt.ylim(-0.02, 0.15)
plt.xlim(4000,400)
plt.xlabel("Wavenumber (cm $^{-1}$)")
# Export plot as .png file
plt.savefig('FTIR-normalized_spectra-PEX-e1-cross_section-ageing_time.png', dpi=300)    #   ----> modify file name


# Plotting average carbonyl region after pre-processing
curves_norm_T0.Mean.plot(alpha=1, color=colors[5], legend="full", label="0 days", ylabel="Absorbance", title="FTIR Spectra - PEX-e1-cross_section - Carbonyl region") #-----> modify accordingly
curves_norm_T30.Mean.plot(alpha=1, color=colors[4], legend="full", label="30 days") #-----> modify accordingly
curves_norm_T60.Mean.plot(alpha=1, color=colors[3], legend="full", label="60 days") #-----> modify accordingly
curves_norm_T90.Mean.plot(alpha=1, color=colors[2], legend="full", label="90 days") #-----> modify accordingly
curves_norm_T150.Mean.plot(alpha=1, color=colors[1], legend="full", label="150 days") #-----> modify accordingly
curves_norm_T210.Mean.plot(alpha=1, color=colors[0], legend="full", label="210 days") #-----> modify accordingly

# control x and y limits  -----> modify accordingly
plt.ylim(-0.0008, 0.12)
plt.xlim(1800,1675)
plt.xlabel("Wavenumber (cm $^{-1}$)")
# Export plot as .png file
plt.savefig('FTIR-normalized_spectra-PEX-e1-cross_section-ageing_time-carbonyl.png', dpi=300)    #   ----> modify file name
```

Calculating area of the carbonyl region:

For the calculation of the carbonyl index, the area of the carbonyl region (1675-1775 cm^{-1}) was calculated with numerical integration.

```
#Creating subsets with spectral regions of interest T0

# SUBSET - Region range = CARBONYL
region_lim_inf = 1675.0
region_lim_sup = 1775.0
subset = curves_norm_T0[curves_norm_T0.index > region_lim_inf]
subset = subset[subset.index < region_lim_sup].drop(['Mean'], axis=1)
```

```
print(subset)


# CALCULATE AREA OF DEFINED REGION OF SPECTRA - in this case Carbonyl region for calculation of Carbonyl index (CI)

# Calculates area of subset (numerical integration of absorbance from 1675-1775cm-1)
CI =[]
for column in subset:
    CI.append(np.trapz(subset[column].values, x=subset[column].index)) #numeric integration of area under the curve

print(CI)

CI_T0 = pd.Series(CI)
# Calculates the MEAN and STD DVE of the area for the three samples

CI_T0.loc[len(CI_T0)] = statistics.mean([CI_T0[0],CI_T0[1], CI_T0[2]])
CI_T0.loc[len(CI_T0)] =  statistics.pstdev([CI_T0[0],CI_T0[1], CI_T0[2]])


# Creates a dataframe with the results that can later be exported as .csv file
samples = pd.Series(['S1', 'S2', 'S3', 'Mean', 'STD DEV'])
CI_frame = {'Sample': samples,
            'Carbonyl index T0': CI_T0}
CI_result = pd.DataFrame(CI_frame)

print(CI_result)
```

Exporting the results:

The results were exported as *comma separates values* (CSV) files that could be latter imported into graphing and data analysis software.

```
# EXPORTS RESULTS .CSV FILES
CI_result.to_csv('PEX-e1-cross_section-carbonyl-index', sep=',', index=True, encoding='utf-8') #  -----> modify file name
curves_norm.to_csv('PEX-e1-cross_section-Normalized-average-spectra', sep=',', index=True, encoding='utf-8') #  -----> modify file name
```

A.3
Supplementary graphs

A.3.1
FTIR spectra: surface analysis

The analysis of the inner surface of the pipes was performed with FTIR-ATR measurements. Three spectra were collected from each pipe at every aging interval, then pre-processed using baseline correction and normalization techniques. The average spectra from these replicate measurements are presented in Figures A.4, A.5, A.6, A.7, for PEX-e1, PEX-e2, PEX-a and PE100, respectively.

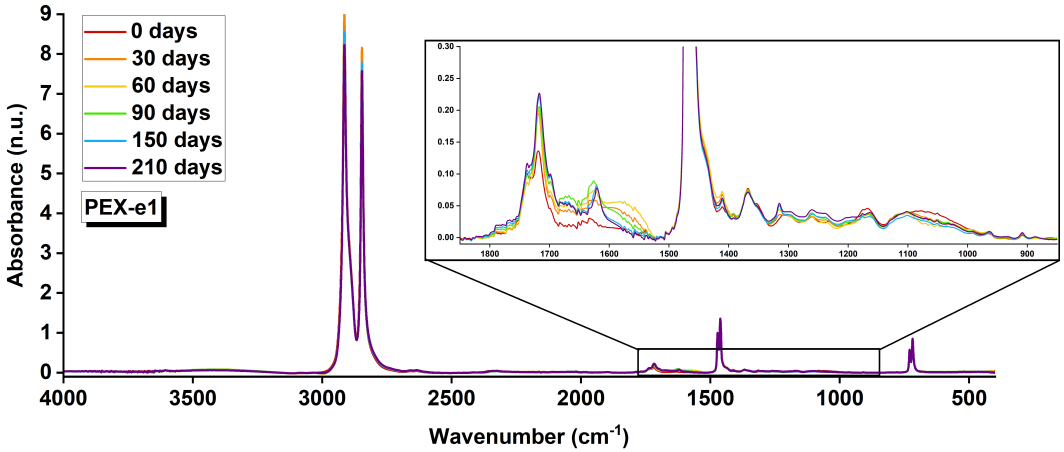

Figure A.4: FTIR spectral evolution of the PEX-e1 surface during thermal-oxidative aging. The zoomed-in region highlights key spectral changes observed with the ageing protocol.

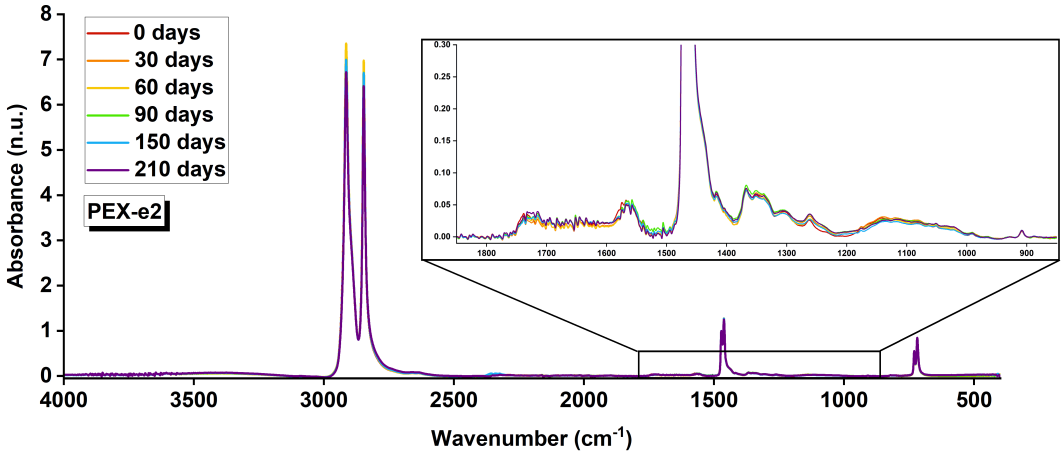

Figure A.5: FTIR spectral evolution of the PEX-e2 surface during thermal-oxidative aging. The zoomed-in region highlights key spectral changes observed with the ageing protocol.

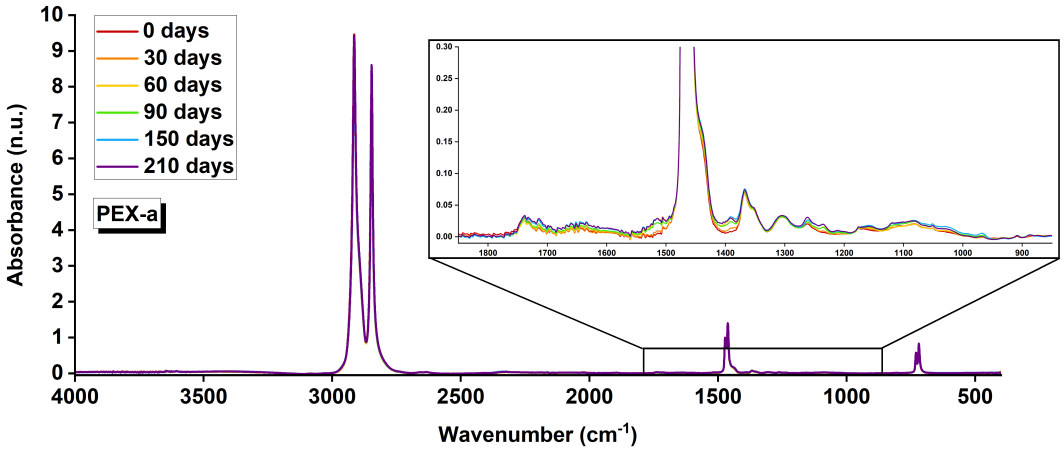

Figure A.6: FTIR spectral evolution of the PEX-a surface during thermal-oxidative aging. The zoomed-in region highlights key spectral changes observed with the ageing protocol.

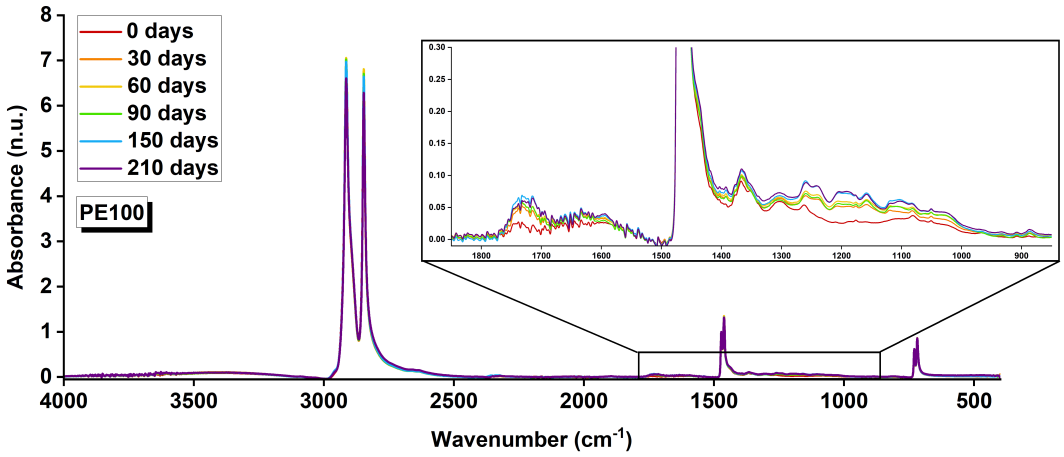

Figure A.7: FTIR spectral evolution of the PE100 surface during thermal-oxidative aging. The zoomed-in region highlights key spectral changes observed with the ageing protocol.

A.3.2
FTIR spectra: bulk analysis

The analysis of the antioxidant additive content on the bulk of the pipes was done by measuring the FTIR-ATR spectra on the center of cross-sectional slices. Similarly to Section A.3.1, three replicate measurements were made and the raw spectra were pre-processed. The average spectra are presented in Figures A.8, A.9, A.10, A.11, for PEX-e1, PEX-e2, PEX-a and PE100, respectively.

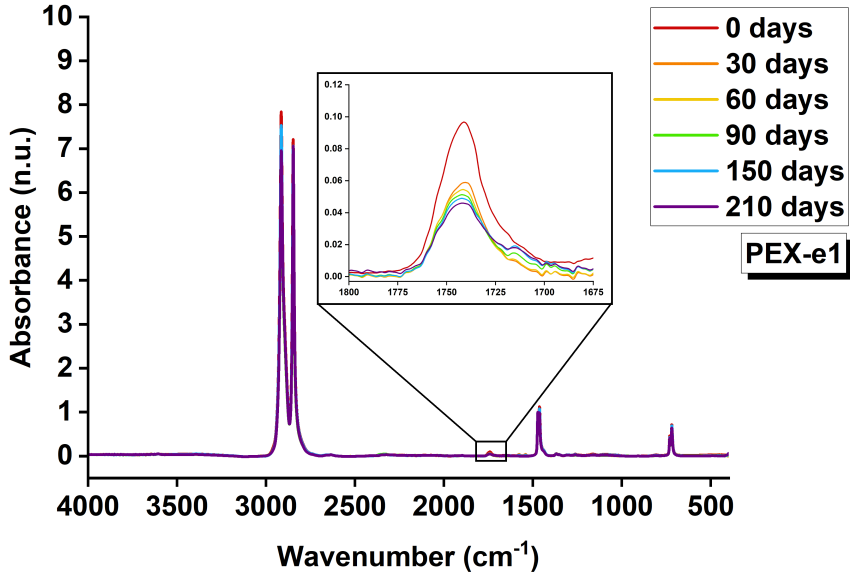

Figure A.8: FTIR spectral evolution of the PEX-e1 cross-section during thermal-oxidative aging. The zoomed-in region highlights key spectral changes observed with the ageing protocol.

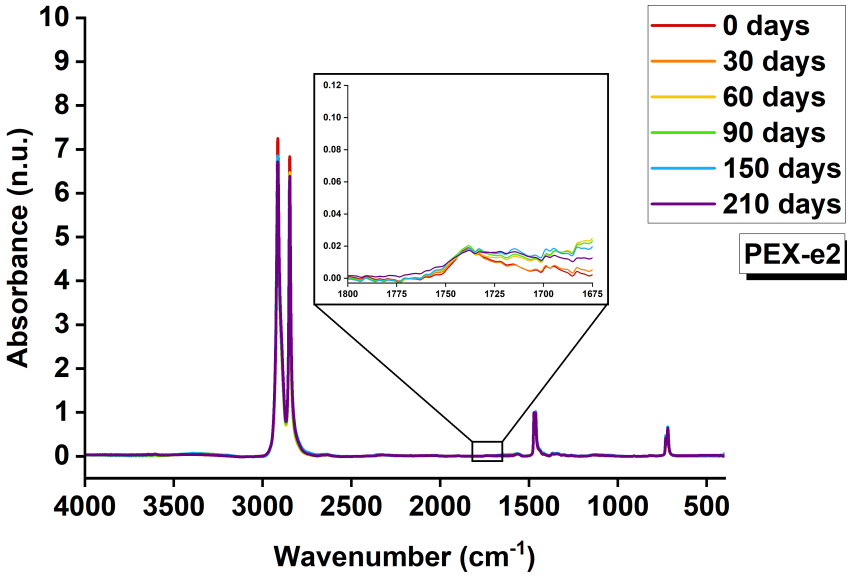

Figure A.9: FTIR spectral evolution of the PEX-e2 cross-section during thermal-oxidative aging. The zoomed-in region highlights key spectral changes observed with the ageing protocol.

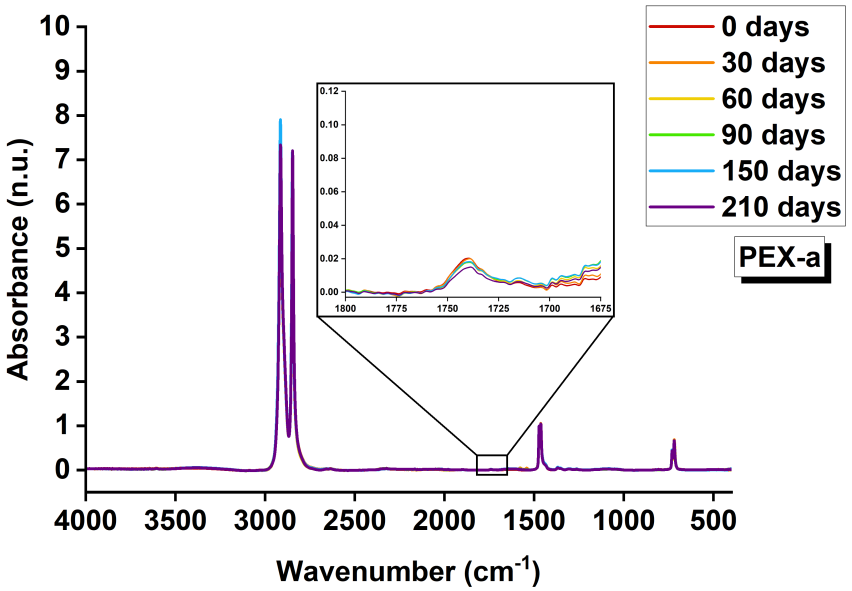

Figure A.10: FTIR spectral evolution of the PEX-a cross-section during thermal-oxidative aging. The zoomed-in region highlights key spectral changes observed with the ageing protocol.

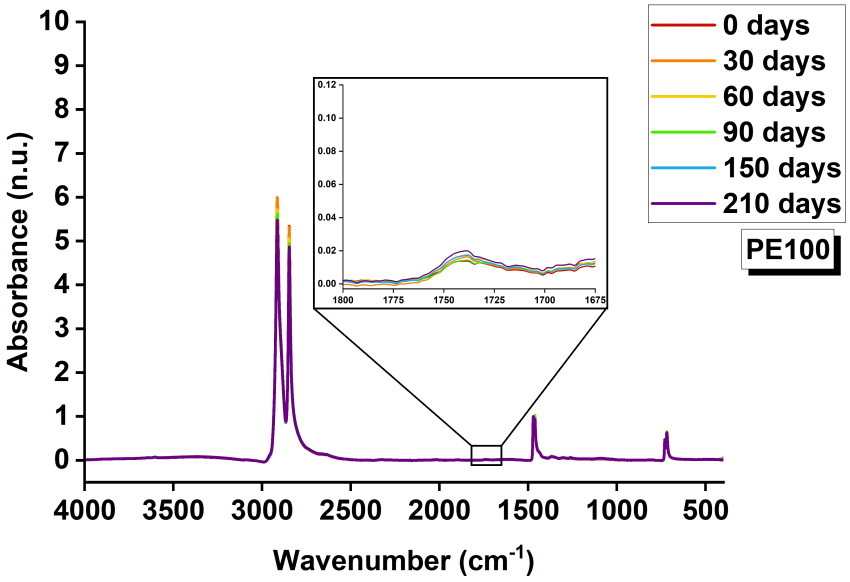

Figure A.11: FTIR spectral evolution of the PE100 cross-section during thermal-oxidative aging. The zoomed-in region highlights key spectral changes observed with the ageing protocol.

A.3.3
Colorimetry: color maps

Color changes were measured with a spectrophotometer and the results were expressed using the CIE (International Commission on Illumination) color coordinate system. The three parameters ΔL, Δa and Δb are a measure of changes in lightness, position on the red-green axis, and position on the blue-yellow axis, respectively. Figures A.12 show the variation in the three parameters with ageing time from 0 to 210 days for PEX-e1, PEX-e2, and PEX-a. The PE100 pipe did not show significant variation in neither parameter after 210 days of ageing, with $\Delta L = 0.38$, $\Delta a = -0.01$ and $\Delta b = 0.02$.

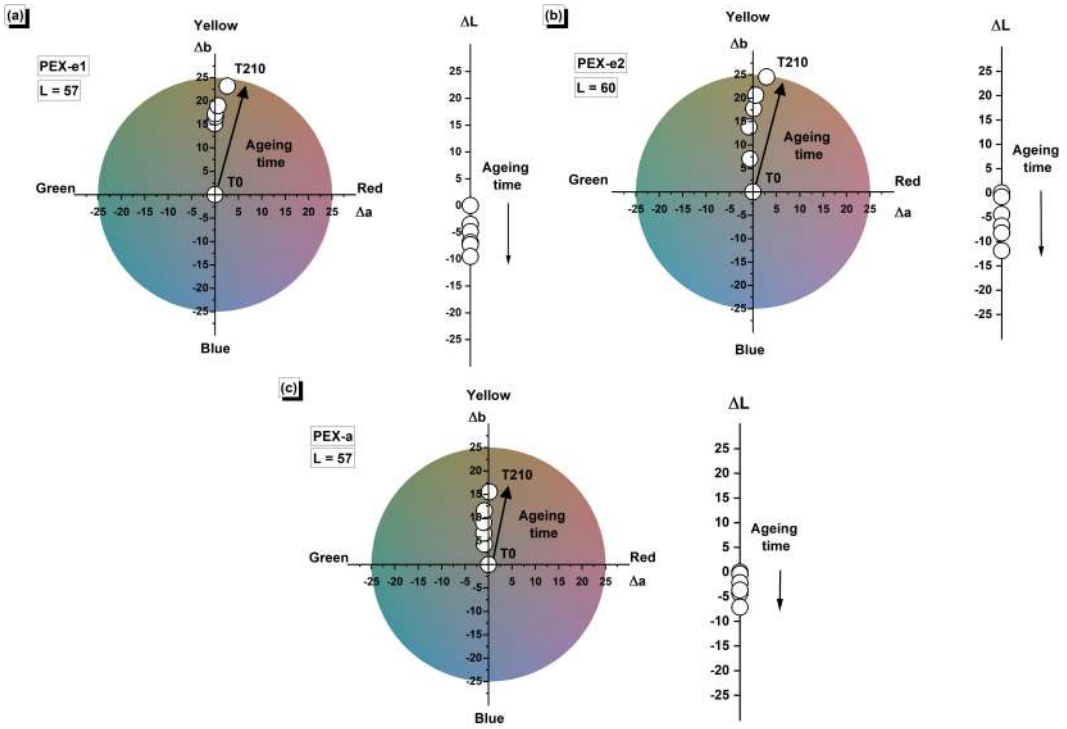

Figure A.12: CIE lab color maps showing progressive variation in color in the surface of (a) PEX-e1, (b) PEX-e2, and (c) PEX-a pipe.

A.3.4 ^{13}C NMR spectra

The main challenge with ^{13}C NMR measurements lies in the quantitation of the NMR signal. In principle, cross-polarisation (CP) is not inherently quantitative, whereas direct excitation MAS (herein referred to as simply MAS) is quantitative, provided that there is a sufficient relaxation delay between acquisitions. However, in ^{13}C MAS experiments, the relaxation time of the crystalline phases of polyethylene (PE) can extend to thousands of seconds. This relaxation time depends on the size of the crystalline domains and their interactions with the interphase region, which can make the analysis of multiple samples significantly time-consuming. Figure A.13 presents a comparison of the ^{13}C CPMAS NMR and ^{13}C MAS NMR spectra of unaged PEX-e2. As shown, the amorphous component of the main chain CH_2 groups is somewhat underestimated in the CPMAS NMR spectra. Consequently, the peak areas between samples can only be compared semi-quantitatively.

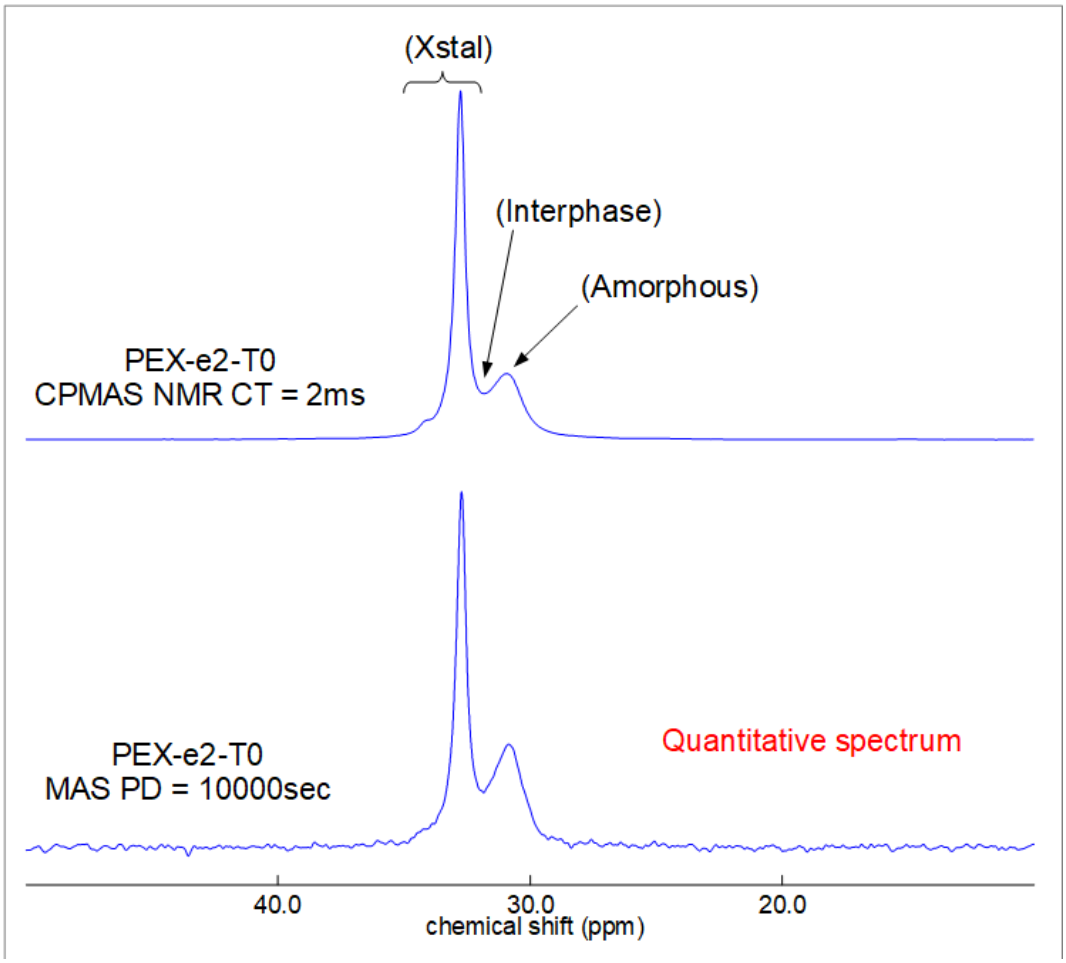

Figure A.13: Comparison of the ^{13}C CPMAS and^{13}C MAS NMR spectra of unaged PEX-e2 (PEX-e2-T0). The peaks corresponding to crystalline ("Xstal"), interphase and amorphous components are identified.

The ^{13} CPMAS NMR spectra of the pipes before (0 days) and after ageing (150 and 210 days) were measured to monitor potential differences in the molecular configurations and the formation/depletion of carbonyl, vinyl, and methyl groups. Figure A.14 shows a comparison of the in the main chain CH_2 peaks in the ^{13} CPMAS NMR spectra of the pipes before and after 210 days of ageing. The crystalline component of the main chain CH_2 groups increased with ageing for all pipes, which corroborates with the increase in degree of crystallinity observed by other techniques.

The analysis of carbonyl, vinyl, and methyl groups was done by vertical expansion of the spectra. A comparison of the vertically expanded spectra of PEX-e1, PEX-e2, PEX-a and PE100 before and after ageing are shown in Figures A.15-A.18.

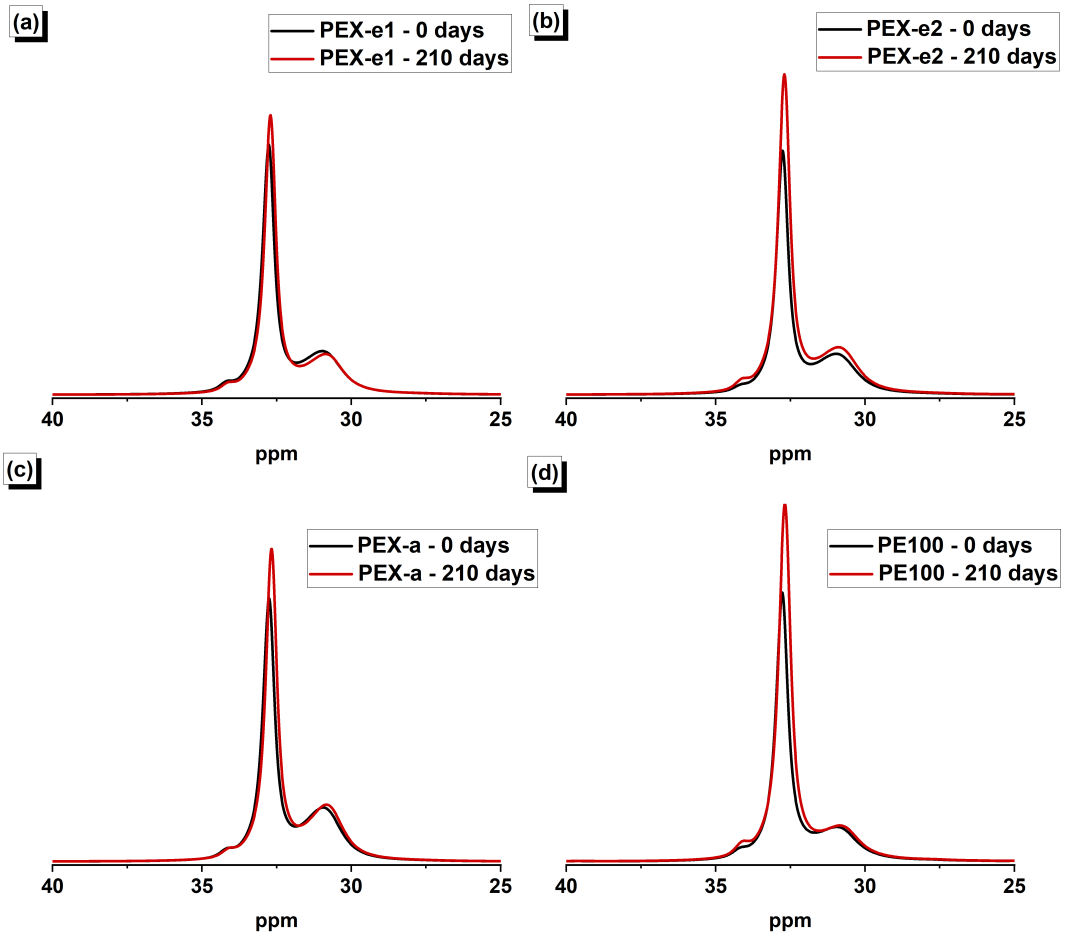

Figure A.14: Comparison of the in the main chain CH_2 peaks in the ^{13} NMR spectra of the pipes before and after 210 days of ageing.

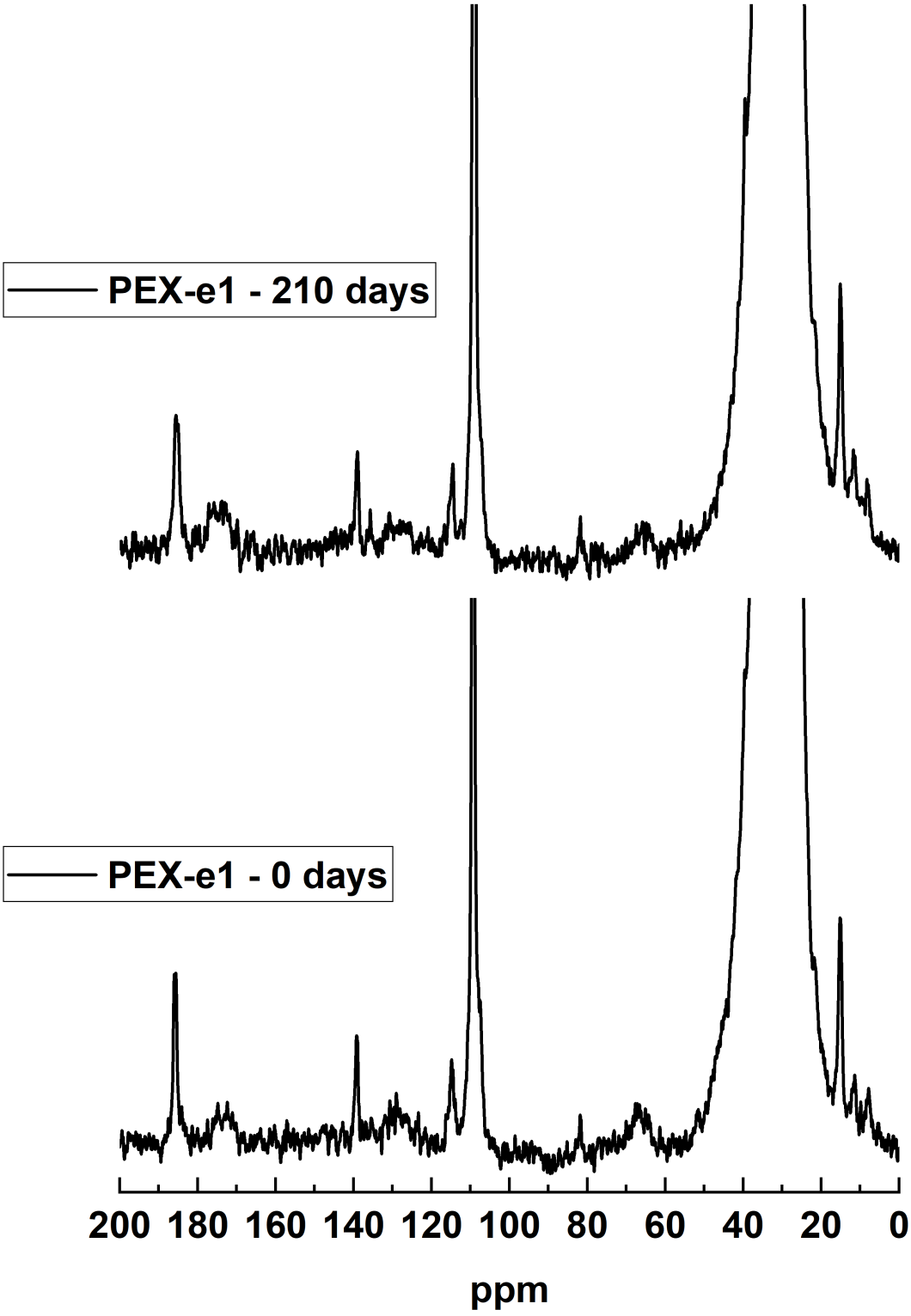

Figure A.15: Vertical expansion of the spectra of the ^{13} NMR spectra of the PEX-e1 pipes before and after 210 days of ageing.

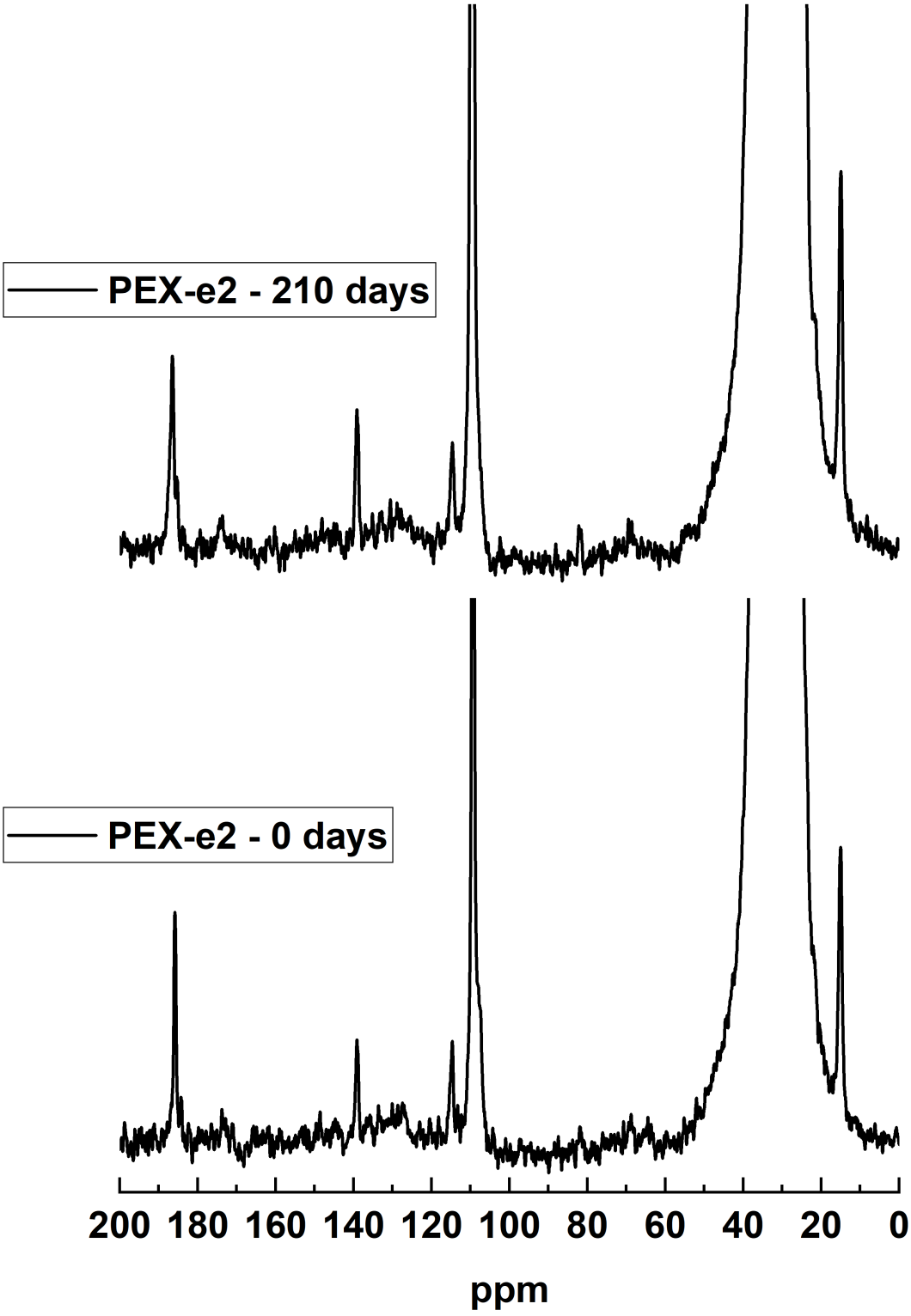

Figure A.16: Vertical expansion of the spectra of the ^{13} NMR spectra of the PEX-e2 pipes before and after 210 days of ageing.

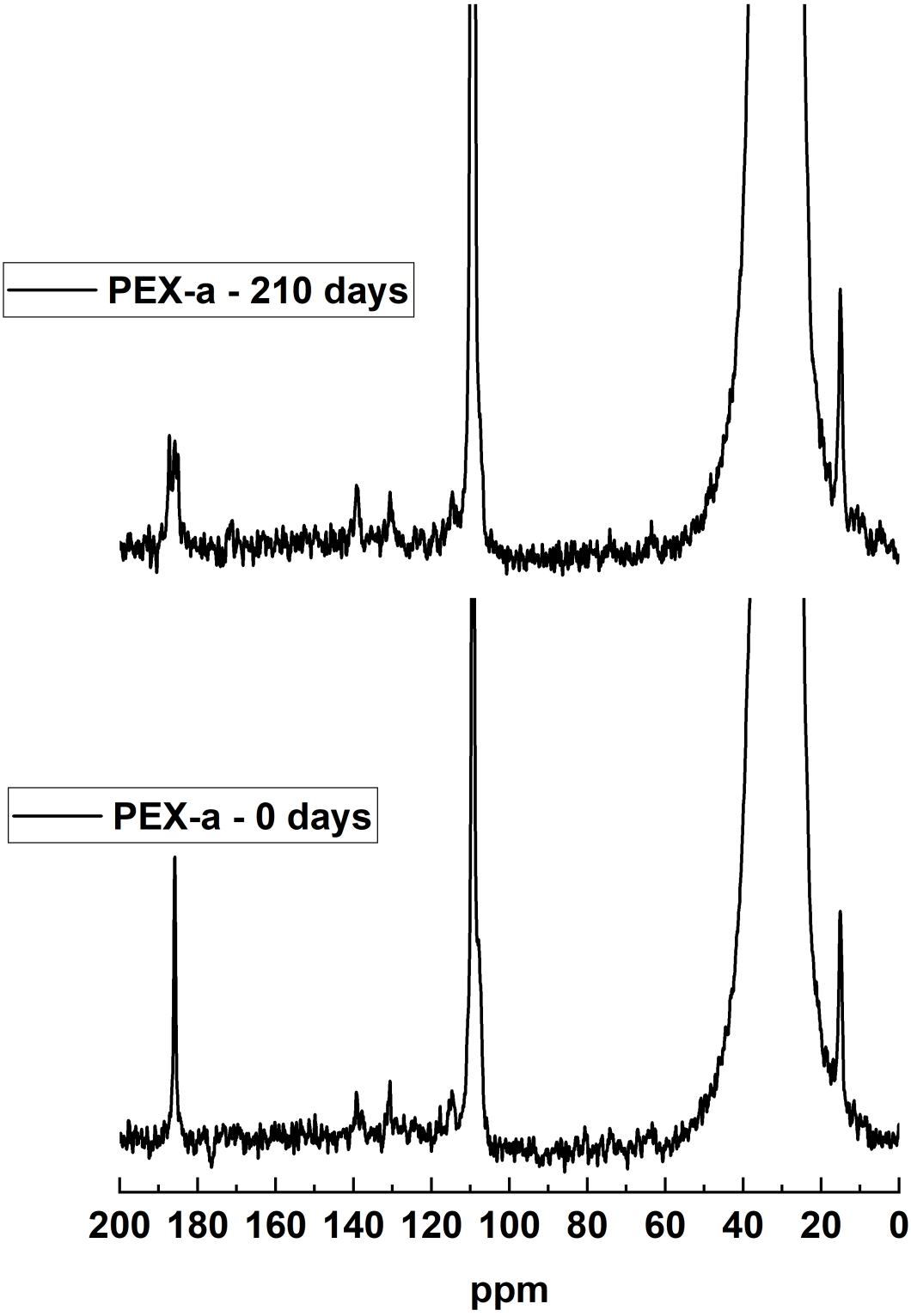

Figure A.17: Vertical expansion of the spectra of the ^{13} NMR spectra of the PEX-a pipes before and after 210 days of ageing.

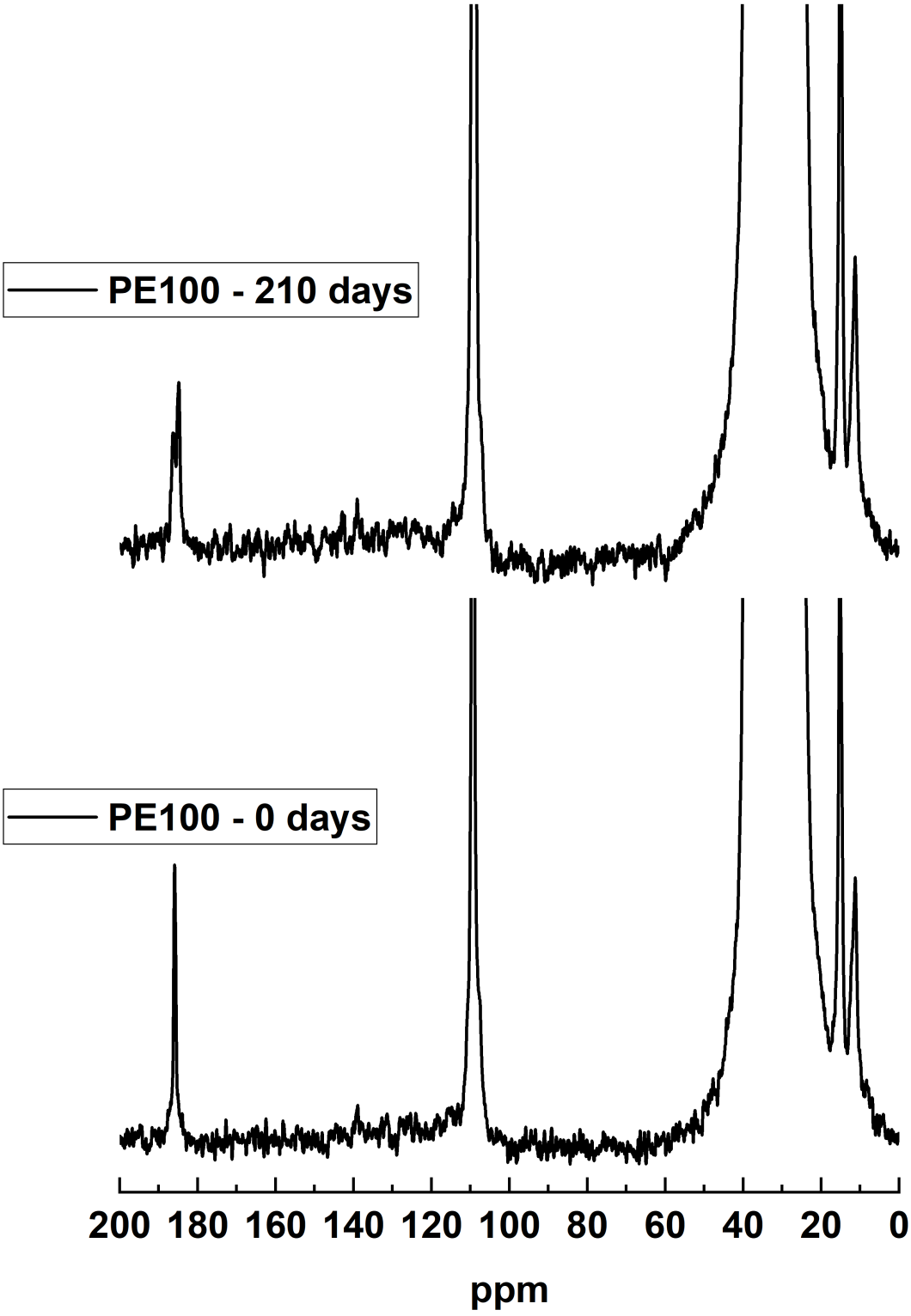

Figure A.18: Vertical expansion of the spectra of the ^{13} NMR spectra of the PE100 pipes before and after 210 days of ageing.

A.3.5
^{1}H NMR spectra

The evolution of the ^{1}H NMR experimental decay signal over ageing time is provided in Figure A.19. Changes in the samples with ageing are better visualized after the three model fitting. The parameters obtained with the fitting are provided in Table

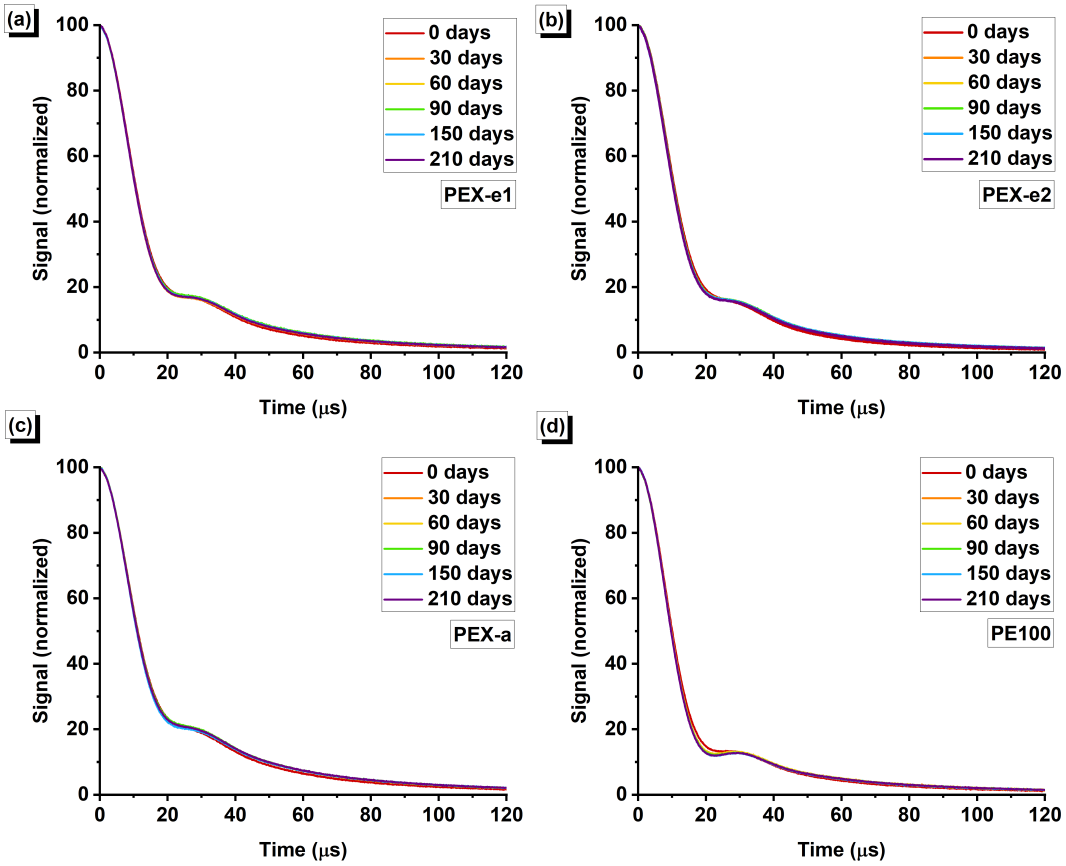

Figure A.19: ^{1}H NMR solid echo decay acquired for PEX and PE pipes samples over time.

Table A.1: Fitting results for the three components with the PEX-e1 data.

		Rigid			Intermediate			Mobile	
Age	Total	T_2	R	Total	T_2	n	Total	T_2
(days)	(%)	(μs)	(-)	(%)	(μs)	(-)	(%)	(μs)
0	54.5	21.7	0.20	36.0	25.5	1.35	9.5	60.2
30	57.6	21.4	0.20	32.6	26.4	1.32	9.8	65.4
60	56.4	21.7	0.21	33.7	26.3	1.29	9.8	67.9
90	55.2	21.8	0.21	34.9	25.8	1.25	9.9	68.4
150	56.7	21.8	0.20	33.1	26.2	1.29	10.2	65.5
210	56.1	22.0	0.21	33.9	25.7	1.28	10.0	65.5

Table A.2: Fitting results for the three components with the PEX-e2 data.

	Rigid			Intermediate			Mobile	
Age (days)	Total (%)	T_2 (μs)	R (-)	Total (%)	T_2 (μs)	n (-)	Total (%)	T_2 (μs)
0	54.4	21.6	0.20	36.8	24.9	1.39	8.8	54.5
30	56.1	21.7	0.21	35.6	25.4	1.30	8.3	65.5
60	56.0	21.8	0.20	35.3	25.3	1.30	8.7	64.4
90	56.6	21.9	0.21	34.8	25.6	1.31	8.7	65.1
150	56.2	21.6	0.21	35.4	25.2	1.28	8.4	66.7
210	56.0	21.9	0.21	34.8	24.8	1.30	9.2	60.6

Table A.3: Fitting results for the three components with the PEX-a data.

	Rigid			Intermediate			Mobile	
Age (days)	Total (%)	T_2 (μs)	R (-)	Total (%)	T_2 (μs)	n (-)	Total (%)	T_2 (μs)
0	50.7	21.7	0.21	36.8	26.9	1.35	12.5	59.2
30	52.2	22.0	0.21	35.0	27.4	1.31	12.8	65.1
60	53.3	21.8	0.21	33.9	28.1	1.35	12.8	65.0
90	51.8	22.0	0.21	35.2	27.7	1.32	13.0	65.0
150	53.8	22.0	0.21	34.0	28.0	1.31	12.3	67.5
210	52.2	22.0	0.21	34.5	27.6	1.31	13.2	64.8

Table A.4: Fitting results for the three components with the PE100 data.

	Rigid			Intermediate			Mobile	
Age (days)	Total (%)	T_2 (μs)	R (-)	Total (%)	T_2 (μs)	n (-)	Total (%)	T_2 (μs)
0	60.0	21.7	0.21	32.7	23.7	1.24	7.3	65.8
30	63.4	21.9	0.21	29.4	24.1	1.17	7.2	74.0
60	63.2	21.9	0.21	29.5	24.3	1.17	7.4	74.5
90	63.2	21.9	0.21	29.8	23.9	1.15	7.0	75.0
150	64.1	21.9	0.21	29.1	24.3	1.17	6.8	76.3
210	64.3	21.8	0.21	28.5	24.3	1.17	7.2	74.6